UNIVERSIDAD CARLOS III DE MADRID

TESIS DOCTORAL

ENHANCING WIRELESS LOCAL AREA NETWORKS BY LEVERAGING DIVERSE FREQUENCY RESOURCES

Autor: Thomas Nitsche, Universidad Carlos III de Madrid and IMDEA Networks Institute
Director: Dr. Joerg Widmer, IMDEA Networks Institute

DEPARTAMENTO DE INGENIERÍA TELEMÁTICA

Leganés (Madrid), 2015

UNIVERSIDAD CARLOS III DE MADRID

Ph.D Thesis

ENHANCING WIRELESS LOCAL AREA NETWORKS BY LEVERAGING DIVERSE FREQUENCY RESOURCES

Author: Thomas Nitsche, Universidad Carlos III de Madrid and IMDEA Networks Institute
Director: Dr. Joerg Widmer, IMDEA Networks Institute

DEPARTMENT OF TELEMATIC ENGINEERING

Leganés (Madrid), 2015

Enhancing Wireless Local Area Networks by Leveraging Diverse Frequency Resources

A dissertation submitted in partial fulfillment of the requirements for the degree of Doctor of Philosophy

Prepared by
Thomas Nitsche, Universidad Carlos III de Madrid and IMDEA Networks Institute

Under the advice of
Dr. Joerg Widmer, IMDEA Networks Institute

Departamento de Ingeniería Telemática, Universidad Carlos III de Madrid

---

Date: January, 2015

Web/contact: thomas.nitsche@imdea.org

This work has been supported by IMDEA Networks Institute.

TESIS DOCTORAL

ENHANCING WIRELESS LOCAL AREA NETWORKS BY LEVERAGING DIVERSE FREQUENCY RESOURCES

Autor: Thomas Nitsche, Universidad Carlos III de Madrid and IMDEA Networks Institute
Director: Dr. Joerg Widmer, IMDEA Networks Institute

Firma del tribunal calificador:

Firma:

Presidente:

Vocal:

Secretario:

Calificación:

Leganés, de de

Acknowledgements

I would like to express my sincere thanks to all those who made this thesis possible and provided help and support. First of all to my supervisor Dr. Jörg Widmer for his guidance and profound advice on writing this thesis as well as his academic mentoring. Further, thanks are owed to Dr. Thomas Fuhrmann and Dr. Edward Knightly, who also took their share in guiding my academic work.

Along the same lines, I would like to thank all those people that I met along the way at Technische Universität München, IMDEA Networks Institute and Rice University for discussion, advice and encouragements: Michael Weiss, Dr. Björn Saballus, Dr. Johanna Amann, Allyson Sim, Arash Asadi, Ignacio de Castro Arribas, Qing Wang, Dr. Jose Felix Kukielka, Dr. Adrian Loch, Dr. Mathias Hollick, Dr. Alexander Kühne, Dr. Kyle Jamieson, Jie Xiong, Jon Gjengset, Pablo Salvador, Maria Isabel Sanchez, Adriana Flores Middelton, Dr. Narendra Anand, Dr. Oscar Bejarano, Ryan E. Guerra, Sadia Quadri, Irene Tejado and Guillermo Bielsa. Special thanks belong to Dr. Benedikt Elser and Dr. Georg Acher for their 'unofficial' academic mentoring.

Finally, I want to express my profound gratitude to my beloved parents, my family and to Daniela for their love and continuous support.

Abstract

In this thesis, signal propagation variations, that are experience over the frequency resources of IEEE 802.11 Wireless Local Area Networks (WLANs) are studied. It is found that exploitation of these variations can improve several aspects of wireless communication systems. To this aim, frequency varying behavior is addressed at two different levels.

First, the intra-channel scale is considered, i.e. variations over the continuous frequency block that a device uses for a cohesive transmission. Variations at this level are well known but current wireless systems restrict to basic equalization techniques to balance the received signal. In contrast, this work shows that more fine grained adaptation to these differences can accomplish throughput and connection range gains.

Second, multi-frequency band enabled devices that access widely differing frequency resources in the millimeter wave range as well as in the microwave range are analyzed. These devices that are expected to follow the IEEE 802.11ad specification experience intense propagation variations over their frequency resources. Thus, a part of this thesis revises, the theoretical specification of the IEEE 802.11ad standard and complements it by a measurement study of first generation millimeter wave devices. This study reveals deficiencies of first generation millimeter wave systems, whose improvement will pose new challenges to the protocol design of future generation systems. These challenges are than addressed by novel methods that leverage from frequency varying propagation characteristics.

The first method, improves the beam training process of millimeter wave networks, that need highly directional, though electronically steered, transmissions to overcome increased free space attenuation. By leveraging from omni-directional signal propagation at the microwave bands, efficient direction interference is utilized to provide information to millimeter wave interfaces and replace brute force direction testing. Second, deafness effects at the millimeter wave band, which impact IEEE 802.11 channel access methods are addressed. As directional communication on these bands complicates sensing the medium to be busy or idle, inefficiencies and unfairness are implied. By using coordination message exchange on the legacy Wi-Fi frequencies with omni-directional communication properties, these effects are countered. The millimeter wave bands can thus unfold their full potential, being exclusively used for high speed data frame transmission.

Table of Contents

List of Tables

List of Figures

Acronyms

A-BFT Association Beamforming Training.
AP Access Point.
ATI Announcement Transmission Interval.

BBS Blind Beam Steering.
BER Bit Error Rate.
BF Beam Forming.
BHI Beacon Header Interval.
BI Beacon Interval.
BPSK Binary Phase Shift Keying.
BRP Beam Refinement Protocol.
BSS Basic Service Set.

CBAP Contention Based Access Period.
CCK Complementary Code Keying.
CDF Cumulative Distribution Function.
CDMA Code Division Multiple Access.
CFP Contention Free Period.
CP Contention Period.
CRC Cyclic Redundancy Check.
CSMA/CA Carrier Sense Multiple Access with Collision Avoidance.
CTS Clear To Send.
CW Contention Window.

DCF Distributed Coordination Function.
DIFS DCF Inter Frame Spacing.
DMG Directional Multi-Gigabit.
DSSS Direct Sequence Spread Spectrum.
DTI Data Transmission Interval.

EDCF Enhanced Distributed Coordination Function.
EIRP Equivalent Isotropically Radiated Power.
ESS Extended Service Set.

FCC Federal Communication Commission.
FEC Forward Error Correction.
FPGA Field Programmable Gate Array.
FST Fast Session Transfer.

HCF Hybrid Coordination Function.
HDMI High-Definition Multimedia Interface.
HPBW Half Power Beam Width.

IBSS Independent Basic Service Set.
IDFT Inverse Discrete Fourier Transformation.
ISI Inter-Symbol Interference.
ISM Industrial Scientific Medical.

LDPC Low Density Parity Code.
LOS Line of Sight.
LOS non-Line of Sight.
LTE Long Term Evolution.

MAC Medium Access Control.
MAC-layer Medium Access Control Layer.
MCS Modulation Coding Scheme.
MIMO Multiple Input Multiple Output.
mm-wave Millimeter Wave.
MPDU MAC Protocol Data Unit.
MSDU MAC Service Data Unit.

MU-MIMO Multi-User Multiple Input Multiple Output.

NAV Network Allocation Vector.

OFDM Orthogonal Frequency Division Multiplexing.

PBSS Personal Basic Service Set.
PC Point Coordinator.
PCF Point Coordination Function.
PCP PBSS Control Point.
PER Packet Error Rate.
PHY-layer Physical Layer.
PIFS Point Coordination Inter Frame Spacing.
PNC Personal Network Coordinator.

QAM Quadrature Amplitude Modulation.
QPSK Quadrature Phase Shift Keying.

RTS Ready To Send.
RXSS Receive Sector Sweep.

SC Single Carrier.
SDM Spatial Division Multiplexing.
SIFS Short Inter Frame Spacing.
SINR Signal to Interference and Noise Ration.
SLS Sector Level Sweep.
SNR Signal To Noise Ration.
SP Service Period.
SPR Service Period Request.
SSO Sub-Carrier Switch Off.
SSW Sector Sweep.

TC Traffic Category.
TCP Transmit Control Protocol.
TDMA Time Division Multiple Access.
TXOP Transmit Opportunity.
TXSS Transmit Sector Sweep.

WARP Wireless open Access Research Platform.
WLAN Wireless Local Area Network.
WPAN Wireless Personal Area Network.

Introduction

IEEE 802.11 Wi-Fi communication is continuously gaining popularity since its first ratified standard in 1997. This surge in popularity results from rapid technological advances and a change in live style towards omnipresent connectivity to telecommunication networks and above all the Internet. With the trend towards more powerful mobile communication devices, also the user's demand for high throughput data connectivity increases. Streaming of high definition video and audio data towards mobile devices is just one shape of this development. However, as cellular data connectivity is limited due to high frequency licensing costs, Wi-Fi communication has been willingly accepted by the users to fill the gap.

With its surge in popularity, also Wi-Fi systems repeatedly came to their limits in terms of available channel resources and throughput. For this reason, continuous enhancements to the IEEE 802.11 standard have been provided. This included continuous advancement of IEEE 802.11 signal encoding mechanisms and optimization of inefficiencies in first generation standards as well as usage of additional channel resources and addition of radically new transmission techniques, e.g. efficient multi-antenna usage.

Nonetheless, the ever increasing use of Wi-Fi and growing network densities have once again brought networks to their capacity limits. This has ultimately lead to the addition of the Millimeter Wave (mm-wave) frequency band, which provides almost ten times as much frequency resources as all legacy bands combined. Further, a radically differing signal propagation behavior compared to currently used frequencies is experienced. This, promises significantly reduced interference and the possibility of parallel data streams even in dense networks. Thus, with the IEEE 802.11ad amendment the next step towards mm-wave communication is taken, which promises to provide the performance for the upcoming technological advancements.

Further, IEEE 802.11 networks will be able to access widely differing frequency resources at the same time. Thus, significant differences in signal propagation behavior will be experienced over the range of accessible frequencies. This thesis exploits these variation of signal propagation, which can hinder but at the same time benefit communication. As a result, novel methods to mitigate and leverage from varying propagation behavior are contributed. In particular, challenges of the upcoming mm-wave technology are identified and approached with novel transmission techniques that are enabled through multi-frequency band access.

Motivation

Wireless transmissions vary significantly with the frequency of the emitted signal. This entails two important facts for wireless communication. First, transmission technology has to account for the varying conditions found over its used frequency range. Second, different frequencies are more suitable for specific types of wireless communication than others. This becomes obvious, e.g. when comparing Long Term Evolution (LTE) cellular networks operating below 1 GHz to 60 GHz backhaul links. While the first provides almost pervasive coverage, even with moving receivers located inside buildings, the usage of the latter is of completely different nature. For these links highly directional antennas are used to overcome strong free space attenuation, which requires precise alignment and a free line of sight. Slight blockage or misalignment easily interrupts transmission of these systems.

Rethinking modern wireless communication, three important aspects determine the user expectation towards theses systems: communication range, reliability and achievable throughput. The latter two are expected even in dense networks. All three characteristics are intrinsically related to the underlying frequency resources.

Communication range almost directly coincides with the free space attenuation of the used transmission frequencies. While in theory, the transmission range can be increased arbitrarily with the used transmit power, this is bounded by physical and regulatory limits. Effectively, the achievable range is thus determined by the frequency of wireless transmissions. While lower frequencies generally receive less attenuation, and allow higher transmission ranges, this property is also impacted by blockages in the path between receiver and transmitter and atmospheric effects. For rather short range indoor communication as prevalent in IEEE 802.11 WLAN, the frequency of a transmission becomes the decisive factor.

The reliability of wireless communication is very much related to the interaction of the radio signal with the environment. When impacting an obstacle, part of the signal energy is reflected, while the remaining part continues its way and penetrates the obstacle. This behavior is strongly frequency dependent, leading to high amounts of reflections or extreme signal attenuation by blockage for certain frequencies. When high reflectivity prevails for a frequency, a multipath propagation environment is created, leading to self interference by multiple copies of the same signal at the receiver. This causes extremely differing reception variations, both over small frequency and location differences. Wireless networks have to cope with these effects and equalize the signal over the used frequency range. Multipath propagation can however also have beneficial effects, e.g. providing coverage behind blocking obstacles, or laying the fundamental for efficient multi-antenna transmission techniques. These Multiple Input Multiple Output (MIMO) approaches leverage from the differing channel conditions at varying antenna positions. When these variations are known, it is possible to separate multiple parallel signal streams at the receiver and potentially multiply throughput by the number of additional transmit and receive antennas.

Throughput and performance under dense network conditions are associated with interfer-

ence effects between transmitters. The impact of interference depends on the coverage area of devices which in turn relates to the communication frequency. Thus, the supported network density depends on the signal frequency, making some frequency ranges more suitable for crowded networks than others. Preventing interference among devices can also be achieved by sharing the transmission medium and limiting the throughput of each user. Medium sharing can happen in different domains, with the most popular being time or frequency. When looking at frequency resource sharing, two different levels have to be distinguished. First, official entities as for example the Federal Communication Commission (FCC) divide the frequency spectrum into different bands. Frequency bands are assigned to specific usages and wireless transmissions in that range need to be licensed. An exception to this rule are the Industrial Scientific Medical (ISM) Bands where Wi-Fi communication takes place in an unlicensed manner. As a drawback, communication at this frequency has to expect unforeseen interference from other spectrum users. Second, frequency bands can further be divided into channels, which confine the amount of spectrum resources that a single transceiver uses. Thus, by subdividing a band into multiple channels, several users can communicate in a band at the same time without interference, but at the cost of utilizing smaller chunks of frequency resources.

As pointed out, performance and behavior of communication systems are strongly influenced by the used frequencies. Generally speaking, different parts of the spectrum are suited towards specific use cases. This has lead to assignment of matching frequencies to different types of wireless communication systems by regulatory entities. For example maritime radio, television and radio broadcasting are located at rather low frequencies with modest reflection and far transmission range. On the contrary, cellular communication systems and local area networking communicate at frequencies above 1 GHz, where spatial reuse of the same frequency is possible due to limited range. However, strong multipath propagation in this range requires careful adaptation to varying transmission conditions. On the other hand, the same multipath effects also open the way for novel transmission techniques and increases the coverage area around blocking obstacles. With technological advances wireless communication is now conquering the millimeter wave frequency range, with frequencies between 30 and 300 GHz. The propagation behavior for such systems significantly differs from systems in use today. Blockage by almost any obstacle poses extreme signal energy loss and even in free space coverage range is severely reduced. E.g. for the IEEE 802.11ad millimeter wave amendment expected range is reduced by a factor of 10 with respect to legacy Wi-Fi. While theses characteristics seems to be a drawback at first, they also form the basis for the vision of extreme spatial reuse due to reduced interference. In fact, due to advanced antenna techniques, strong signal energy focussing is envisioned, which enables multiple non interfering pencil-beam transmissions in the same room.

While the millimeter wave revolution in itself promises significant advances for wireless communication, it possesses particularly stunning opportunities for future IEEE 802.11 networks. These systems will be multi-band enabled and thus capable of able to accessing multiple frequency bands with varying propagation behavior. While this is already the case for current devices

which communicate at 2.4 and 5 GHz, for these bands propagation properties were still relatively alike. With the addition of frequency resources at 60 GHz this however changes, and combination of transmissions with radically differing behavior becomes possible. This allows for completely new transmission techniques that leverage from the individual strength of each frequency band.

Scope

This thesis explores novel ways to enhance WLAN performance considering frequency varying propagation conditions and proposes solutions to leverage from spectrum access at different frequency bands. To this end, this work is divided into two parts.

At first, frequency varying propagation characteristics are investigated at the intra-channel level for classical IEEE 802.11g compliant communication. For these systems, throughput and reliability are increased, adding a minimal feedback loop for channel state information. This information is used to prevent the usage of strongly attenuated parts of the channel, reducing transmission error probability and increasing throughput. Due to the benefits of an adaptation to frequency dependent variations, we then explore multi-band systems, which feature even stronger variations in propagation behavior.

The second part of this thesis therefore studies the benefit of frequency varying behavior for multi-band systems that operate on millimeter wave frequencies. It begins with an in-depth analysis of multi-band capable Wi-Fi networks, which is twofold. First an introduction to the IEEE 802.11ad amendment with focus on the beamforming aspects at the millimeter-wave band is given. As high throughput on millimeter wave frequencies can only be achieved with directional communication, these beamforming mechanisms are the most critical addition to the IEEE 802.11 protocol. Second, the theoretical evaluation is complemented by a practical measurement campaign of first generation millimeter wave networks that rely on electronic beam steering.

This study reveals, that devices are still limited in terms of interference reduction through directional antenna patterns. In the azimuthal range, where highly directional gain can be achieved also strong side lobes exist even when aiming for the optimal beamforming direction. This behavior worsens when beamforming towards the boundary of an antenna arrays serviceable area. As a result the device's coverage area is increased, which benefits current systems as communication protocols still can behave close to legacy Wi-Fi communication. The observed shortcomings are expected to be resolved by further advancement of antenna technology with resulting reduction in coverage area. Thus, for directionally communicating future millimeter wave systems, two main challenges are identified.

- The *setup of highly directional millimeter wave links* is a high overhead process, which also leads to network wide interference due to the sweeping of all possible transmit directions. Due to decreased coverage area and higher directivity, more antenna configuration have to be tested, resulting in increased interference and overhead.

• *Carrier sensing*, the process of detecting ongoing transmissions, becomes less and less reliable when the signal coverage area is reduced. This effect, known as deafness problem, negatively impacts IEEE 802.11's most popular medium access scheme leading to efficiency loss and increased medium access delay [10].

To theses challenges, solutions that benefit from the variation of propagation characteristics over frequency are presented. The first mechanism leverages omni-directional communication and direction estimation capabilities in the micro-wave band to align directional high speed throughput at the mm-wave frequencies. This reduces the need for sweeping communication that is originially used in IEEE 802.11ad for direction estimation, thus reducing interference and leading to an overall throughput increase. Second, omni-directional communication at lower frequencies is exploited to improve carrier sensing in directional mm-wave networks. This resolves the deafness effects created by directional communication, reduces collision probability and ensures correct medium access behavior.

Contributions

This thesis studies the impact of frequency varying propagation behavior on IEEE 802.11 networks with a focus on the recently evolving millimeter wave Wi-Fi systems. Further, through analysis of first generation millimeter wave devices, research questions arise for the challenges of upcoming millimeter wave systems. Solutions to these questions, as well as to challenges for classic microwave Wi-Fi communication experiencing frequency varying propagation behavior, are proposed. In particular, the contributions of this thesis are as follows:

1. First, Sub-Carrier Switch Off (SSO) for Orthogonal Frequency Division Multiplexing (OFDM) modulated microwave wireless local area networks is presented. SSO addresses frequency selective behavior, which effects the transmission over a single wireless channel. As certain OFDM sub-carriers are attenuated more than others, using only a subset of possible carriers increases throughput and frame delivery rate. Further, an optimization problem for SSO is identified, namely how many sub-carriers to switch-off. Removing a higher number of attenuated carriers allows to drive the remaining ones with less robust encoding which provides higher throughput. However, data of the switched off sub-carriers has to be transmitted over the remaining ones, resulting in longer frames. A threshold based solution is derived from experimental evaluation of SSO and the performance of a dynamic SSO algorithm is shown. Unfortunately, applying SSO to millimeter wave networks is not promising, as the used directional antenna technology at these frequencies suppresses frequency varying propagation effects [16, 103]. Thus, for the strong frequency dependent propagation variations of millimeter wave enabled multi-band Wi-Fi, alternative approaches are explored.

2. Second, to the best of our knowledge the first beamforming and interference evaluation of off-the-shelf millimeter wave networks is presented. As a key finding, first generation millimeter wave systems are shown to suffer from interference through imperfect beamforming and reflections, as well as difficulties to implement omni-directional antenna patterns. The latter results in the need to sweep multiple antenna patterns with the same replicated signal for proper reception, thus increasing interference and overhead. These findings are complemented by a reassessment of the IEEE 802.11ad amendment for millimeter wave enabled multi-band Wi-Fi. Form this, next generation networks are expected to implement even stronger directionality as the vision of highly directional parallel antenna beams can not be achieved otherwise. This however complicates the communication principles for these networks. A further key observation is, that the theoretical assumption of strongly focused and side lobe free beams, found in almost all theoretical work on millimeter wave networks, has to be revalidated.

3. Third, the BBS mechanism is presented, which enhances the beamforming training process for high speed data transmissions at mm-wave frequencies. To this aim, the differing signal propagation characteristics for multi-band Wi-Fi systems following the IEEE 802.11ad amendment are exploited. As lower frequencies offer the possibility of omni-directional signal propagation, incidence angle estimation can be performed with high efficiency. The retrieved direction information is then used on mm-wave frequencies, where directional communication needs complex link setup procedures otherwise. As a result, no sweeping of probing frames into all possible directions is required, which prevents interference and breakage of parallel directional transmission. Also less overhead on the high speed millimeter wave band promises increased throughput rates, especially for mobile use cases.

4. Last, a mechanism for improvement of Carrier Sense Multiple Access with Collision Avoidance (CSMA/CA) channel access in mm-wave band Wi-Fi is proposed. This mechanism also leverages from the difference in signal propagation between microwave and mm-wave bands. As directional high throughput communication lacks efficient ways of sensing the usage of a channel, unfairness is introduced in a network. By exploiting omni-directional propagation at lower frequencies for multi-band traffic flow coordination, significant fairness improvements can be achieved. Also link initialization frames that are transmitted in vain to already transmitting stations are prevented removing interference into directions differing from established directional links.

Part I

Adapting IEEE 802.11 to Intra-Channel Propagation Variations

The first part of this thesis focuses on improvement of IEEE 802.11 networking by leveraging from frequency varying propagation behavior at the intra-channel level. The contribution presented in this part is a feed-back mechanisms that enables fine grained adaptation to the experienced channel variations. The level of adaptation is beyond the one found in current commercial communication systems while the required signaling overhead is negligible. Further, this part of the thesis is divided into two chapters. First, a background chapter explains the fundamentals of the presented intra-channel optimization. This chapter also forms the basis for Part II of this thesis that focuses on multi-band millimeter wave Wi-Fi, as these systems build on the IEEE 802.11 networks described in the following.

Frequency varying signal propagation behavior can be observed at two levels. First, significant difference can be found between widely separated frequency ranges in the order of multiple hundred MHz or even GHz. These differences mainly results from free space attenuation, described in Section 1.1.1 and 1.1.2, and differences in material reflection and transmission properties (see Section 1.1.3.1). Second, multipath propagation can lead to frequency varying behavior at a much smaller frequency scale. This can lead to diverse effects on the frequency resources used by a single device for one cohesive transmission, which is referred to as the *intra-channel* level in the following. Multipath propagation, described in Section 1.1.3 results from a signal's interaction with objects in the vicinity of transceivers, leading to multiple copies of a signal overlaying at the receiver.

This part of the thesis focuses on the adaptation of IEEE 802.11 systems to intra-channel propagation variations caused by multipath. These variations result in varying signal reception qualities in terms of amplitude and phase as described in Section 1.1.3.4. High throughput IEEE 802.11 systems identify these variations through a channel estimation preamble prepended to every transmission as described in Section 1.4.1, and perform basic channel equalization (see Section 2.1.2). The presented adaptation mechanism targets IEEE 802.11 systems that rely on an OFDM Physical Layer (PHY-layer). In-depth background information about the PHY-layer definition of IEEE 802.11 and OFDM modulation are given in Section 1.4. The basic principle of OFDM is to separate the used channel in multiple smaller frequency blocks to realize multiple transmissions, parallel in frequency, with lower transmit speed. The parallel transmitted signals on these sub-divided resource blocks are also known as sub-carriers.

The presented improvement for IEEE 802.11 networks is called Sub-Carrier Switch Off. It identifies sub-carriers with low signal quality and disables them, transmitting the excessive data from switched off sub-carriers through the remaining strong sub-carrier. While this mechanism has been mentioned by other works before [72, 73] and [24] it has not been considered to be an independent mechanism but as a borderline case for more complex mechanisms that also require higher amount of signaling overhead. We find from the experimental evaluation, presented in Section 2.3 that SSO can achieve significant throughput and link robustness increases by it self. Further, we present an optimization problem that SSO needs to solve to balance between longer transmission length through sub-carrier switch off and higher throughput encoding on the

remaining sub-carriers. From the experimental evaluation, a threshold based solution to this optimization problem is derived that leads to a dynamic SSO algorithm, which is experimentally shown to select configurations close to the optimum on arbitrary channels.

SSO proves that fine grained adaptation to the frequency varying behavior of wireless systems on the intra-channel level is a profitable approach. It also points to additional research directions that promise to yield further potential at the intra-channel level. With the upcoming consumer millimeter wave technology, multi-band Wi-Fi devices can access frequency resources with strong frequency varying behavior. These systems, which are studied in Part II of this thesis, promise even higher potential for leveraging from said behavior. The SSO mechanism itself is however not suitable for these device class. As highly directive antenna technology is used for millimeter wave systems, much smaller multipath impact is expected. The intra-channel variations, central for SSO, are thus not as strong on millimeter wave frequencies [16, 103].

Chapter 1

Background on IEEE 802.11 Communication

This chapter summarizes the relevant background for Part I of this thesis which details on adaptation to frequency varying propagation behavior at the intra-channel level. First, a brief introduction into the most relevant signal propagation effects is presented, that lead to frequency varying behavior of wireless transmission. Second, an introduction to the IEEE 802.11 standard is given, which is subject to improvement in this thesis. The IEEE 802.11 standard is presented with respect to its standardization history as well as general network and channel architecture followed by a description of its PHY and Medium Access Control Layer (MAC-layer) features relevant for this thesis. The background information given in this chapter also forms the basis for the description of millimeter wave enabled multi-band IEEE 802.11ad networks that are discussed in Part II of this work.

1.1 Radio Wave Propagation

Radio communication has formed the foundation for several technologies, that have revolutionized the society throughout the 20th and 21th century. While the speed of evolutionary steps for wireless communication systems has steadily increased, their basic physical principles remain the same. Every radio communication system emits electro magnetic waves from a transmitter towards a receiver. At both devices, antennas are used to convert between an electric signal and electromagnetic waves. While these waves propagate towards the receiver, they interact with obstacles and spread out over space. Thus, they experience several propagation effects, as for example, attenuation, reflection, refraction, diffraction and scattering. In this section the basic effects, that are relevant for the topics described in this thesis, are explained.

1.1.1 Free Space

When propagating through free space from an isotropic antenna (i.e. uniform radiation into all three dimensions of space), an electro magnetic wave gets attenuated. This results from the fact, that the originally transmitted energy P_t is spread over the complete area covered by the wave. According to the Friis free space equation [77] the received power P_r at a distance d from the transmitter can be formulated as in Equation 1.1. Hereby, L is a system loss factor, related to effects in the transmitter and receiver devices and λ the wave length of the transmitted signal. The wavelength is related to a signal's frequency f as shown in equation 1.2, with c being the speed of light.

$$P_r(d) = \frac{P_t \lambda^2}{(4\pi)^2 d^2 L} \tag{1.1}$$

$$\lambda = \frac{c}{f} \tag{1.2}$$

Eq. 1.1 points to an important insight with respect to this thesis. The received signal power in free space scales with the frequency of a transmitted signal. Thus, lower frequencies suffer less attenuation than high frequencies, making low frequency communication especially attractive for long distance communication. The increased attenuation with frequency results from the reducing antenna aperture A_e, which is the antenna's perpendicular area to the received radio wave. The antenna aperture for an isotropic antenna scales with the wavelength as shown in equation 1.3.

$$A_e = \frac{\lambda^2}{4\pi} \tag{1.3}$$

Figure 1.1 depicts the free space attenuation over distance for various frequencies. It can be clearly seen that the frequency can induce a major attenuation difference at the same distance. E.g. while transmissions at 2.4 GHz experience an attenuation of -60 dB at a distance of 15m, transmissions at 60 GHz suffer almost -30 dB more attenuation. In contrast, frequencies at 2.412 GHz and 2.462 GHz, corresponding to Wi-Fi channel 1 and 11 show almost negligible attenuation differences. To account for practical antennas, equation 1.1 is generalized to include varying gain for transmitter G_t and receiver G_r leading to equation 1.4 (see e.g. [77]). An antenna's gain depends on its effective aperture A_e can be described as in equation 1.5.

$$P_r(d) = \frac{P_t G_t G_r \lambda^2}{(4\pi)^2 d^2 L} \tag{1.4}$$

$$G = \frac{4\pi A_e}{\lambda^2} \tag{1.5}$$

1.1.2 Atmospheric Absorption

A second attenuation effect that varies with frequency is atmospheric absorption. Figure 1.2 shows the attenuation in excess of free space attenuation due to atmospheric components. Notable peaks in the attenuation are observed, that result from absorption by specific molecules

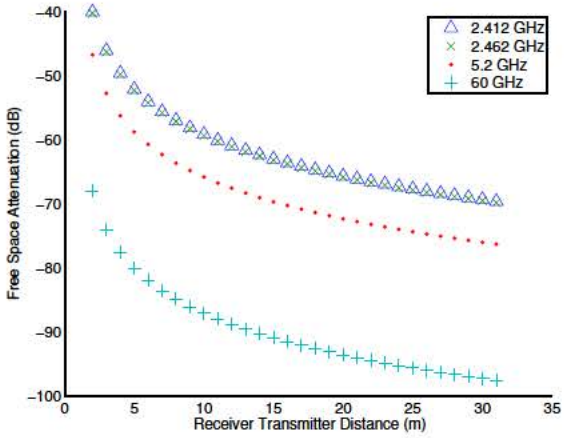

Figure 1.1: Free space attenuation at different frequencies for isotropic transmitters.

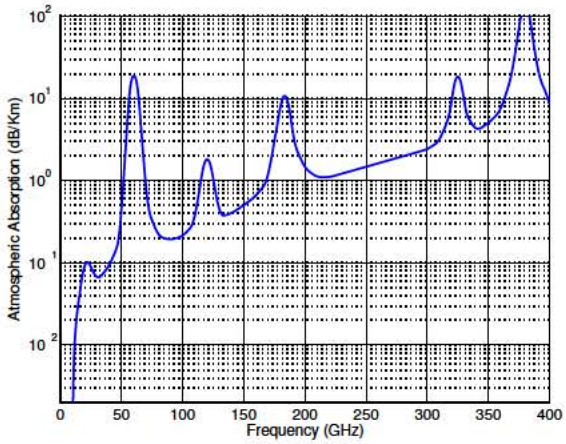

Figure 1.2: Attenuation due to atmospheric absorption.

in the atmosphere. The peaks at 22 and 60 GHz are e.g. caused by absorption from oxygen (O_2) respectively water vapor (H_2O). As the amount of molecules in the atmosphere reduces with height, the given numbers are valid from sea level up to 1 km of altitude. Further details can be found in [78].

Equal to free space attenuation, the atmospheric absorption curves show, that low frequency electro magnetic waves are to be preferred for long range communications. For higher frequencies, especially those matching the absorption frequency of certain atmospheric molecules, the additional attenuation sums up over distance, reducing the reception area. While this is a drawback for long range communication, it can be beneficial for short range communications. Due to the increased attenuation, signals from interfering transmissions are severely limited in range, allowing for frequency reuse.

1.1.3 Multipath Propagation

For almost every real world propagation scenario, assuming simple free space propagation through an atmosphere neglects important propagation effects. This is even the case if a clear line of sight exists. Especially in indoor scenarios, the transmitted electromagnetic waves interact heavily with obstacles in the vicinity of receiver and transmitter. Several effects lead to the replication of the signal, resulting in multiple copies of the same signal to overlay at the receiver. This phenomenon is very well known as multipath propagation. The most important effects that create multipath are explained in the following. A result of multipath propagation are highly fluctuating wireless channel variations, also known as small-scale or frequency selective fading. This effect is explained at the end of this section.

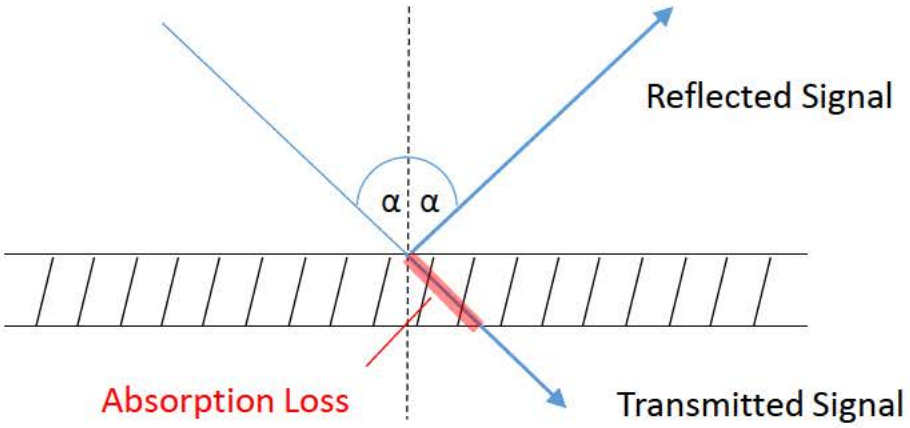

Figure 1.3: Electro magnetic wave reflection.

1.1.3.1 Reflection

The environment of radio communication systems typically entails objects that impact the propagation behavior of the emitted electro magnetic waves. One of the most important caused effects is reflection. Reflection will occur whenever a radio wave impinges on the boundary between two media with different electrical properties that is significantly larger then the wave length [77].

The effect of radio wave reflection equals the commonly known reflection of light, thus an incoming wave front is reflected under an angle equal to the incidence angle (see Figure. 1.3). For real world materials however only a part of the incoming energy is reflected while another part is transmitted and partially absorbed. Hereby, the ratio between transmission, reflection and absorption is typically expressed with respective coefficients, stating each effect's ratio with respect to the incidence energy. Every coefficient varies with reflecting material, incidence angle, polarization and frequency of the reflected electro magnetic wave. Examples for variations in reflection coefficients between 17 and 60 GHz can be found in [76]. A comparision of transmission coefficients between 5 and 41 GHz is given by [14]. A precise prediction of the reflection property in complex indoor scenarios is therefore very challenging. However, materials with electric properties close to a perfect conductor (e.g. metallic objects) show improved reflection behavior, and can generally be assumed to be strong electromagnetic wave reflectors. Further details about electromagnetic wave reflection can be found in [77].

1.1.3.2 Scattering

Scattering is a further important phenomenon, that impacts radio wave propagation in non isolated environments. It is strongly related to reflections, but caused by much smaller obstacles that do not behave like proper reflectors. These objects, which are in the size of the wave length or smaller, remit the impinging wave, but under an angle uncorrelated to the incidence angle (see Figure. 1.4).

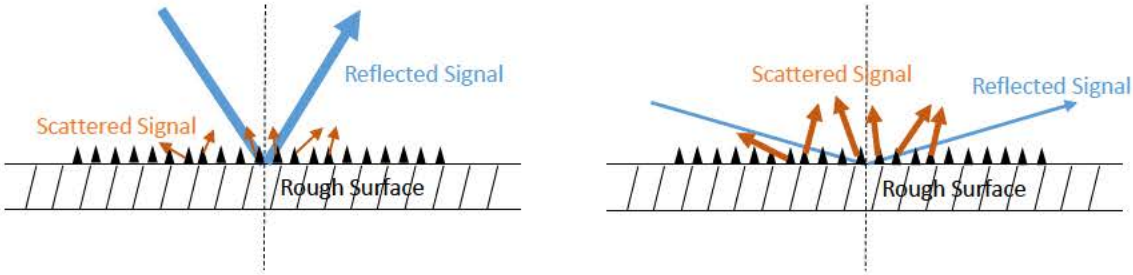

Figure 1.4: Elector magnetic wave scattering.

Scattering can have significant impact on the reflection behavior of a surface. When a surface is rough, part of the otherwise reflected signal is scattered instead, leading to a weaker reflection. At the same time, randomly scattered signal energy can illuminated regions, otherwise are not hit by reflections.

As the random scattering behavior is hard to predict, it is usually not explicitly described when modeling radio propagation. Instead, the reflection coefficient of a surface is multiplied by a scattering loss factor depending on the roughness of the surface [77]. To this aim not only the size of irregularities in the surface has to be considered but also the incidence angle of the radio wave. A steeper incidence angle increases the scattering effect of the irregularities.

1.1.3.3 Diffraction

Diffraction is a further major propagation principle that occurs whenever a radio wave is blocked by an obstacle with a sharp edge. Under this condition, instead of being completely blocked by the obstacle, an electro magnetic wave is diffracted around the edge into the shadowed region behind the obstacle. An example is shown in Figure 1.5.

A theoretical model, that can explain the diffraction behavior, was developed by Huygens in 1678 and is well known under the name Huygen's principle. Its key idea is that every point of a wave front can be considered as a secondary point source for the wave [77]. However, when blocking certain points of a wave front, the overlay of the remaining point sources does not lead to an undisturbed continuation of the wave front. Instead, the signal from the remaining secondary point sources will propagate into the space blocked by the obstacle (see Figure 1.5). The amount of diffracted energy depends on the phases of the wave fronts which pass the obstacle as well as the blocked signal parts. Thus, the exact behavior of multi diffraction that frequently occurs in indoor propagation scenarios is hard to predict. Its impact however becomes more significant at obstacles close to the direct path between a receiver and transmitter. Also, as a rule of thumb, lower frequency transmissions experience stronger diffraction [77].

1.1.3.4 Small-Scale Fading

The aforegoing propagation effects lead to the creation of multiple copies of a transmitted radio signal in non isolated propagation environments. Multiple of these copies travel over dif-

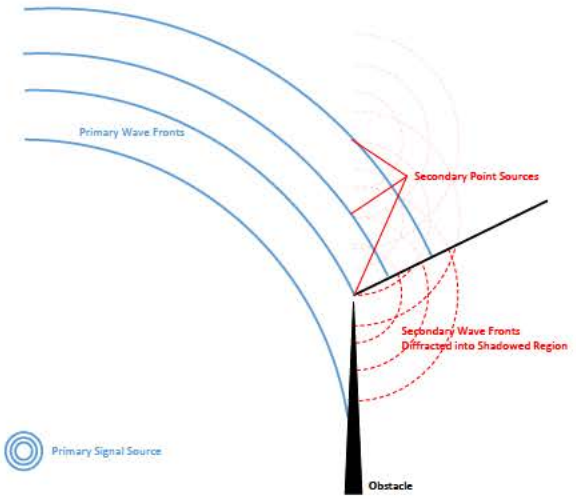

Figure 1.5: Elector magnetic wave diffraction.

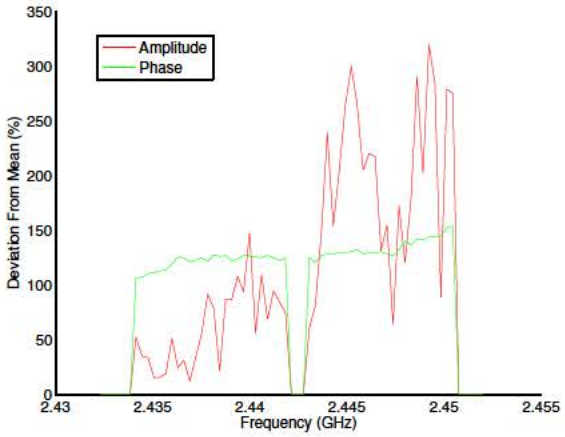

Figure 1.6: Channel state measurement for an IEEE 802.11a transmission on Wi-Fi channel 6.

ferent paths towards the receiver, each arriving with unique delay, phase shift and attenuation. At the receiver several of these copies overlay, which leads to constructive or destructive interference depending on the respective phase offsets. Further, due to mobility in the environment, the multipath scenario varies over time.

Mathematically, the impact of multipath propagation can be described by a series of attenuated and phase shifted impulses, each corresponding to one of the received signal copies. Equation 1.6, as found in [77], sums up N signal copies that overlay at a receiver at time t and represents a formulation to represent the multipath behavior of a wireless channel. Hereby, $a_i(t,\tau)$ is the individual attenuation of every multipath component and $\tau_i(t)$ is its propagation delay relative to the first received signal, also known as excess delay. The term $2\pi f_c \tau_i(t))$, with f_c as the signals frequency, describes the phase shift due to free space propagation and $\phi_i(t,\tau)$ any additional phase shift encountered on the traveled path. $\delta(\tau - \tau_i(t)$ discretizes the impulse response into excess delay bins with equal size $\Delta\tau$ with $\tau_i = i\Delta\tau$

$$h\left(t,\tau\right) = \sum_{N-1}^{i=0} a_i\left(t,\tau\right) e^{j(2\pi f_c \tau_i(t) + \phi_i(t,\tau))} \delta(\tau - \tau_i(t)) \tag{1.6}$$

The multipath representation as given by Equation 1.6 is widely known as the channel impulse response, as it is also observed at the receiver upon transmission of an infinite impulse from the transmitter. When convoluted with a transmitted signal $x(t)$ the received signal $y(t)$ can be determined using the impulse response as in Equation 1.7.

$$y(t) = \int_{-\infty}^{\infty} x(\tau) h(t,\tau) d\tau \tag{1.7}$$

From Equation 1.6 it can be seen that the multipath behavior depends on the frequency of the signal. This leads to significantly different channel responses for different input frequencies

in terms of attenuation and phase. Over the frequency range of a band pass signal this causes frequency selective fading. Practical systems have to address these differences that vary considerably depending on the dynamics of the propagation scenario. When not addressed, frequency selective fading results in significant distortions in the received signal. An example for the attenuation and phase variations introduced by a indoor multipath channel are shown in Figure 1.6. It can be seen that phase and amplitude vary significantly over the channel average. The gap for both measurements at the center frequency of channel 6 is not due to strong attenuation but results from the fact that this range is not used for signal transmission. At this frequency range, the transceiver architecture requires the signal to be filtered.

1.2 IEEE 802.11

IEEE 802.11 is the most popular protocol family for wireless local area networks and widely adopted by industry. The 802.11 standards are developed by the IEEE LAN/MAN Standards Committee, with the first version of the standard released in 1997. From there on, several amendments to the standard have been ratified to introduce new features as well as maintain previous parts of the standard. 802.11 defines a set of media access control (Medium Access Control (MAC)) and physical PHY-layer specifications, that ensure interoperability between devices following the standards.

This thesis addresses the improvement of IEEE 802.11 compatible WLAN networks. Thus, this section addresses the key aspects of the 802.11 communication standard, relevant for the understanding of the thesis. First, a general overview of the standardization history together with a description of the used frequency resources is given. Then, the basic network architectures defined by the 802.11 standard are explained. Finally, an overview of the PHY and MAC-layer specifications is given, with a focus on the OFDM PHY-layer, which is subject to improvement in Chapter 2.

1.2.1 Standardization History

IEEE 802.11 has significantly evolved over time, adding new communication features and adopting addition frequency ranges not specified by the initial standard. In the following an overview of the significant evolution steps is given.

The initial standard [31] defined two PHY-layers operating in the license free ISM frequency band at 2.4 GHz. The two PHY-layers used frequency-hopping spread spectrum and direct-sequence spread spectrum modulations supporting throughput rates of up to 2 Mbps. While this version of the standard was not very popular, it was quickly superseeded by the IEEE 802.11a [32] and 802.11b [33] amendments in 1999, which became widely adopted. 802.11a added a PHY-layer definition for OFDM modulation at the 5 GHz ISM band and increased throughput rates to 54 Mbps. The 802.11b amendment continued using the 2.4 GHz frequency, but increased throughput rates to 11 Mbps by application of Complementary Code Keying (CCK) modulation.

As the propagation range at 2.4 GHz is higher compared to 5 GHz and also higher connection reliability is provided, 802.11b became the more popular amendment among the two. Finally, in 2003 the 802.11g [34] amendment defined OFDM PHY-layer operation with up to 54 Mbps throughput also for the 2.4 GHz frequencies.

In 2007 an updated standard [36] was ratified, that merged the formerly mentioned documents together with several maintenance amendments, making the original documents obsolete. Among the maintenance amendments, particularly IEEE 802.11e [35] deserves to be highlighted, as it introduced advanced quality of service mechanisms at the MAC-layer. The next important evolutionary step took place in 2009 with the IEEE 802.11n [37] amendment. It introduced MIMO techniques to the IEEE 802.11 PHY-layer and added a new channel aggregation feature allowing 802.11n compliant devices to use up to twice the bandwidth as before. Also, a modification to the MAC-layer introduced frame aggregation and significantly reduced the per frame overhead, overall leading to increased throughput of up to 600 Mbps. IEEE 802.11n was super seeded in 2014 by the 802.11ac [40] amendment, which further increases the performance introducing higher MIMO degrees (up to 8 parallel streams), channel aggregation up to 160 MHz, Multi-User Multiple Input Multiple Output (MU-MIMO) and beamforming. At the time of writing, the first high end Wi-Fi products compliant with the IEEE 802.11ac specification, supporting throughput rates of up 1.7 Gbps, are commercially available.

In parallel to the 802.11 main development branch targeting the 2.4 and 5 GHz bands, several amendments introduce novel PHY-layers for different bands. This development has recently accelerated with 802,11ad, af, ah and aj, that target a broad range of new frequency resources, from coexistence with TV transmissions below 1 GHz to transmission in the 45 and 60 GHz millimeter wave bands. Further details about the evolution of the IEEE 802.11 standard can be found in [18–20].

1.2.2 Channelization and Frequency Bands

For radio communication, typically a base band signal with a given frequency bandwidth is modulated onto a carrier frequency before transmission over the air. The amount of information which can be transmitted with a signal depends on its bandwidth and the signal to noise ratio at the receiver. This relation can mathematically be calculated according to the Shannon theorem [77]. The benefit of modulating a base band signal onto a carrier frequency lies in the fact that it can be transmitted on different regions of the frequency spectrum. This allows to modulate several signals onto different carriers without their bandwidth overlapping and thus parallel transmission of multiple signals over the same medium. Otherwise, if signals overlap in frequency and time they sum up at the receiver and distort the final reception, an effect called interference.

In order to prevent interference, the frequency spectrum is managed by national regulation agencies. For example in the United States the FCC is in charge of this task, the respective entity in the United Kingdom is the office of communications (Ofcom) and in China the Ministry of Information Industry (MII). To homogenize the use of frequency spectrum superordinate institutions

like the international telecommunication union (ITU) or European telecommunications standards institute (ETSI) issue recommendations to the national entities. Certain frequency ranges (also called frequency bands) are hereby assigned to specific use cases and users. These differ widely, including for example commercial use cases (e.g. cellular networks), scientific usage (e.g. radio astronomy) or military applications. While licensing a frequency band is an effective way to prevent interference, acquiring it is cumbersome and expensive.

As an alternative, certain frequency bands are assigned for unlicensed use. This opens the way for inexpensive wireless consumer devices, which do not require the manufacturer to spend high amounts of money on frequency licensing. Unlicensed frequency bands also enable wireless communication systems deployed by small institutions incapable of obtaining a licensed frequency block. Particularly popular unlicensed frequency blocks are the ISM bands around 2.4 and 5 GHz. As a drawback, communication on these frequencies always has to expect unforeseen interference from other users. It is further important to highlight that the users of unlicensed frequency resources do not necessarily use the same communication protocols. In case of different communication systems working in the same frequency range, inter-system interference problems arise. These are especially severe, as coordination among users with different communication behavior is difficult and time sharing the channel resources may fail.

The popular IEEE 802.11 amendments operate on the 2.4 and 5 GHz ISM bands, which are further subdivided into several channels. Separation into channels allows multiple Wi-Fi users to transmit at the same time by using different frequency resources. At the 2.4 GHz band, however, the channels partially overlap, resulting in remaining interference effects between adjacent channels. Overall, the 2.4 GHz band has 14 channels between 2.412 and 2.484 GHz, with three non overlapping channels. At the 5 GHz band, significantly more frequency resources between 4.980 GHz to 5.825 GHz are available. However, this spectrum is undergoing widely differing national regulations, prohibiting the use of several channels depending on the region and also requiring dynamic frequency selection and transmit power control adaptation at many channels. The last two methods are required to minimize the interference impact on coexisting communication systems.

To increase throughput, the popular amendments 802.11n and 802.11ac propose a channel bonding feature. This technique combines multiple channels for transmission of wider bandwidth signals. Bonding channels does not only benefit the throughput rate because of the increased bandwidth but also because mandatory frequency guard intervals between the smaller channels can be used for data transmission instead [17]. While 802.11n supports only bonding of two channels resulting in 40 MHz signal bandwidth, 802.11ac relaxes this limit up to 160 MHz and allows bonding of non consecutive channels [3, 40]. Usage of bonded channels however still increases the load on the available frequency band, thus leaving less channel resources for other devices. Also, for the use of channel bonding, the channel resources have to be idle at the same period of time, which can lead to inefficient channel usage in combination with legacy devices [65].

1.2.3 Network Structures

In its basic definition, IEEE 802.11 allows two different network architectures. These differ by the existence of a so called Access Point (AP) that is responsible for management of a set of communicating stations. When an AP exists, a set of nodes communicating with coordination by the AP is called infrastructure based Basic Service Set (BSS). This may not be confused with an Independent Basic Service Set (IBSS) which is a set of nodes that communicate directly, without an access point. The IBSS network architecture is also known as ad-hoc network.

In infrastructure mode, the AP is among other tasks responsible for announcement of the network and time synchronization. To this aim, a beacon frame is transmitted at certain time intervals. Stations that receive the beacon frame and wish to join the network have to associate with the AP first. After that, all communication between stations is relayed by the AP, which resolves the hidden terminal problem [102] for nodes in the network but also reduces throughput by half, as every frame is transmitted twice.

In IBSS mode the stations themselves are responsible for network announcement and time synchronization. To this aim every node tries to transmit a beacon frame with a slight random time offset around the beacon timing given by the beacon frequency. The node with the earliest beacon transmission time will effectively announce the network while all other nodes overhear the frame and refrain from their transmission. Despite the higher throughput of the ad-hoc network structure because of direct frame transmission without relaying by the AP, the infrastructure mode has become by far more popular.

In addition to the two basic network architectures the more complex structure of interconnected infrastructure BSS is also characterized by the IEEE 802.11 standard. Many of the details regarding the implementation of these architectures are however implementation dependent and not specified by the standard. The architecture of multiple BSS that are connected via cabled APs is known as an Extended Service Set (ESS).

1.3 MAC-Layer

In this section aspects of the IEEE 802.11 MAC-layer, that are relevant for the understanding of this thesis are explained. The purpose of the MAC-layer is to organize multiple stations in a network to exchange data in a non interfering manner. This includes several aspects, from frame addressing (each transceiver has its unique MAC-address) over rules to share the medium (medium access schemes), to special frame exchanges to manage the network. In an IEEE 802.11 network, the last point for example comprises association in an infrastructure network or negotiating quality of service parameters.

1.3.1 Medium Access Techniques

The IEEE 802.11 evolution stages until the release of the 802.11-2007 standard support two different medium access schemes. These are CSMA/CA and polling based access with a central controller. The first technique is described by 802.11 under the name Distributed Coordination Function (DCF) while the later is referred to as Point Coordination Function (PCF). In addition to CSMA/CA access, an optional protection frame exchange is defined which is especially effective against the hidden node problem [91]. However, the only access mode, that received wide spread popularity was the CSMA/CA approach. Both other techniques incur additional overhead that is only justifiable under specific traffic conditions.

With the addition of the IEEE 802.11e amendment to the 802.11-2007 standard, additions to the original access methods have been defined, that enable quality of service (QoA) [52]. First, the Enhanced Distributed Coordination Function (EDCF) improves the Distributed Coordination Function (DCF) access, allowing prioritization of frames. Also definition of different Traffic Categories (TCs) is supported, resulting in different sized shares of the available channel resources being allocated to each TC. Second, the Hybrid Coordination Function (HCF) extends Point Coordination Function (PCF) coordinated channel access, also allowing traffic categories to prioritize certain types of traffic. Further, the Hybrid Coordination Function (HCF) allows stations to broadcast the state of their packet queues and the controller to modify the polling strategy according to a station's load and traffic type. In the following section the basic MAC techniques defined by IEEE 802.11 are explained.

1.3.1.1 DCF

802.11 defines CSMA/CA access with exponential backoff, where coordinated access of the shared medium is reached through stations sensing the medium to be idle before transmission. By choosing random backoff times after every frame transmission an alternation between the transmitting nodes can be reached, which leads to a coordinated shared medium access without a central controller. The steps that every node follows when transmitting a frame according to DCF access are as follows:

- **Backoff Procedure.** Every node maintains a backoff interval, from where it draws its waiting time to initialize its backoff counter. This counter has to decrease to zero before the next transmission is attempted. The backoff interval is defined as the range from one to the nodes current maximum backoff which changes depending on successful or unsuccessful transmissions. When currently in backoff state, a node senses the channel for other frame transmissions. If the channel is found to be idle, the node reduces its backoff counter on a time slot basis. The uniform slot length varies over the different 802.11 amendments. When another frame is overheard, its length is decoded from the PHY header and decreasing the backoff counter is paused for the duration of the frame plus a DCF Inter Frame Spacing (DIFS). This process is also known as virtual carrier sensing.

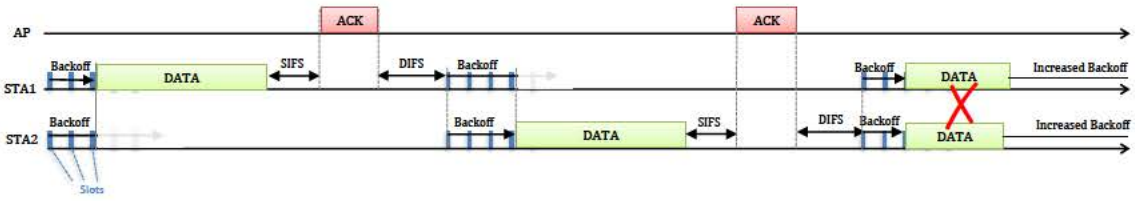

Figure 1.7: IEEE 802.11 DCF operation.

- **Transmission.** When a node's backoff counter expires, it attempts to transmit a frame. For this it first physically senses the channel to be idle, i.e. comparing the energy level of the medium against a threshold. In case the channel is found to be busy, the node returns into the backoff state and doubles the size of its maximum contention window. Otherwise, the transmission is performed and the station waits a Short Inter Frame Spacing (SIFS) time for an acknowledgment by the receiver. If the acknowledgment is received, the station resets its maximum contention window to the initial value defined by the 802.11 standard. Otherwise, the maximum contention window is doubled and the station returns into the backoff state to wait and retransmit the frame.

- **Acknowledgment.** Whenever a station receives a frame addressed to it, it checks the content of the received frame using the added Cyclic Redundancy Check (CRC) sum. When the frame is found to be error free, it answers the frame with an acknowledgment frame. Between the end of the data frame and the acknowledgment, the station waits for a SIFS. As the SIFS is shorter than the DIFS no other station following the DCF will try to obtain the channel between data and its corresponding acknowledgment. The acknowledgment frame thus has a higher priority on the medium.

An example for DCF access is shown in Figure 1.7. Two stations attempt to transmit data frames to the AP of an infrastructure BSS. At the beginning, both stations initialize their backoff counter with a random value from their backoff interval, with station one waiting two slots and station two waiting 5 slots. Station ones data transmission is overheard by station two, which in turn defers and stops its counter. After the first data frame is acknowledged by the AP and a DIFS interval has passed, both stations resume backoff with station reinitializing its backoff counter to 5 and station two resuming its remaining 3 slots waiting time. This time station two wins contention and successfully exchanges data with the AP. As can be seen, an alteration in transmitting stations is reached due to the virtual carrier sensing that continuously reduces the back off timer of stations, unsuccessful in winning contention. Finally, both data transmissions collide, as both stations' backoff counter has the same value. As a result, both stations increase their maximum contention window and have higher chances to initialize their backoff counters with a high value. This in turn reduces the risk of further collisions.

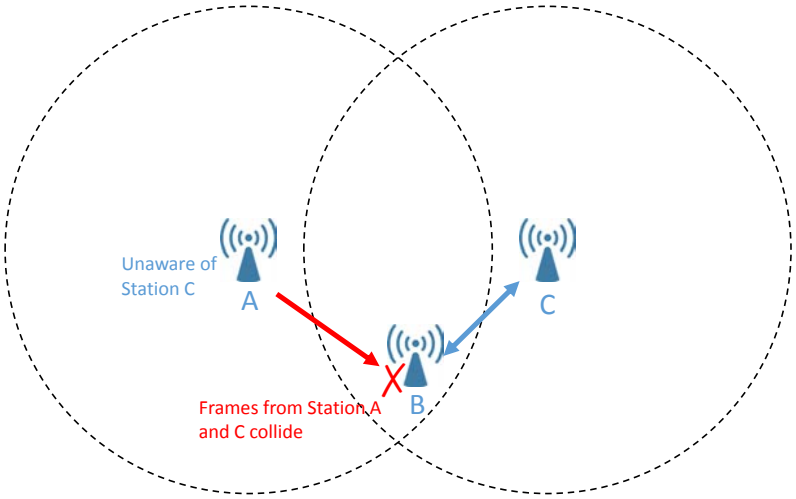

Figure 1.8: Hidden node problem.

1.3.2 Hidden Node Problem

A common problem in CSMA/CA networks is the interference between nodes that are not in communication range but are received by a third station. This phenomenon is known as the hidden node problem [91] and is depicted in Figure 1.8. The IEEE 802.11 standards propose an optional collision avoidance mechanism to protect wireless communication against the hidden node problem. Therefore, the twofold message exchange between two stations (data and acknowledgment) is expanded, adding Ready To Send (RTS) and Clear To Send (CTS) messages before the data transmission. Both frames inform about the upcoming data frame and ensure that stations out of the reception area of one of the stations receive the information. All stations will thus refrain from using the medium throughout the following transmission except for the two stations engaged in the data exchange. Further, in case of the RTS colliding with a hidden interferer, the loss of the short RTS frame wastes less channel time compared to the loss of the entire data frame.

The RTS/CTS exchange has not gained much popularity in IEEE 802.11 networks, because of two reasons. First, it implies additional per frame overhead that reduces overall network throughput. Especially for small data frames the overhead created by RTS and CTS frames often is excessive. Further, IEEE 802.11 networks operation in infrastructure mode already reduces hidden terminal situations between nodes in the network. This is due to the fact, that the AP relays every frame that is to be transmitted between two stations. As every connected station is in the reception area of the AP no hidden terminal situation can arise. Thus, hidden terminal issues are limited to interference from outside of the network or networks operating in the rather unpopular ad hoc network mode. The RTS/CTS exchange thus has not been widely adopted into commercial devices.

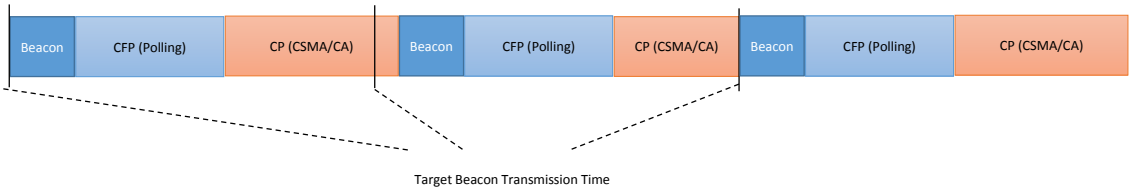

Figure 1.9: PCF beacon interval structure.

1.3.2.1 PCF

The Point Coordination Function (PCF) defined by 802.11 uses a central coordinator or Point Coordinator (PC). This station, which is usually the AP, has higher priority to access the medium and polls other stations to transmit data. The increased priority is achieved by allowing the Point Coordinator (PC) to transmit frames after a Point Coordination Inter Frame Spacing (PIFS) which is shorter than the usual DIFS. Thus, other stations do only access the medium after the PC and refrain from transmission when the PC is active.

When PCF channel access is enabled in an IEEE 802.11 network, the transmission time between transmitted beacon frames is divided into two. Directly following the beacon a Contention Free Period (CFP) is established by the PC using its prioritized channel access. During this period, stations are polled for pending frames and the PC can coordinate channel access such that stations can comply with formerly solicited delay constraints. Following the PCF a Contention Period (CP) occupies the remaining time until the next beacon. During the CP all stations can communicate according to the DCF. An example for the beacon interval structure during PCF access is shown in Figure 1.9. It can be seen, that the channel access between the beacon frames is divided between CFP and CP. Further, at the second target beacon transmission time, a station is still transmitting according to the DCF. This prevents the transmission of the beacon and delays it until the active frame transmission is finished. The following beacon thus is delayed, which also effects the following CFP and CP. While the PCF mode allows to enable basic QoS features, equally to the RTS/CTS exchange, it did not gain much popularity. This is due to several drawbacks that PCF operation brings [9]. First, additional overhead is caused when the polled stations do not have any data to transmit, as the polling request is transmitted in vain. Second, the length of the transmission of a polled station can not be controlled by the PC. This makes it difficult to comply with guaranteed QoS for other stations, as the PC can not integrate this information into its access strategy. Last, the beginning of the CFP follows directly after a beacon, which however might be delayed as it requires an idle medium. A long frame transmission at the end of the previous CP can thus result in additional delay for the next CFP which is not controllable by the PC.

1.3.3 Frame Aggregation

IEEE 802.11 communication until the 802.11-2007 standard suffered from high per frame overhead, especially for bursts of short MAC-layer payloads. In order to improve throughput performance, the IEEE 802.11n amendment added frame aggregation as an optional feature. Frame aggregation allows a transmitter to concatenate multiple frames dedicated to a single receiver to reduce per frame overhead. This reduces the number of PHY preambles and headers to just one for an aggregated frame.

Two different types of frame aggregation are enabled by 802.11n [87]. Hereby, the actual aggregation strategy is not specified, but the frame structures for both mechanisms are defined. First, MAC Service Data Unit (MSDU) aggregation allows to package multiple data chunks received for transmission from higher protocol layers. While MSDU aggregation is the more efficient mechanism (only one MAC header required), aggregated data in MSDU frames are more sensitive to noisy channels due to their length [50]. The number of aggregated MSDUss thus has to be chosen carefully to prevent costly retransmissions. Second, aggregation of MAC Protocol Data Units (MPDUs) is defined. MPDU aggregation concatenates multiple MAC payloads separated by reduced delimiters which are shorter than a full PHY preamble. While this form of aggregation causes a higher amount of overhead compared to MSDU aggregation, each MPDU is separately acknowledged in a block acknowledgement frame. In case of retransmissions this reduces the amount of repeated data to the MPDUs that were actually corrupted. Last, a mix of both aggregation techniques is possible, combining multiple MPDUs that contain aggregated MSDUs.

With IEEE 802.11ac a significant change has been introduced, requiring that every MSDU is transmitted in the MPDU aggregation format. This is even the case when only one MSDU is to be transmitted. The reason lies in the header structure which is more efficiently encoded at higher throughput rate in the MPDU delimiter than in a normal unaggregated frame [20].

1.4 PHY-Layer

The PHY-layer specification in the IEEE 802.11 standard defines the transmission of data payload provided from the MAC-layer over the wireless medium. Hereby, data from the MAC-layer is provided in chunks, which are prepared for transmission in one uninterrupted transmission, known as MPDU. For such a MPDU the PHY-layer defines the parameters for conversion into the physical signal, that is emitted onto the medium. The conversion process comprises several aspects, from scrambling the data bits over forward error correction coding to modulation and addition of preambles and PHY header information.

IEEE 802.11 defines a variety of different PHY-layer specifications using different transmission techniques and targeting various frequency bands. In the following, a general overview over the common characteristics is given. Finally, the relevant internals of the most popular PHY-layer clauses, that are necessary for the understanding of this thesis, are explained.

1.4.1 Frame Format

IEEE 802.11 networks are packet switched networks and exchange data on a frame basis. Every station encapsulate higher protocol layer payload data into frames and tries to send these whenever the medium is idle. Hereby, the mechanisms described in Section 1.3 ensure that frames do not overlap in time and interfere. A frame needs to be structured, such that a receiver with sufficient Signal To Noise Ration (SNR) can decode the transmitted data without additional signaling.

While the details of the frame design change over the evolutionary stages of IEEE 802.11, a general common structure is found. Figure 1.10 shows this structure. Overall, frames are characterized by a separation of MAC-layer data and preceding PHY-layer additions.

Each frame starts with a PHY-layer preamble needed for synchronization and frame detection. This preamble is split in two different parts, first a known preamble for timing and frame offset synchronization (SYNC) followed by a channel estimation field (CEF). The second part is not present for the original 802.11 and 802.11b amendments. Following the preambles, a PHY header is transmitted, which contains basic information about the frame which allow the receiver to decode the following payload. The most important information in this header is the signal field, which indicates the bit rate and the PHY-layer used to transmit the payload. It is followed by a service field which is reserved for future use and a length field indicating the length of the payload part of the frame. Last, the PHY header is protected against corruption by an CRC sum. The PHY header of IEEE 802.11 frames is transmitted with the most robust PHY-layer, which is the direct sequence spread spectrum described in Section 1.4.2.1. [1]

With 802.11n and 802.11ac, modifications to the preamble structure have been introduced. These modifications shorten the preamble in order to reduce the per frame overhead. In order to keep backward compatibility, parts of the preamble however were kept unchanged, allowing legacy devices to detect frames and infer their length from the PHY header. This allows the devices to detect a busy channel and reduce interference effects, even though they can not decode the full frame. For this purpose the PHY header of 802.11n and ac devices is split into two sections. One compatible with legacy devices and a second one carrying additional information needed to decode the advanced frames [71]. The PHY-layer prefix is followed by the payload which is transmitted using the data PHY-layer indicated in the PHY header. To protect the PHY payload, another CRC sum is added at the end of the payload. Further, the payload is separated into a header and the actual MAC payload, which is formed by higher layer protocol data. The MAC header depends on the transmitted frame type, which can be one out of three general groups: Management, control or data. These groups are further sub-divided, a detailed description can be found in [18, 71].

[1] An exception is found in the 802.11a amendment which only supports OFDM PHY-layers. Thus, headers are transmitted with the most robust 6 Mbps OFDM PHY-layer.

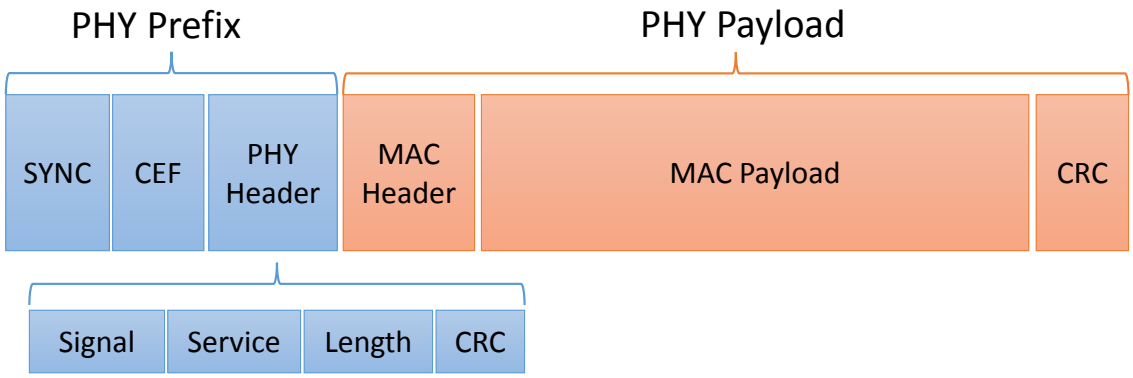

Figure 1.10: IEEE 802.11 frame structure.

1.4.2 Modulation

IEEE 802.11 defines several different PHY-layers that can be used to encode and modulate MPDUs before transmission over the air. The popular amendments for communication on the 2.4 and 5 GHz band rely on a subset of these PHY-layers that make use of 3 different modulation techniques. The initial 802.11-1997 [31] standard, relied on direct sequence spread spectrum modulation supporting throughput of up to 2 Mbps. For the follow up 802.11b [33], throughput was increased by applying complementary codes to the spread spectrum technique. From there on all following standards used OFDM. In the following an overview is given of the three modulation schemes, with focus on OFDM modulations, that is subject to improvement in Chapter 2.

1.4.2.1 Direct Sequence Spread Spectrum

The most basic modulation used for IEEE 802.11 transmissions at 1 and 2 Mbps is Direct Sequence Spread Spectrum (DSSS). DSSS modulated PHY rates implemented by 802.11 achieve transmission with high range and robust signals. Further, this modulation is used to encode the frame header of 802.11 frames that needs to be received reliably by as many nodes in the network as possible.

DSSS modulation spreads the bandwidth of a digital data signal (i.e. stream of data bits) by modulating it with a spreading sequence that has a higher frequency rate [27, 77]. In fact, this leads to a higher bandwidth used for signal transmission than is actually needed to transmit the data signal. As the amplitude of the data signal is not increased throughout this process, the spread signal has a very low amplitude close or even below the noise level. A frequency spectrum example for DSSS modulation is shown in Figure 1.11. The bandwidth of the outlined signal is inversely proportional to the fraction of data symbol length T over chip length T_c. By the use of specifically designed spreading sequences it is possible to recuperate the signal at the receiver. For this, strong autocorrelation properties of a spreading sequence are needed, that allow a receiver to restore the signal when it knows the same sequence used for transmission. DSSS modulation has a variety of properties that made it interesting for military usage, as for example

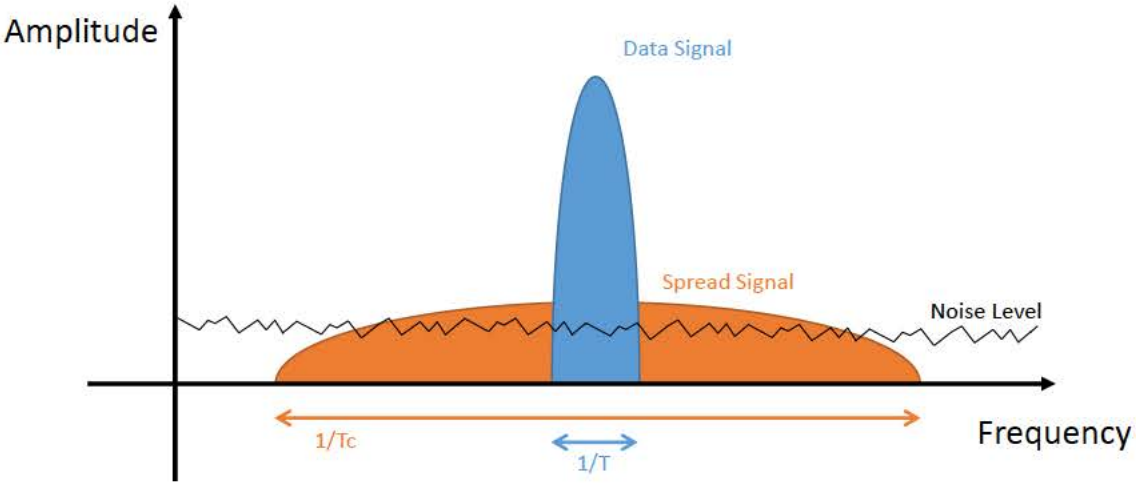

Figure 1.11: DSSS signal characteristics in the frequency domain.

its low amplitude and thus hard detectability. Further, wide spreading makes a signal much harder to be jammed. DSSS encoding also allows multiple receivers to use the same frequency resources at the same time. For this, the spreading sequences used by every transmitter need to have low correlation properties among each other. This property is used for Code Division Multiple Access (CDMA) networks to share frequency resources, which however is not considered for IEEE 802.11 communication. The reason IEEE 802.11 applies DSSS modulation is the high resilience against noise and multipath echoes achieved by the redundancy added by the spreading sequence. Together with the high autocorrelation properties, the redundancy leads to very low bit error rates of DSSS signals [93].

The spreading sequence used by IEEE 802.11 is an 11 chip barker sequences [38] with a chip rate of 11 Mchips/s. Each chip hereby is a signal change in the spreading sequence, comparable to a symbol at the data signal. As the used barker sequence consists of 11 chips, 10^6 sequences are transmitted per second, each carrying one bit of information leading to a throughput rate of 1 Mbps. The 2 Mbps modes uses two 90 degree rotated sequences in the complex signal plane at the same time, doubling the transfered information.

1.4.2.2 Complementary Code Keying

With the 802.11b amendment the set of supported PHY rates was extended by use of an additional modulation allowing transmission rates of 5.5 and 11 Mbps. The introduced modulation, complementary code keying, is an extension of DSSS explained in Section 1.4.2.1. Instead of using barker sequences, polyphase complimentary codes are used as spreading signal [69]. The advantage of these codes is that multiple sequences with strong autocorrelation properties are defined that have low correlation between each other. By selection of one of the sequences, multiple bits can be encoded in one chipping sequence. In addition, the chip length of the used complimentary codes is shorter, leading to the increased throughput of CCK modulated PHY rates.

1.4.2.3 OFDM

Current high speed 802.11 PHY-layer designs are based on OFDM modulation. OFDM has become very popular especially for a wide range of wireless communication systems including cellular networks and digital video broadcasts. In the following, the concept of OFDM is discussed, followed by details of its application in 802.11 systems.

OFDM Concept. OFDM systems place closely spaced orthogonal sub-carriers inside the frequency range of the communication channel. Usually, signals have to be spaced sufficiently far apart to allow them to be filtered properly by the receiver. Additionally, the sidebands of every carrier will overlap and corrupt signal quality if insufficient spacing is applied. OFDM circumvents these difficulties by spacing its sub-carriers reciprocal to the symbol period. With this, the sub-carriers are orthogonal to each other and do not interfere, although being placed very closely in the spectrum. The baseband representation of the OFDM signal can be expressed using the Inverse Discrete Fourier Transformation (IDFT) [43].[2]

$$\begin{aligned} x_t(n) = \text{IDFT}\{X(m+tN)\} = \sum_{k=0}^{N-1} X(k+tN)e^{j2\pi kn/N} \\ m = 0, 1, ..., N-1 \\ n = 0, 1, ..., N-1 \\ t = 0, 1, ..., \left\lceil \frac{D}{N} \right\rceil - 1 \end{aligned} \tag{1.8}$$

Here, N is the number of available sub-carriers, $X(k), k = 0, ..., D-1$ is a sequence of D data symbols to be modulated onto these sub-carriers, and $x_t(n)$ is the time domain representation of the t-th symbol, which is a series of $N-1$ consecutive samples in time denoted by n. Accordingly, m denotes the current sub-carrier in the frequency domain, with the number of sub-carriers equaling the number of time domain samples per symbol. If necessary, zero-padding is added, i.e., $X(k) = 0, \forall k \geq D$. On the receiver side, the received signal $y_t(n)$ is demodulated using discrete Fourier transformation to regain the per sub-carrier data symbols.

$$\begin{aligned} Y(k+tN) = \frac{1}{N} \sum_{n=0}^{N-1} y_t(n)e^{-j2\pi kn/N} \\ k = 0, 1, ..., N-1 \\ t = 0, 1, ..., \left\lceil \frac{D}{N} \right\rceil - 1 \end{aligned} \tag{1.9}$$

The parallel transmission structure of an OFDM systems is its key advantage. In a typical wireless channel, the received signal consists of overlapping arbitrarily delayed copies of the original message due to multipath effects. Therefore, energy from one symbol may bleed into other sym-

[2] For simplicity, we omit guard interval, packet header, and pilot carriers.

bols; this effect is known as Inter-Symbol Interference (ISI) and lowers reception quality. The parallel transmission structure of OFDM with its increased symbol duration lessens this effect, as explained in the following subsection.

In a frequency selective fading channel, the different OFDM sub-carriers may experience different channel qualities. This results in certain sub-carriers being more or less error prone. It is important to take these differences in sub-carrier qualities into account. Neglecting the higher error probability of weak sub-carriers easily leads to packet loss and hence throughput degradation due to retransmissions.

OFDM in IEEE 802.11. The 802.11a and g amendments, which defined the first OFDM based PHY-layers, are limited to single channel usage and thus a maximum bandwidth of 20 MHz. Both amendments define the same OFDM modulation parameters which result in a 16.66 MHz signal to be transmitted over a channel. The remaining 3.34 MHz separate adjacent channels from the signal. The amendments define 52 sub-carriers with a signal spacing of 312.5 KHz and a symbol duration of 4 μs. From these 52 sub-carriers, 4 are used for pilot signals, which are used to compensate for remaining frequency offsets, as well as inaccuracies introduced through clock drift between devices. Depending on sub-carrier modulation and coding, data rates between 6 and 54 Mbps are achieved.

In order to counter multipath reflection, the 802.11 OFDM PHYs define a guard interval to be added to the beginning of every OFDM symbol. The duration of this interval is 800 ns for the basic OFDM PHY-layers. Throughout the guard interval, a transmitter cyclically repeats the beginning of the ofdm signal, which does not alter the signal in the frequency range. It however allows possible reflection from the previous symbol, that arrive with a delay inside the guard interval, to settle. By discarding the signal part received during the guard interval in front of every symbol, inter symbol interference from multipath propagation can be severely reduced.

With the 802.11n and 802.11ac amendments several modifications to the OFDM PHY-layer have been introduced. For 20 MHz single channel operation, 802.11n compliant OFDM waveforms add 4 more data sub-carriers and allow optional reduction of the guard interval to 400 ns. When channel aggregation of two channels is applied, the frequency guard interval between the two channels can be used for data transmission. Further, the number of pilot symbols is set to 6 for the combined channels, resulting in 108 sub-carriers available for data transmission [58]. With 802.11ac channel bonding of up to 8 channels becomes possible and the relative number of pilot sub-carriers is further reduced. This leads to an increase in the number of usable sub-carriers to 468 [20].

1.4.3 MIMO

MIMO techniques have revolutionized IEEE 802.11 WLAN communication in terms of throughput and reliability. First introduced with the 802.11n amendment in 2009, MIMO techniques have increased throughput by a factor of approximately 30. The basic idea leading to this increase is to use multiple transmit respectively receive chains with spatially separated antennas

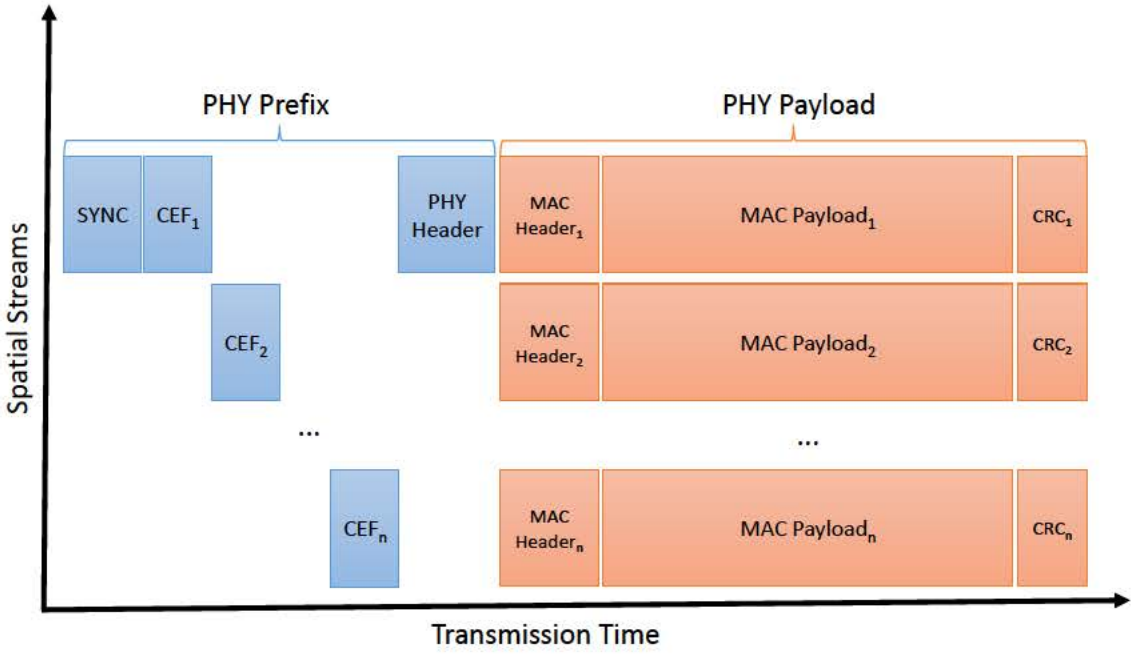

Figure 1.12: IEEE 802.11 MIMO frame structure.

at a device. While this is supposed to generate interference, multipath environments lead to heavily varying channel conditions even at relatively close by antenna locations. When sufficiently placing antennas apart from another (at least half wave length), uncorrelated channel conditions are found and the signals can be separated. In fact, one could argue, that MIMO transmissions effectively exploits the fluctuating propagation characteristics in the spatial dimension. While this is related to the concept explored in this thesis, the presented work in turn exploits the variation in the frequency dimension. I.e. it adapts to the channel state which varies over frequency or between frequency bands, while MIMO adapts to the channel state at different spatial locations.

Several different techniques have been proposed to exploit MIMO channels and several of them have been adopted by the IEEE 802.11 standard. The most popular and commonly used technique in 802.11n and ac networks is Spatial Division Multiplexing (SDM). SDM transmits several spatial streams in parallel, whereas each stream needs to be transmitted over a different antenna [5]. Hereby, 802.11n requires all streams to be transmitted between the same two devices. One of the advantages of this technique is that it does not require any kind of feedback between receiver and transmitter before transmission. Further, with sufficiently distinct channel conditions the throughput rate is multiplied by the number of supported spatial streams. For IEEE 802.11n the maximum number of streams is 4. In order to decode a MIMO transmission, the PHY preamble structure of 802.11 frames had to be modified [71]. In particular, for every spatial stream, a separate channel estimation field is transmitted (see Figure 1.12). This allows the receiver to separately measure the channel from everyone of the N transmit antennas to each of its M receive antennas resulting in a $N \times M$ channel state matrix. When inverting this matrix, it can be multiplied with the following data transmission, resulting in the N transmitted data streams [5].

In addition to SDM, further MIMO techniques have been adopted by the IEEE 802.11 standards. A technique to increase resilience of transmissions, space time block coding (STBC), was introduced by 802.11n. STBC also combines multiple spatial streams without prior feedback, however it does not increase throughput but adds resilience. IEEE 802.11ac introduces MU-MIMO [3] which allows to transmit several spatial streams with multiple devices. This however requires the receiving devices to feedback their channel state before data transmission which creates significant overhead. With the knowledge of the channel state for every receiver, the transmitter can weight (in terms of amplitude and phase) the signal transmitted from every antenna to reduce interference between the spacial streams. Further, transmit beamforming was introduced by 802.11ac. [3] Transmit beamforming also requires explicit feedback and allows the transmitter to weight every antenna's signal to increase the received signal strength at multiple receivers. In contrast to MU-MIMO, transmit beamforming does not cancel out interference between multiple spatial streams, which makes it more robust to channel state estimation errors [40]. Overall, 802.11ac severely increases the throughput, by increasing the number of spatial streams for SDM to 9 and also implementing up to 4 spatial streams for MU-MIMO which benefits low complexity receivers with low number of antennas.

[3] In fact it was already an optional part of 802.11n which however was not adopted by implementors [3, 71].

Chapter 2

OFDM Sub-Carrier Switch Off

Since the IEEE 802.11a/g amendments to the IEEE 802.11 standard, OFDM has become the most used PHY-layer modulation for high speed data transmission (see Section 1.2.1). As described in Section 1.4.2.3, OFDM divides the available frequency spectrum of a channel into several sub-carriers. These sub-carriers allow for the parallel transmission of multiple data streams with longer symbol duration compared to single channel schemes. In combination with a guard interval between symbols, this reduces Inter-Symbol Interference (ISI) and thus lowers sensitivity to complex multipath environments. Additionally, while single carrier modulation uses more bandwidth compared to an OFDM sub-carrier, the same throughput is achieved due to multiple simultaneous data streams.

In typical IEEE 802.11 indoor scenarios, the signal transmission undergoes frequency selective fading as explained in Section 1.1.3.4. As every sub-carrier is located on a slightly different portion of the frequency spectrum, varying propagation behavior results in different fading characteristics. Adapting to these frequency variations is typically done in two steps by IEEE 802.11 systems. The first step requires phase and amplitude of each sub-carrier to be measured from the channel estimation field in the frame preamble (see Section 1.4.1). This information is used to equalized all sub-carriers to a common mean amplitude and phase offset. While this is sufficient to map the transmitted signal into the quantization range of known symbols, equalization can significantly increase noise induced distortion of strongly faded sub-carriers. Demodulation of weak sub-carriers results in bit errors when their modulation is not robust enough to account for equalization exacerbated noise effects. Thus, as a second step sub-carrier modulation has to be adapted to the respective signal quality.

Adapting the Modulation Coding Scheme (MCS) on a per sub-carrier basis is one option to counter this effect. This method ensures high throughput while maintaining acceptable bit error rates but at the same time comes at an increase in transceiver complexity. In addition to the signal processing and computational overhead of such so-called loading algorithms [24], they also incur a considerable signaling overhead for the feedback of channel states and preferred MCS per sub-carrier. As a consequence, no current wireless system adapts the MCS at such a fine granularity.

WLAN as standardized by IEEE 802.11, including the most recent 802.11ac amendment, use the same MCS for each sub-carrier. Even sophisticated OFDMA based systems such as LTE only allow to adapt the MCS per user, but use the same MCS on all the sub-carriers of a given user. This however unnecessarily reduces the throughput of strongly received sub-carriers, as they are encoded with a low throughput but robust modulation coding scheme.

A simple but powerful alternative to adaptive MCS is to simply deactivate sub-carriers with severe fading. Such Sub-Carrier Switch Off (SSO) very effectively combats frequency selective fading and at the same time has much lower computational complexity and feedback overhead. Using SSO to deal with frequency selective fading has been first proposed in [73], [72] and [24]. These works investigate the merits of SSO in conjunction with power loading approaches by means of simulation.

In this chapter, we present our implementation and experimental results of SSO. SSO lowers the average bit error probability and thus increases the packet reception probability, by adapting to frequency varying propagation characteristics in a more elaborate way than any commercial wireless communication system before. However, at the same time the data that formerly was to be transmitted on the disabled sub-carriers will be appended to the remaining sub-carriers, resulting in longer packets. An efficient SSO mechanism needs to carefully balance these two effects. We design an SSO scheme that enables or disables sub-carriers with respect to the sub-carrier channel estimation. Our implementation is based on Wireless open Access Research Platform (WARP) [68], a Field Programmable Gate Array (FPGA) based software defined radio system. To the best of our knowledge, our implementation is the first to analyze the effect of SSO in an actual IEEE 802.11 style Wi-Fi system.

From our measurements we observe that SSO provides throughput gains of up to 250%. Also, we found that SSO can decrease the necessary signal strength for successful data transmission. Under certain fading conditions we noticed a difference in the necessary signal strength of up to 5 dB. Thus, we consider SSO a highly promising mechanism to improve future wireless local area networks while maintaining low complexity.

The rest of this chapter is structured as follows. A detailed description of SSO for OFDM modulated wireless systems is given in Section 2.1. In Section 2.2 we outline the experimental setup used to evaluate SSO. Then, experimental results are presented in Section 2.3. Finally, we give an overview over related work in Section 2.4.

2.1 Mechanism

SSO provides throughput gains through adequate reaction to frequency selective fading which is caused by varying propagation behavior through multipath propagation over the frequency range of the channel. It operates on the basis of sub-carriers, which are a consecutive series of frequency blocks that a wireless channel is split into when OFDM modulation is used by a wireless system (see Section 1.4.2.3). SSO shares some characteristics with adaptive modulation

and coding, however instead of choosing a different MCS for every sub-carrier, SSO just has two options: it either transmits data on a sub-carrier using the MCS chosen for the packet or it makes no use of the sub-carrier. In the latter case, data that would have been transmitted on the deactivated sub-carriers is appended to the other active sub-carriers. This lowers the throughput of the transmission as it takes more time to transmit all the payload data on the remaining active sub-carriers. At the same time, it is possible to use higher order MCSs on the active sub-carriers, while maintaining a low Packet Error Rate (PER) respectively Bit Error Rate (BER). In contrast to adaptive modulation and coding, the feedback overhead consists of only one bit per sub-carrier to signal whether it is active.[1]

The main principle of SSO is to insert a complex zero whenever a data symbol falls onto a deactivated sub-carrier. With χ as the set of deactivated sub-carriers, the base-band representation of SSO-enabled OFDM transmission can be expressed as:

$$\begin{aligned} x_t^{sso}(n) &= \text{IDFT}\{X^{sso}(m+tN)\} \\ m &= 0,1,...,N-1 \\ n &= 0,1,...,N-1 \\ t &= 0,1,...,\left\lceil \frac{D}{N-|\chi|} \right\rceil - 1 \end{aligned} \tag{2.1}$$

Hereby, the notation from Section 1.4.2.3 is used, with N being the number of available sub-carriers and X a sequence of D data symbols. Accordingly, $x_t^{sso}(n)$ is the time domain representation of the t-th symbol, having $N-1$ consecutive samples in time (denoted by n), which also corresponds to the number of sub-carriers in the frequency domain (denoted by m). The number of symbols t that are needed to transmit the complete data stream increases with the number of deactivated sub-carriers. The data symbol stream modified for SSO can be expressed as follows.

$$X^{sso}(l) = \begin{cases} X(\gamma(l)), & \text{if } l \bmod N \notin \chi \\ 0, & \text{otherwise} \end{cases} \tag{2.2}$$

Here, $\gamma(l)$ maps from a sub-carrier index in the SSO encoded OFDM transmission to the corresponding data symbol index that is to be placed in this sub-carrier.

$$\gamma(l) = l - ((\lfloor l/N \rfloor)|\chi| + |\{x \in \chi \,|\, x < l \bmod N\}|) \tag{2.3}$$

[1] For example, 802.11ac supports at most 512 sub-carriers corresponding for the maximum bandwidth of 160MHz (see Section 1.2.1), resulting in a signaling overhead of only 64 bytes. Certain of these sub-carriers are not used for data transmission and therefore do not need to be included in the signaling. In addition, this overhead can be reduced further due to the fact that neighboring sub-carriers tend to have similar channel quality, allowing for efficient aggregation of state information for neighboring sub-carriers.

2.1.1 Adaptive Sub-Carrier Switch Off

When determining χ, the set of sub-carriers to deactivate for SSO, we aim to improve transmission quality and performance. This can be seen as a optimization problem. Therefore, we formulate the packet error rate P of a SSO enabled OFDM link as follows:

$$P(M,c) = 1 - \prod_{k=1}^{N}(1 - p(M,c,h(k),w(k))) \tag{2.4}$$

Here, $p(M,c,h(k),w(k))$ is the error probability for sub-carrier k with channel $h(k)$ and AWGN noise $w(k)$, given modulation scheme M and coding scheme c. Furthermore, we define the throughput for a channel with conditions h and w as follows:

$$T_{h,w}(M,c,\chi) = b(M) \cdot r_{\text{fec}}(c) \cdot r_{\text{sso}}(\chi) \cdot (1 - P(M,c)) \tag{2.5}$$

The rate of the convolutional coder is given by r_{fec}, the reduction caused by switching of the sub-carriers in χ is $r_{\text{sso}}(\chi) = 1 - \frac{|\chi|}{N}$, and the throughput rate for modulation M is denoted $b(M)$.

The SSO optimization problem to be solved is thus to select the set of sub-carriers to switch off together with a modulation and coding scheme that maximizes throughput, given channel conditions $h(k)$ and $w(k)$.

$$\arg\max_{M,c,\chi}(T_{h,w}(M,c,\chi)) \tag{2.6}$$

2.1.2 Threshold-Based Adaptive Sub-Carrier Switch Off

For a practical solution, we simplify the general optimization problem given by Equation 2.6 by splitting the joint optimization of MCS and SSO into two separate optimization problems. On the one hand, we adapt the number of sub-carriers to be deactivated in order to increase the throughput given a MCS. On the other hand, we select the modulation and coding scheme that best utilizes the available channel. For the latter, we use one of the existing rate adaptation mechanisms, e.g., [44], [82]. When continuously running these mechanisms on a SSO enabled system, the used MCS will adapt to the deactivated weak sub-carriers by successively increasing the MCS of the remaining sub-carriers.

To decide on the quality of a sub-carrier, we make use of the channel estimation techniques of OFDM systems that are used to handle frequency selective fading. This mechanism uses part of a wireless packet's preamble to predict the channel state of every sub-carrier (see Section 1.4.1). For the decoding of the payload, every symbol transmitted on a sub-carrier is equalized based on this estimate. This is done e.g. by multiplication with the inverse channel estimate $\hat{H}(k)$ [30].

$$\hat{X}(k) = \frac{Y(k)}{\hat{H}(k)}, k = 0,1,...,N-1 \tag{2.7}$$

The influence of the multipath fading channel that causes frequency varying behavior and leads

to selective fading can be described as (see also Section 1.1.3.4):

$$y(n) = x(n) \otimes h(n) + w(n), \tag{2.8}$$

Here, $w(n)$ is the additive white Gaussian noise (AWGN) and $h(n)$ is the channel impulse response. From the equalization process given in Equation 2.7, it can be seen that the AWGN noise $w(n)$ affecting a sub-carrier is scaled by the inverse of the channel estimate $\hat{H}(n)$ in the same way as the transmitted signal. This means a low magnitude of the channel estimate (highly attenuated channel) will result in amplification of $w(n)$ during equalization. By this, even in case of perfect channel estimation and presence of AWGN noise, a low magnitude for $\hat{H}(n)$ may lead to a significant distortion in the received sub-carrier signal. For this reason we consider $|\hat{H}(n)|$ as a suitable measure for the decision whether to deactivate a sub-carrier or not.

As all the sub-carriers are independent and their error rate only depends on the sub-channel quality, they will be switched off in the order of their channel qualities. The resulting optimization problem for adaptive sub-carrier switch off of the ξ weakest sub-carriers is:

$$\arg\max_{\xi} \left(T_{h,w}(M, c, min(\mathcal{N}, \xi))\right) \tag{2.9}$$

With $\mathcal{N}$ as set of sub-carriers and $min(\mathcal{N}, \xi)$ describing the ξ weakest sub-carriers from $\mathcal{N}$. With a measure for the sub-carrier channel quality we now propose a threshold-based heuristic solution to Equation 2.9. We define a channel quality threshold τ to decide whether a sub-carrier should be added to χ. This threshold specifies the sub-carrier quality at which the loss in throughput due to deactivating the sub-carrier equals the loss introduced due to the carrier's contribution to the error rate. The value for τ is equal for every sub-carrier but is MCS dependent. Therefore, for a channel estimate $|\hat{H}(k)|$ we define as a solution to Equation 2.9:

$$\xi = |\{k, |\hat{H}(k)| < \tau\}| \tag{2.10}$$

It is obvious that SSO can not provide any gains for flat fading channels. Under this special condition, it is possible that all sub-carriers will be switched off. However, this can be easily detected and the SSO functionality could be disabled for this extreme case.

2.2 Hardware Platform and Experimental Setup

For the experimental evaluation of OFDM sub-carrier switch-off we use the Wireless open Access Research Platform (WARP). WARP provides an open source FPGA driven software defined radio platform, where the MAC and PHY-layers can be modified in software. Our work builds upon the WARP reference implementation of an IEEE 802.11a-style OFDM PHY-layer implementation that allows for real-time frame encoding and decoding.

Index	Utilization
0 (DC)	Must be empty
7,21,43,57	BPSK pilot tones
1-6, 8-20, 21-26, 38-42, 44-56, 58-63	Data Carriers
27-37	Must be empty

Table 2.1: WARP: Sub-carrier assignment.

2.2.1 PHY-Layer Structure

WARP's OFDM PHY-layer provides a 10MHz bandwidth OFDM channel that consists of 64 sub-carriers as shown in Figure 2.1.[2] When comparing to the IEEE 802.11a PHY-layer as described in Section 1.4.2.3, it can be seen that our test implementation supports less bandwidth than standard compliant devices. This however only limits the impact of frequency selective fading, as higher channel state fluctuations can be found over wider frequency spacing [73]. Out of the 64 used sub-carriers, 49 can be used for actual data transmission. The rest are assigned to the DC carrier, pilot carriers, or are left empty according to the IEEE 802.11a specification (see Table 2.1).

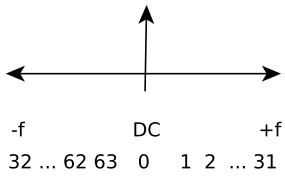

Figure 2.1: Sub-carrier allocation of the WARP OFDM PHY-layer.

The data packets generated by the WARP OFDM implementation have the packet structure given in Figure 2.2, that is similar to the one of the IEEE 802.11 protocol family as described in Section 1.4.1. It starts with a predefined preamble and training symbol sequence. These parts are needed to correct the carrier frequency offset, determine the signal strength and estimate the channel coefficients. After the training sequence follows a packet header. It is encoded with a robust MCS in order to transmit basic parameters for the packet, such as for example source and destination addresses, packet length or CRC. The rest of the packet contains the payload data. It is encoded with the full rate MCS that is a combination of one of the modulation schemes Binary Phase Shift Keying (BPSK), Quadrature Phase Shift Keying (QPSK), or 16-Quadrature Amplitude Modulation (QAM) together with rate $1/2$, $2/3$ or $3/4$ punctured convolutional coding. Additionally, the convolutional coding can be deactivated. While the base rate is fixed and known to both sender and receiver, the full rate is signaled in the packet header and can vary. Therefore, the sender can decide on a full rate MCS while the receiver adapts to it during header decoding. In our experi-

[2]Note that we use the sub-carrier numbering from 1 to 64 as given in Figure 2.1 for all sub-carrier related figures, i.e., the empty sub-carriers at the left and right border of the frequency spectrum appear in the middle of these figure.

ments we choose the WARP default MCS of QPSK with rate 1/2 punctured convolutional coding for the packet header.

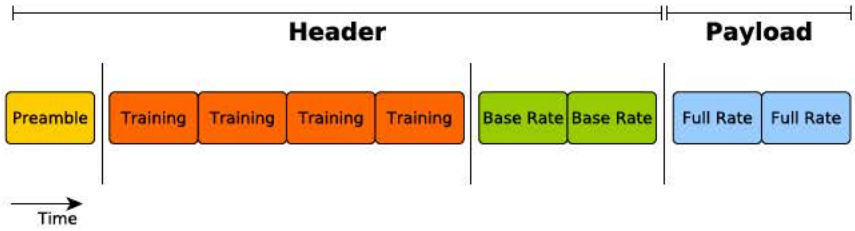

Figure 2.2: WARP OFDM PHY-layer frame format.

2.2.2 WARPnet Measurement Setup

The intended scenario for our SSO algorithm is a wireless local area network with a slowly varying, pseudo-static channel, as experienced for example by notebooks in an office that usually keep their positions for long periods of time compared to the duration of a wireless packet transmission.

For our implementation we use the WARPnet framework. One key advantage of WARPnet is the ability to transfer large amounts of measurement data from the WARP boards via Ethernet to a commodity PC system for further processing. There, data analysis can be done without the restrictions of WARP's embedded FPGA environment.

WARPnet consists of three main components: a MAC-layer running on the WARP system, data co-processors running on the commodity PC system, and a python script to configure the experiment parameters. The MAC-layer component receives control messages from the experiment control script via Ethernet to configure transmission parameters and to start and stop the packet exchange between the wireless nodes. On the receiver side, the MAC-layer sends the received data together with other measurement values via Ethernet to the WARPnet co-processors for further processing. Figure 2.3 gives an overview of the WARPnet setup. Although the WARPnet framework is very well suited for the testing of SSO, it has one drawback. WARP lacks the correction of phase offsets that arise from channel coefficient changes or sampling frequency offsets. As a consequence, the longer the duration of a packet transmission, the higher the risk that the phase offset results in packet loss. The maximum packet duration with WARP results from transmitting the maximum payload length of approximately 1400 bytes with the BPSK modulation and code rate $1/2$. To avoid the adverse effects of phase offsets, we limit the maximum number of sub-carriers that can be switched off. In our experiments, we do not switch off more than 22 sub-carriers. That means, less than half of the available sub-carriers can be switched off, which roughly doubles the packet duration. In turn, we use a payload of approximately half

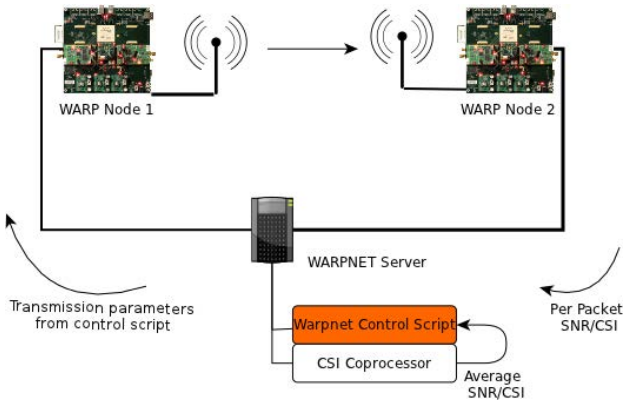

Figure 2.3: SSO experimental setup.

Table 2.2: WARP: Modulation base rates.

Modulation	BPSK	QPSK	16-QAM
Base Rate	5.72Mbit/s	11.44Mbit/s	22.88 Mbit/s

the maximum payload length for all experiments, so that the maximum packet duration remains unchanged.

The throughput of the wireless links established in our testbed can be determined by Equation 2.5. For WARP, values for the throughput base rates $b(M)$ and Forward Error Correction (FEC) throughput reduction are given in Tables 2.2 and 2.3, respectively. The packet error rate P (see Equation 2.4) is determined from the number received packets with and without payload errors, per SNR level and MCS. For the 10MHz Bandwidth OFDM implementation of WARP, throughput for the available modulations is defined according to Table 2.2. The throughput reduction due to SSO is given by $r_{\text{sso}}(\chi) = 1 - \frac{|\chi|}{49}$.

2.2.3 Measured Values

To evaluate SSO performance we use WARPnet to collect PHY-layer information for further analysis. This information can be separated into two groups:

- Transmission quality measures
- Channel state information

Table 2.3: WARP: Throughput reduction due to FEC.

Puncturing	1/2	2/3	3/4
Reduction Factor	0.5	0.67	0.75

Transmission quality measures are used to determine throughput, and in particular the throughput gain achieved by SSO. Packets that are lost due to a corrupted header will be lost with or without SSO. Therefore, we ignore them in the performance comparison. We thus investigate the PER as the ratio between the successfully received packets and packets with an erroneous payload, given a certain payload MCS. Additionally, we measure every packet's signal strength. The WARP platform measures this value during packet preamble detection. Equal to Camp et al. in [7] we consider this factor as a proxy to the SNR value, and in the following refer to it as the packet's SNR value.

The channel state information describes the characteristics of the channel and is used to decide on a suitable link configuration, including SSO. The channel state consists of two values. First, we consider the average signal strength of recently received packets as an indicator of the channel's overall attenuation. The second value that forms the channel state are the channel coefficients estimated from the preamble and training sequence. They consist of a complex fixed point number for every sub-carrier describing the magnitude of the channel estimation for this sub-carrier.

2.2.4 General Measurement Setup

Our basic test setup consists of two WARP boards running the OFDM PHY-layer with the modified WARPnet MAC-layer implementation. The nodes are placed in two neighboring testbed rooms so that no line of sight path exists. In order to analyze the behavior of SSO in a frequency faded channel we investigated a range of antenna configurations. Here, we report results that were obtained for experiments where live monitoring of the channel estimation showed heavily faded carriers.

This kind of fading can be found in around 30%-40% of antenna settings. We also remark that WARPnet's bandwidth is limited to 10MHz, which is considerably less compared to current Wi-Fi standards. IEEE 802.11ac for example uses channels with a bandwidth of up to 160MHz (see Section 1.4.2.3). For comparable indoor scenarios, channels with this bandwidth have a higher probability of deep faded sub-carriers.

The measurements were performed during night time to avoid that moving persons lead to varying channel conditions. Through continued logging of the channel estimation we verified that the channel conditions were relatively stable. An experiment configuration is given by the transmit gain, modulation and coding scheme, set of deactivated sub-carriers χ, and packet length. For each such configuration we run an experiment for a duration of 20 seconds, and average the results over all of the packets transmitted during that time interval. This is necessary, as the estimated channel coefficients and detected SNR might vary slightly due to noise that affects the preamble detection process.

2.2.5 Feedback Mechanism

As we consider a pseudo-static channel (see 2.2.2) we use an implicit feedback mechanism. The WARPnet control script decides which sub-carriers to switch off and sets the transmission parameters accordingly for the next time slot. An explicit feedback mechanism for a 802.11 like system could for example included the feedback in the acknowledgment packet that follows every received data packet. This way, no additional signaling packets need to be transmitted, reducing the feedback overhead solely to the bits added to the acknowledgment. For systems with 64 sub-carriers comparable to the WARP setup, this amounts to an additional overhead of only $8B/1460B = 0.5\%$, assuming maximum length data packets.

2.3 Results

In this section we present the results for the SSO measurements that we conducted on our WARP testbed. The results are separated threefold. First we present throughput measurements that give insights into the gains achievable with SSO. Next we report on a series of measurements to determine the threshold described in section 2.1.2. Finally these findings are validated with additional adaptive throughput measurements.

2.3.1 Throughput Gain for SSO

To determine the gains that SSO can achieve in different settings, we measure the transmission quality for the same frequency faded channel with different transmission configurations. To this end, we compare the throughput for the best performing MCS with and without SSO. In addition, this analysis provides us with insights about the influence of channel conditions on the performance of SSO.

As measuring the transmission quality for all possible configurations is cumbersome, we restrict ourselves to measuring a representative subset of channel configurations. For a first insight into the effect of SSO, we use different values for ξ and conduct experiments for all four possible coding rates in conjunction with WARP's three available modulation schemes. Furthermore, to determine the behavior over a range of signal reception strengths, we perform measurements for different transmit power settings.

In the following, we present the results of the throughput measurement for a frequency selective channel where SSO shows a significant throughput gain. In this experiment, we deactivate the 6, respectively 12, weakest sub-carriers. As a reference, the performance of the transmit configuration with all sub-carriers active is measured.

Figure 2.4 shows the corresponding channel coefficients over time according to the sub-carrier order described in Section 2.2. As can be seen from the figure, the basic fading pattern remains stable throughout the complete experiment run. Note that the spectrum shows considerable fading for the sub-carriers around sub-carrier number 15. The gap comprises more than 6 heavily faded

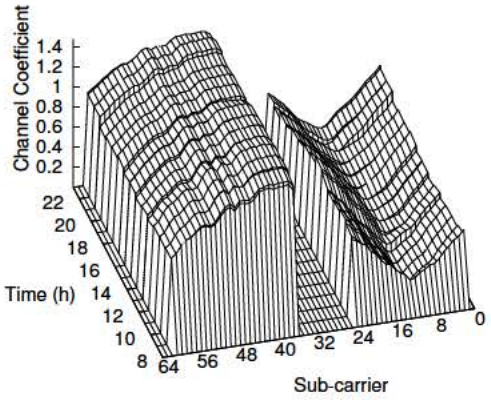

Figure 2.4: Channel coefficients during SSO throughput evaluation.

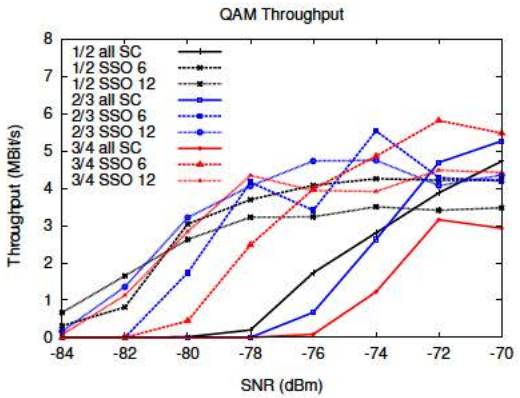

Figure 2.5: Throughput comparison for SSO enabled and plain QPSK modulated transmissions.

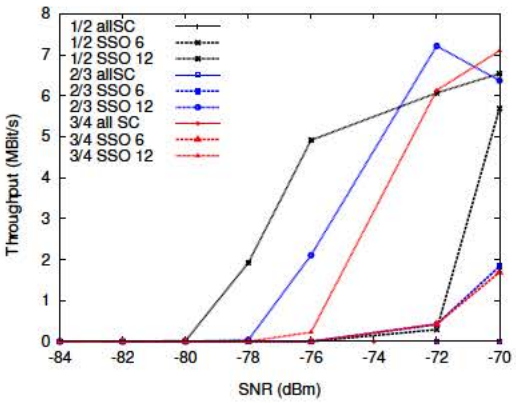

Figure 2.6: Throughput comparison for SSO enabled and plain 16-QAM modulated transmissions.

carriers which suggests that the configuration disabling more than 6 sub-carriers might lead to higher gains. [3]

Figure 2.5, shows the performance of SSO for QPSK modulation. It can be seen, that QPSK still successfully delivers packets under these channel conditions even without SSO. However, the sub-carrier configuration with all sub-carriers active only reaches the throughput level of the switched off configuration for high SNR values. Furthermore, for low SNR values a successful data transmission without SSO is not possible. It can be seen that SSO significantly decreases the minimum SNR that is needed for successful packet transmission. If we consider for example a throughput of 2Mbit/s we can see that SSO improves the reception by a value of roughly 5dBm. While a QPSK transmission with 1/2 coding and SSO still transmits with this throughput at a

[3]The results for BPSK basically give the same insights.

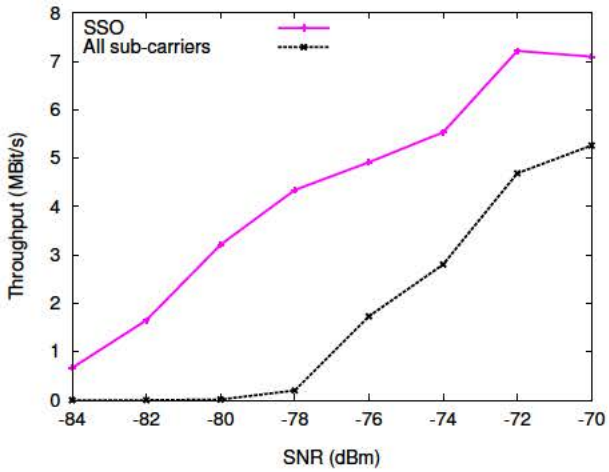

Figure 2.7: SSO throughput gain.

SNR of -81dBm the equivalent without SSO reaches this throughput at -76 dBm. Further, it is obvious that the order of error protection strength for the different coding variants is preserved when SSO is applied. For all MCS, 1/2 coded transmission still are the most resilient while 3/4 coding are the least robust. As expected for this channel state deactivating 12 sub-carrier performs better than switching off 6.

Figure 2.6 shows throughput for the same channel using 16-QAM. It is obvious that for these channel conditions, 16-QAM without SSO is not feasible. In contrast, when disabling the weakest sub-carriers it is possible to successfully transmit data with 16-QAM. Note that disabling 12 sub-carriers performs significantly better than only deactivating 6 sub-carriers. We explain this with the higher error proneness of 16-QAM compared to QPSK and BPSK. Note that, in comparison to Figure 2.5 the SSO enabled QPSK transmissions performs better for lower SNR values while 16-QAM provides higher throughput for higher SNR values.

In Figure 2.7 we show the maximal throughput for this experiment. This plot combines the data of all measured modulations. The throughput of the best configuration with all sub-carriers active compared to the best configuration with SSO is shown over the measured SNR range. The maximum absolute throughput gain can be found at -78dBm and has a magnitude of 4.1Mbit/s, where the conventional scheme achieves a throughput of 0.2Mbit/s, whereas SSO achieves 4.3Mbit/s.

2.3.2 Parameter Configuration for SSO

In a second step we experimentally determined the threshold τ described in Section 2.1.2. To this end we use the previously described setup for throughput measurements to collect the throughput for one specific MCS and all possible values for ξ. For every experiment we determine the MCS dependent value for τ from the best performing configuration as the channel state of the

weakest active sub-carrier. We find that the measured channel estimates do not correspond to the exact channel approximation $\hat{H}$. This effect is caused by WARP's gain control which amplifies the packets before the channel estimation is done. Therefore, we extend τ_s to be a vector of thresholds depending as well on the receivers gain factor, which corresponds to the measured packet SNR.

We repeat the measurement procedure for several different pseudo-static channels and record the channel states and transmission quality measures. For every MCS, we average the values for τ_s over all conducted experiments. Our low-complexity adaptive SSO strategy determines the number ξ_s of weakest sub-carriers to deactivate depending on the signal strength and the vector of averaged thresholds τ_s as follows:

$$\xi_s = \{k, |\hat{H}(k)| < \tau_s\} \tag{2.11}$$

We then validate the calculated vector τ_s through further experiments. Hence, we determine the values for ξ that the adaptive SSO approach chooses when applied to the formerly saved experiment data. By comparing these values to the optimum values we can see the performance of the adaptive SSO approach with τ_s.

In the following, we exemplarily show the results of one of these experiments that measures the complete SSO configurations for the 16-QAM 1/2 MCS. Note that this experiment is run on a arbitrary channel, that is not related to the channel shown in the previous section on which the τ_s configuration is based. Figure 2.8 shows the channel state for this experiment. Figure

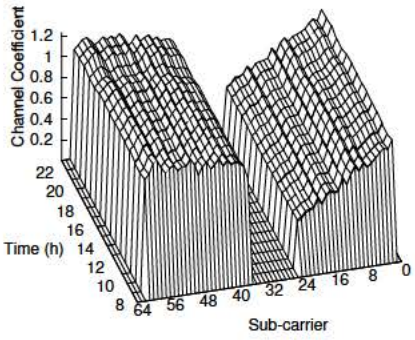

Figure 2.8: Channel coefficients during SSO threshold determination measurements.

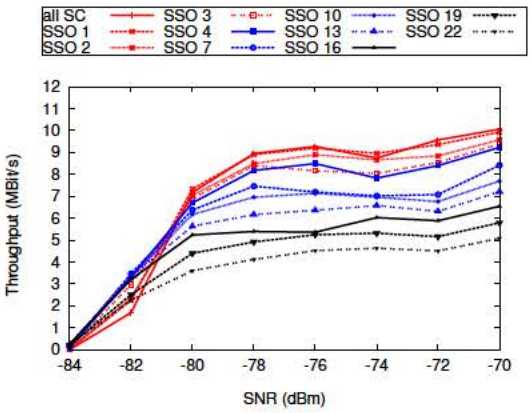

Figure 2.9: Throughput for different SSO configurations and 16-QAM 1/2 modulation.

2.9 shows the throughput graphs for this measured channel. For better readability we do not show all SSO configurations for higher values of ξ. The behavior of the curves that were left out is similar to that of the shown configurations. For high SNR values where all sub-carriers only suffer low error rates, switching off sub-carriers has negative impact on throughput, that is directly proportional to the number of deactivated carriers. This behavior changes at around -80dBm when the error rate of the weakest sub-carriers reaches the threshold τ. For even lower SNR values, the

configuration with all sub-carrier active turns out to be the worst performing configuration with respect to throughput.

To verify the configuration of τ, we show an a posteriori analysis of the performance of our adaptive SSO strategy on the same data set in Figure 2.10. We compare the throughput that the adaptive strategy would have achieved, against the best performing transmit configuration, i.e., the maximum of the curves with a fixed number of sub-carriers switched off. For the former, for each data point we take the performance of the scheme with a fixed number sub-carriers switched off, where the deactivated sub-carriers conform to the threshold τ. As can be seen from the throughput curve of our adaptive strategy, it chooses configurations that are very close to the optimal decision. However, due to the averaging nature of our determination of τ, small deviations from the optimum exist.

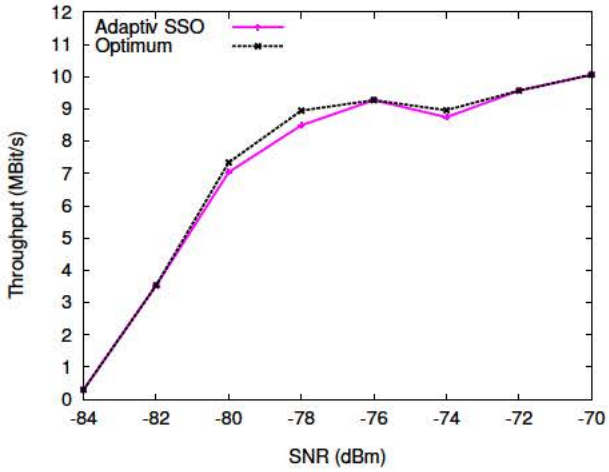

Figure 2.10: Adaptive SSO evaluation: Throughput compared to optimal switch off throughput.

2.3.3 Adaptive Sub-Carrier Switch Off

In order to further confirm our findings for the threshold vectors, we apply the adaptive SSO strategy to live throughput measurements. In contrast to the validation approach in Section 2.3.1, the adaptive strategy directly sets the SSO parameters based on the channel quality measurements reported by the receiver. Furthermore, note that the channel for this measurement differs from the one in section 2.3.2 that was used for the determination of the threshold vector τ. A successful adjustment of the transmission parameter therefore shows that the adaptive approach also works for unknown channels. Figure 2.11 depicts the channel state for the adaptive throughput measurement. Figure 2.12 shows an overview of the results. We compare the adaptive strategy with the static switch off of 6 and 12 sub-carriers for the 16-QAM 1/2 MCS. As a further reference we also show the throughput for the all active configuration. It can be seen from the graph that the adaptive strategy always performs similar to the best static scheme. The small deviation from the

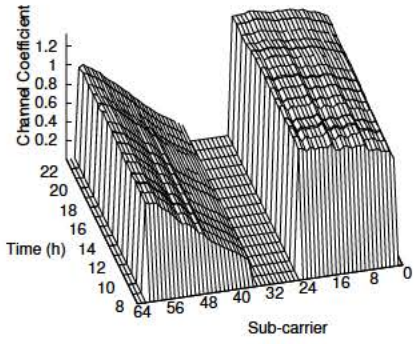

Figure 2.11: Channel coefficients during adaptive SSO evaluation.

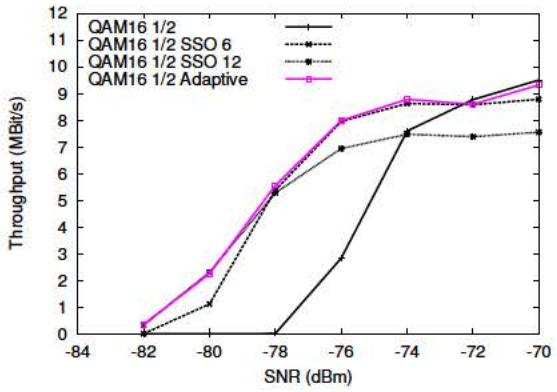

Figure 2.12: Throughput for adaptive SSO with QAM 1/2 modulation.

optimum configuration at higher SNR values results from the averaging in the threshold determination. It can easily be prevented by disabling SSO when very low packet error rates for the all active configuration are measured.

2.4 Related Work

Sub-Carrier Switch Off is related to adaptive modulation for OFDM transmission, which varies the used MCS according to the channel quality for every sub-carrier. Cheong et. al [96] propose OFDM with adaptive modulation per sub-carrier to be a promising counter-measure for wireless channels with multipath induced frequency selective fading. They also refer to the possibility of not transmitting data on a deeply faded sub-carrier during the period of a symbol, similarly to the basic idea of sub-carrier switch off. Nonetheless, adaptive modulation systems include higher computational costs for determining the optimal MCS for every sub-carrier and higher transmitter and receiver complexity. Furthermore signaling back the desired MCS combination requires a certain bandwidth overhead (see [70], [88], [83]).

A further method to combat frequency selective fading is to assign different transmit powers for every sub-carrier, referred to as power loading [24]. In [45] the authors use SSO (referred to as 'sub-band blocking') in order to meet signal power limitations on the proposed power loading scheme. Also the combination of power loading and adapting the MCS has been analyzed, a technique known as bit loading [2]. The idea of SSO as a self contained frequency selective fading counter-measure has first been considered by Puñal and Gross in [73], [72] and [24]. As the newly released IEEE 802.11ac amendment has channels with bandwidths of up to 160MHz, they argue that frequency selective faded sub-carriers will have even more impact in the future. Motivated by this, they compare different loading algorithms by means of simulation, namely power loading, bit loading, and SSO. They show that power loading has a minor influence compared to SSO and also show that their proposed combination of SSO and power loading comes close to the results

achieved by bit loading.

Our results from a real testbed confirm and extend the findings on SSO that were investigated by Puñal et. al. by means of simulation. We show that in case of deeply faded sub carriers, SSO can archive significant performance gains even for a far smaller bandwidth of only 10 MHz and without the complexity of power loading or bit loading techniques. As the simulation results presented in the works [73], [72] and [24] do not include pure SSO results but results for a combination of SSO and powerloading, and the simulated packets are modulated using a higher modulation scheme (256-QAM), the simulation results are unfortunately not directly comparable to our measurements.

The idea to switch off certain sub-carriers of a OFDM transmission can also be beneficial to cognitive radio (CR) systems [51]. Here however, the idea is to disable sub-carriers that coincide with used parts of the spectrum, thus decreasing interference between CR transmitters and incumbent transmitters.

2.5 Conclusion

In this chapter we analyzed the performance of Sub-Carrier Switch Off in IEEE 802.11 style OFDM wireless local area networks. We designed a light-weight mechanism to select the set of sub-carriers to switch off, based on the channel coefficients. This technique allows to adapt wireless transmission to the variations in signal propagation over the used frequency resources, in which SSO operates at the intra-channel level. The variations found over the frequency range of a single channel result from multipath propagation as detailed in section 1.1.3.4. In contrast to existing techniques, SSO is the most elaborate, yet low overhead involving, way of adapting to these variations.

SSO was implemented on the WARP software-defined radio platform to conduct a range of performance measurements. With the help of extensive channel state analysis for all possible SSO configurations, we developed a simple but effective method to decide which sub-carriers to switch off. This method maximizes throughput, while having very low computational complexity and feedback overhead.

In case of frequency selective fading, SSO turns out to be a very efficient measure to increase throughput and link stability. Under certain fading conditions we were able to transmit packets with a SNR range increase of up to 5 dBm, with corresponding significant increases in throughput from 0.2 Mbit/s without SSO to 4.3 Mbit/s with SSO. In summary, our analysis indicates that SSO is a very promising method to improve performance and resilience of future IEEE 802.11-style networks.

Our findings also open interesting questions for future work. At the intra-channel level, the combination of rate selection and SSO leaves room for additional improvements and measurements. Further, SSO can be applied to the packet headers with the goal of further improving the packet detection rate. These ideas promise modest improvement gains, when leveraging from

frequency varying propagation characteristics.

However, with the upcoming multi-band millimeter wave technology for consumer wireless networks, the propagation variations over the range of used frequency resources become significantly higher. Thus, future millimeter wave Wi-Fi systems, promise increased opportunities to exploit such variations. Therefore, the second part of this thesis shifts the focus from the intra-channel level perspective to multi-band systems, where channel resources with frequency differences of multiple tens of GHz can be accessed. At this level, entirely new approaches to exploit varying frequency resources become possible. Expansion of the SSO principle itself to millimeter wave communication however is not promising. This is due to the directional antenna technology which is commonly used at millimeter wave frequencies (see Section 3.1.3) and significantly reduces multipath [16, 103]. Thus, also the intra-channel signal quality variations, which SSO addresses are not as expressed as on legacy Wi-Fi frequencies.

Part II

Leveraging from Varying Multi-Frequency Band Propagation

The second part of this thesis expands the idea of adapting wireless communication to frequency varying propagation characteristics on the level of different frequency bands. An especially promising candidate technology to profit from this approach is multi-frequency band millimeter wave Wi-Fi. This technology emanates from the recent development of millimeter wave Wi-Fi that is complemented by legacy microwave Wi-Fi at 2.4 and 5 GHz. Multi-band millimeter wave Wi-Fi is supposed to gain momentum with the ratification of the IEEE 802.11ad amendment, which has been ratified in late 2013. Millimeter wave communication is expected to not fulfill traditional customer expectations towards Wi-Fi systems on stability and range. Thus, the IEEE 802.11ad amendment defines multi-frequency band features for range extension and increase in reliability. The trend towards accessing multiple frequency bands from one Wi-Fi device is thus continuing, with chip set manufacturers already announcing tri-band (2.4/5/60 GHz) chipsets for multi-gigabit streaming [6].

With the anticipated availability of these chipsets, new possibilities to leverage frequency varying propagation arise. The main differences between the two frequency bands is the significantly increased attenuation at millimeter wave frequencies (see Section 1.1.1), that requires the use of directional transmissions. Thus, millimeter wave systems are expected to experience much less interference, enabling parallel transmission over pencil-beam antenna patterns, which is a significant advantage for dense networks. On the other hand, the reception area of millimeter wave transmissions is much smaller than in the micro wave range and omni-directional communication is extremely difficult to realize (see Section 3.2.2.2 and [28]). Further, achievable transmission ranges as well as impact of Line of Sight (LOS) blockage varies widely between the two bands. This renders the microwave band suitable for longer link distances and resilient to blockage while millimeter wave communication best suits in-room LOS applications. The behavior of the used frequency resources thus varies more strongly than the intra-channel variations explored in Part I of this thesis. As the behavior of millimeter wave and microwave frequencies is complementary, upcoming multi-band millimeter wave devices are promising candidates to exploit the diverse behavior.

The second part of this thesis is subdivided into three chapters. First, Chapter 3 gives in-depth background information on multi-frequency band millimeter wave Wi-Fi to identify perspectives and challenges of this new technology. This discussion particularly focuses on the changes introduced to adapt IEEE 802.11 communication to the novel communication characteristics at 60 GHz frequencies. Among the most relevant additions is an elaborate beamforming protocol that facilitates directional communication and a multi-MAC-layer that allows to choose between three different medium access schemes. Further, modifications to network architectures, association and network announcement are described. The discussion on the concepts incorporated in the IEEE 802.11ad amendment is complemented by a practical analysis of millimeter wave communication systems. As at the time of writing no IEEE 802.11ad compliant devices are available, this analysis targets first generation millimeter wave systems (WiGig,WiHD) with commercially available hardware. IEEE 802.11ad has its origin in these standards (the WiGig Alliance merged

into the IEEE 802.11ad consortium [59]), which suggest that the studied devices will show performance comparable to first upcoming IEEE 802.11ad devices. The results of this study thus reveal challenges to next generation millimeter wave Wi-Fi communication, which this thesis addresses by leveraging frequency varying propagation behavior of the announced multi-band systems. In particular, the beamforming capabilities and interference impact are analyzed. The measurement results show, that the vision of interference free pencil-shaped antenna beams does not hold for first generation devices. Strong side lobes and interference created by reflections still contradict with the expected behavior. Thus, first generation devices still can rely on some of legacy Wi-Fi's omni-directional communication principles, as directionality is still limited. With next generation devices, this is about to change with particular challenges arising for the beam training process between devices and the operation of CSMA/CA medium access, which is well established for Wi-Fi networks.

Second BBS , a novel multi-frequency band approach, is presented in Chapter 4. It utilizes indoor localization at 2.4 GHz to improve the beam steering process in highly directional 60 GHz Wi-Fi networks. This improvement benefits future millimeter wave networks in several ways. First, the beam training overhead is reduced as less in-band probing is required. The overhead is problematic at highly directional millimeter wave devices as the amount of directions to probe increases. Further, especially for the mobile use-case of the IEEE 802.11ad amendment, frequent retraining of beam directions becomes necessary. Second, beam training resembles omni-directional transmissions, as all possible directions are probed in a brute force approach. Therefore, each beam training creates interference in all directions, which potentially breaks parallel transmissions. The proposed approach significantly reduces this problem.

Finally, directionality is known to pose a problem for the well established CSMA/CA carrier sensing mechanisms of IEEE 802.11 networks. Chapter 5 therefore analyzes the impact of this impairment on a simulation basis and finds that unfairness effects can be caused by that phenomenon. Therefor, a dual-band communication scheme is proposed that benefits from the combination of millimeter and microwave bands. It resolves the deficiencies of CSMA/CA in millimeter wave Wi-Fi, by moving RTS/CTS message exchanges from the 60 GHz interface to the legacy bands. Using the dual-band approach does not only achieve throughput improvements, but also prevents RTS frames that are mistakenly sent to busy stations. This reduces interference from transmission outside of established data streams and helps to enable parallel non interfering transmissions on the 60 GHz band.

Chapter 3

Background on Multi-band WiFi

Communication in the millimeter wave frequency range has not been used for consumer-grade wireless communication until very recently. In fact, very few devices compliant with the WiHD and WiGig haven been made available so far, and they have not reached wide consumer attention. This is supposed to change with the IEEE 802.11ad amendment, which merges the standardization efforts from the WiGig consortium into the popular IEEE 802.11 protocol stack that is widely accepted. While this promises a wide leap for consumer millimeter communication, a second trend is implied. Next generation millimeter wave networks are likely to be multi-frequency band capable. This is supported by the fact that first tri-band chips supporting the 802.11ad amendment have been announced [6]. Further, the 802.11ad amendment incorporates mechanisms that make use of these multi-band capabilities for range extension.

Due to the novelty of millimeter wave capable multi-band wireless transceiver technology, this background chapter is sub-divided into two main sections. The first gives a detailed analysis and background information on the IEEE 802.11ad amendment. It details the modifications made by the IEEE 802.11ad protocol to adapt Wi-Fi communication to frequencies in the millimeter wave range. These changes mainly result from the need for directional communication and target several key aspects of IEEE 802.11 networking. First, an elaborate beam training protocol is introduced that communicating stations use to focus signal energy between them. This also brings several changes to the network announcement and association process, which are impacted by the lack of long range omni-directional communication. Second, an enhancement of the MAC access schemes (see Section 1.3.1) allows IEEE 802.11ad devices to choose between three different schemes (CSMA/CA, Polling and Time Division Multiple Access (TDMA)). This enables adaptation with regard to the diverse 802.11ad use cases.

As little is publicly known about practical challenges and behavior of upcoming IEEE 802.11ad devices, the second part of this chapter contains a practical study of first generation millimeter wave devices. This performance analysis focuses especially on the aspects related to the application of antenna array techniques which is a key enabler for millimeter wave communication as it is required to overcome increased attenuation (see Section 1.1.1). Thus, achievable

directionality of first generation devices is analyzed, as well as antenna array performance when wide coverage is necessary, for example during device discovery. Last, as high directionality and attenuation at millimeter wave frequencies promise extremely low interference, the potential for spacial frequency reuse and interference effects is analyzed.

Finally, this chapter combines the results from first generation device analysis with the presented information on the upcoming IEEE 802.11ad amendment. This allows to identify challenges for millimeter wave communication that arise from practical limitations and problems that next generation networks will face.

3.1 IEEE 802.11ad

With the worldwide availability of a large swath of spectrum at the 60 GHz band for unlicensed use, we start to see an emergence of new technologies enabling Wi-Fi communication in this frequency band. However, signal propagation at the 60 GHz band significantly differs from that at the 2.4 and 5 GHz bands. Therefore, efficient use of this vast spectrum resource requires a fundamental rethinking of the operation of Wi-Fi and a transition from omni-directional to directional wireless medium usage. The IEEE 802.11ad amendment addresses these challenges, bringing multi-Gbps throughput and new application scenarios to Wi-Fi users. These new usages include instant wireless synchronization, high speed media file exchange between mobile devices without fixed network infrastructure, and wireless cable replacement, e.g., to connect to high definition wireless displays. The most significant difference in 60 GHz propagation behavior is increased signal attenuation. At a typical IEEE 802.11ad range of 10 meters, additional attenuation of 22 dB compared to the 5 GHz band is experienced according to the Friis transmission equation, resulting from the frequency dependent difference in antenna aperture (cp Section 1.1.1). In contrast, oxygen absorption plays a minor role over short distances, even though it peaks at 60 GHz [81]. Further, compared to legacy Wi-Fi frequencies, reflection, absorption and transmission characteristics of materials vary between frequency bands (see Section 1.1.3.1). 60 GHz communication has been found to be characterized by a quasi-optical propagation behavior [100] where the received signal is dominated by the LOS path and first order reflections from strong reflecting materials. As an example, metallic surfaces were found to be strong reflectors and allow non-Line of Sight (LOS) communication [100]. Concrete materials, on the other hand, cause large signal attenuation and can easily create a blockage. Thus, 60 GHz communication is more suitable to in-room environments where sufficient reflectors are present. This section discusses the design assumptions resulting from the mm-wave propagation characteristics and resulting changes to the 802.11 architecture. We further present typical device configurations, an overview of the IEEE 802.11ad physical PHY-layer, and the newly introduced personal basic service set network architecture. This is followed by an in depth description of the IEEE 802.11ad Beam Forming (BF) mechanism and hybrid medium access control (MAC) design, which are the central elements to facilitate directional communication.

3.1.1 Directional Communication

The IEEE 802.11ad amendment to the 802.11 standard defines a directional communication scheme that takes advantage of beamforming antenna gain to cope with increased attenuation in the 60 GHz band [81]. With quasi-optical propagation behavior, low reflectivity and high attenuation, 60 GHz signals with highly directional main beam focus can be achieved. Based on this behavior, the amendment introduces a novel concept of virtual antenna sectors [39] that discretize the antenna azimuth. IEEE 802.11ad sectors can be implemented either using pre-computed antenna weight vectors for a phased antenna array [92] or by equipping a system with multiple directional antenna elements. In both cases, the wave length in the millimeter range allows significantly smaller antenna form factors compared to legacy Wi-Fi at 2.4/5 GHz. A sector focuses antenna gain in a certain direction. Communicating nodes thus have to agree on the optimal pair of receive and transmit sectors to optimize signal quality and throughput. This process, referred to as beamforming training, takes advantage of the discretized antenna azimuth that reduces the search space of possible antenna array configurations. After a first sector matching, a second beam training stage allows further refinement of the found sectors. During this stage, antenna weight vectors that vary from pre-defined sector patterns can be evaluated to further optimize transmissions on phased antenna arrays. While in general higher antenna gain is desirable, it imposes stronger directionality and a higher number of narrow antenna sectors. This increases coordination overhead to adapt the antenna steering between communicating nodes, and it has been shown that link budget loss by misalignment increases with directionality [103]. Figure 3.1 shows an example for two nodes communicating over IEEE 802.11ad sectors. The highlighted selection of sectors that match the line of sight direction usually offers the optimum link quality in absence of blocking obstacles.

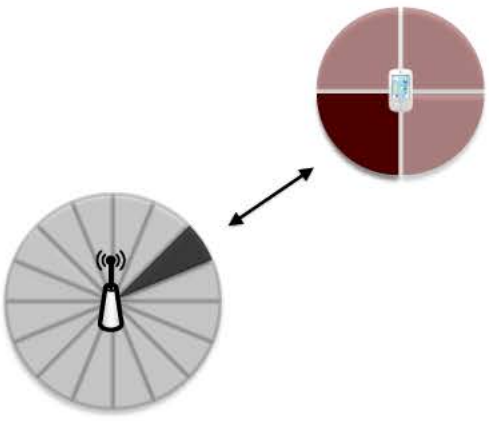

Figure 3.1: Virtual antenna sectors.

3.1.2 IEEE 802.11ad Device Classes and Use Cases

Communication in the mm-wave band enables extremely high throughput at short-ranges ($\leq$ 10m), and promises high potential for spatial reuse. Thus, not only does it suit typical Wi-Fi usage, but it also expands the uses of Wi-Fi into other application areas. Among these areas are wireless transmission of high definition video, wireless docking stations, connection to wireless peripherals or high speed download of large media files. To meet the requirements for these novel use cases, the IEEE 802.11ad amendment allows for a broad variety of Directional Multi-Gigabit (DMG) devices ranging from energy constrained handheld equipment with low complexity antennas (1-4 antenna elements) to stationary access points with multiple antenna arrays and permanent power supply. Table 3.1 shows typical configurations for several device classes. It states the number of sectors that correlates with range and throughput, differences between receive and transmit direction and special traffic characteristics for every class. Further, the expected number of antenna arrays is given for every device class. Multiple phased antenna arrays enable high gain coverage in all directions. They are not used in a MIMO fashion, but treated like a set of additional sectors with only one antenna array used at a time.

3.1.3 Design Assumptions

Communication in the mm-wave frequency band has different characteristics compared to legacy 2.4/5 GHz Wi-Fi frequencies. Thus, the development of the IEEE 802.11ad amendment followed a number of design assumptions that result from the change of frequency band.

Highly directional transmissions. Increased transmission loss and the application of high gain beamforming techniques lead to a strong directional signal focus. In contrast to omni-directional legacy Wi-Fi signal propagation, IEEE 802.11ad communicates over narrow beams that follow quasi-optical propagation characteristics.

Quasi-omni-directional antenna patterns. Implementation of truly omni-directional mm-wave antenna patterns is not practical, as signal blockage and deviation by device components in the vicinity of the antenna have a much stronger effect than on legacy Wi-Fi frequencies. Therefore, IEEE 802.11ad introduces quasi-omni-directional patterns that allow gain fluctuations over the pattern. Further measures are taken to cope with the resulting effects.

Inefficient omni-directional communication. The increased attenuation in the mm-wave band leads to severely reduced transmission range and throughput when quasi-omni-directional antenna patterns are used. However, when the direction to a communication partner is unknown (e.g. during beamforming training) quasi-omni patterns are still needed. Thus, directional antenna gain is added at least at one side of a link to achieve a sufficient communication range. Typically, quasi-omni-directional antenna configurations are used at the receiver side. Only de-

Device	Antenna Sectors	Expected Range(m)	Max. Throughput (Gbps)	Traffic Type	Antenna Arrays
AP, Docking Station	32 to 64	20	7	Bursty Traffic on Downlink	≤ 3
Wireless Peripheral (Hard drive, Memory Stick)	≤ 4	0.5 to 2	4.6	Bursty	1
Wireless Display, TV	32 to 64	5 to 10	7	Continuous, RX more important	≤ 2
Notebook	16 to 32	5 to 10	4.6 - 7	Various, symmetric TX and RX	1
Tablets	2 to 16	2 to 5	4.6	Various, symmetric TX and RX	1
Smartphone, Handheld, Camcorder, Camera	≤ 4	0.5 to 2	1.2 - 4.6	Various, symmetric TX and RX, TX more important for video streaming devices	1

Table 3.1: IEEE 802.11ad: Typical device configurations.

vices with extreme space or energy restrictions are expected to implement quasi-omni-directional transmit modes. These devices will be severely limited in range and throughput (see Table 1).

Extreme efficiency loss on poorly trained beams. The throughput difference between the highest and lowest transmission scheme defined by IEEE 802.11ad lies in the range of 6.5 Gbps. A poorly trained beam that uses a low throughput scheme severely reduces the system performance and should be avoided at all costs.

Reduced interference. Directional transmission properties of IEEE 802.11ad devices have the potential to reduce interference outside of the beam direction. Applying transmit and receive beamforming allows in many cases to reuse the same frequency band and significantly increase the system's overall throughput.

Deafness and directional communication drawbacks. Highly directional IEEE 802.11ad transmissions have hindering effects on common Wi-Fi MAC mechanisms. Directional transmit patterns prevent devices from passively overhearing ongoing transmissions, leading to additional collisions during channel access. Further, the deafness effect caused by misaligned transmit or receive antenna patterns may lead to frame loss, unnecessary long contention back-off and lower throughput. An in depth discussion of these impairments can be found in [10]. IEEE 802.11ad adapts the 802.11 CSMA/CA mechanism and further introduces a multi-MAC architecture, with alternative medium access schemes suited to directional communication.

3.1.4 Physical Layer

IEEE 802.11ad introduces three different PHY-layers dedicated to different application scenarios. The Control PHY is designed for low SNR operation prior to beamforming. The Single Carrier (SC) PHY enables power efficient and low complexity transceiver implementation. The low-power SC PHY option replaces the Low Density Parity Code (LDPC) encoder by a Reed-Solomon encoder for further processing power reduction. The OFDM PHY provides high performance in frequency selective channels achieving the maximum 802.11ad data rates. Despite having different PHYs, all of them share the same packet structure with common preamble properties. Specifically, the same Golay sequences are used for the preamble training fields. Also, a common rate LDPC structure is used for channel encoding. Moreover, 802.11ad defines a single bandwidth of 2.16 GHz, which is 50 times wider than the channels available in 802.11n and roughly 14 times wider than the channels defined in 802.11ac. The IEEE 802.11ad packet structure is shown in Figure 3.2. The packet consists of typical IEEE 802.11 elements (compare Section 1.4.1), e.g., a short training field (STF) and a channel estimation field (CEF) that is also used for auto-detection of the PHY type. They are followed by the PHY header and the PHY payload that is protected by a CRC. Finally optional automatic gain control (AGC) and training (TRN) fields, unique to IEEE 802.11ad, might be appended. These are used for the beamforming

mechanism described in Section 3.1.7. To provide robust discovery and detection, the control PHY has a longer STF than the SC and OFDM PHYs, comprising 48 Golay sequences, each 128 samples long. The SC and OFDM PHY only use 17 Golay sequences for the STF. The channel estimation field that follows the STF has 9 Golay sequences. The OFDM PHY uses a different combination of Golay sequences in the CEF to distinguish between OFDM and single carrier modulation.

The Control PHY uses MCS 0. It implements a 32 sample Golay spreading sequence along with rate $\frac{1}{2}$ LDPC encoding (spread from the common rate LDPC code) to extend range and reliability for management frames, giving a throughput of 27.5 Mbps. The Control PHY uses $\frac{\pi}{2}$-differential BPSK modulation to further enhance robustness to distortion like phase noise. The mandatory Control PHY defines the minimum rate that all devices use to communicate before establishing a high-rate beamformed link. It is used for transmitting and receiving frames such as beacons, information request and response, probe request and response, sector sweep, sector sweep feedback, and other management and control frames. The SC PHY (MCS 1-12) and low power SC PHY (MCS 25-31) allow for low complexity and energy efficient transceiver implementations with a throughput of up to 4.62 Gbps. The lowest SC data rate is 385 Mbps (MCS 1). It is implemented using BPSK modulation and rate $\frac{1}{2}$ code with a symbol repetition of two. All modulation types use $\frac{\pi}{2}$ rotation to reduce the peak-to-average power ratio for BPSK and to enable GMSK equivalent modulation. To provide interoperability between different device types, MCS 1-4 are mandatory for all devices. These four MCSs are all based on $\frac{\pi}{2}$-BPSK modulation. MCS 2, 3, and 4 use code rate 1/2, 5/8, and 3/4, respectively. The OFDM PHY (MCS 13-24) is an optional mode for maximum throughput at the cost of a more complex and energy intensive transceiver structure. The OFDM PHY type utilizes 64-QAM and a rate 13/16 code to achieve the highest 802.11ad data rate of 6.75 Gbps. In order to keep transceiver complexity and energy consumption low, mobile and low cost devices are likely to implement only single carrier PHYs. In contrast, stationary devices with fixed power supply and high throughput requirements (access points, wireless displays) implement the full spectrum of MCSs including complex OFDM transceivers.

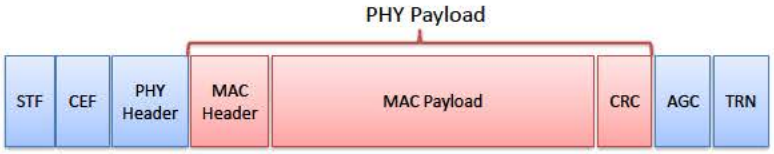

Figure 3.2: IEEE 802.11ad packet structure.

3.1.5 Network Architecture

This section describes the changes to the IEEE 802.11 network architecture defined by IEEE 802.11ad. First, we describe the changes to the Beacon Interval (BI). Next, a novel network type

called Personal Basic Service Set (PBSS) is discussed, that complements infrastructure BSS and IBSS network architectures (see Section 1.2.3). Finaly, a description of the IEEE 802.11 network and schedule announcement mechanisms is given.

3.1.5.1 Beacon Interval

IEEE 802.11 in lower frequency bands organizes the medium access through periodically reoccurring beacon intervals that are initiated by a single beacon frame transmitted omni-directionally by the AP or coordinating station. The beacon announces the existence of a Wi-Fi network and carries further management data. The rest of the BI is used for data transmissions between stations, usually following a contention based access scheme. The length of a BI is limited to 1000 ms, but typically chosen in the range of 100 ms. While longer BI durations increase the connection delay for nodes waiting for the beacon, a longer interval reduces management frame transmission and increases throughput. The IEEE 802.11ad amendment extends this concept in several ways to cope with the challenges of mm-wave propagation. First, a beacon interval is initiated with the Beacon Header Interval (BHI) that replaces the single beacon frame of legacy Wi-Fi networks. The BHI facilitates the exchange of management information and network announcements using a sweep of multiple directionally transmitted frames. The BHI sweeping mechanism is required due to increased attenuation and unknown direction of unassociated devices. Additional functionality of the BHI is described later on. The BHI is followed by a Data Transmission Interval (DTI), which can implement different types of medium access. The schedule and medium access parameters, which are necessary for stations to participate in a BI, are announced by the central network coordinator, the PBSS Control Point (PCP) or AP, during the BHI. This ensures that stations receive this information even though no efficient broadcasting mechanism is available.

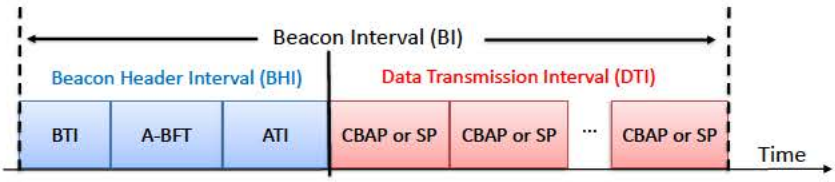

Figure 3.3: IEEE 802.11ad beacon interval structure.

A typical beacon interval, consisting of BHI and DTI, is shown in Figure 3.3. The BHI consists of up to three sub-intervals. First, the Beacon Transmission Interval (BTI) comprises multiple beacon frames, each transmitted by the PCP/AP on a different sector to cover all possible directions. This interval is used for network announcement and beamforming training of the PCP/AP's antenna sectors. Second, the Association Beamforming Training (A-BFT), is used by stations to train their antenna sector for communication with the PCP/AP. Third, during the Announcement Transmission Interval (ATI), the PCP/AP exchanges management information

with associated and beam-trained stations. While communication during BTI and A-BFT uses MCS 0 to increase range for untrained beams, communication during the ATI takes place with beam-trained stations and thus is more efficient. The DTI comprises one or more Contention Based Access Periods (CBAPs) and scheduled Service Periods (SPs) where stations exchange data frames. While in CBAP multiple stations can contend for the channel according to the IEEE 802.11e EDCF (see Sections 1.2.1 and 1.3.1), an SP is assigned for communication between a dedicated pair of nodes as a contention free period.

3.1.5.2 Personal Basic Service Set

IEEE 802.11ad introduces the PBSS, where nodes communicate in an ad-hoc like manner. However, one of the participating nodes takes the role of the PBSS Control Point. This PCP acts similar to an AP, announcing the network and organizing medium access. This centralized approach allows the directional network and schedule announcement process described in the next section to be used for an ad-hoc like network. The PBSS network has been introduced to satisfy new applications targeted by IEEE 802.11ad such as, for example, wireless storage and peripherals or wireless display usage. For these applications, usually no preinstalled infrastructure exists and communication takes place between a set of personal devices. An ad-hoc like network with a centralized controller poses two main challenges. First, for energy-constrained devices, increased power consumption at the PCP penalizes a single device while a fair sharing of the energy costs is desirable. Second, outage of the PCP paralyzes the entire PBSS. To respond to these challenges, a PCP Handover procedure is defined [39]. This procedure can be used for explicit (initiated by the current PCP) or implicit (after PCP becomes unavailable) handovers. Further, when selecting between a set of possible PCPs, the unique capabilities of PCP candidate stations are considered to choose the PCP providing the most complete set of services to the network.

3.1.5.3 Network and Schedule Announcements

Network announcements in legacy IEEE 802.11 are traditionally propagated periodically, using beacon frames by the AP. Due to the limited antenna gain of quasi-omni-directional mm-wave transmissions the coverage range is severely restricted. Consequently, the beacon is sent as a series of directionally transmitted beacon frames. To have the largest possible range, the beacon frames are transmitted at the most robust MCS (MCS 0). IEEE 802.11ad also specifies additional signaling for network scheduling and beam training appended to every beacon frame. Collectively, this results in a significantly increased overhead in comparison to legacy Wi-Fi. Thus, it becomes critical to control the amount of information that is transmitted in each BTI. In addition, transmissions during the A-BFT, which also use MCS 0, create overhead reoccurring with every BI where the A-BFT is present. The overhead becomes especially problematic when short BI durations are applied for delay critical application as, for example, video streaming. The IEEE

802.11ad amendment defines a number of counter strategies. First, it is possible to split a beacon sweep over several BIs. This, however, increases the time a node needs to set up its link to the PCP/AP, as not every direction is served at every BI. The result is an increased association delay. Second, it is possible to periodically schedule BIs without A-BFT, which also results in additional association delays. Third, IEEE 802.11ad introduces the ATI. During the ATI, beam-trained and associated nodes can be served with management data using individually addressed directional transmitted frames encoded with a more efficient MCS. Thus, it is possible to move information from the spectrally inefficient beacon frames to the frames transmitted during the ATI, limiting beacons to the minimal information necessary. Also, for beacon intervals with split beacon sweeps, stations that do not receive a beacon miss network and timing information. Without this information, stations cannot participate in a BI. Implementing an ATI solves this problem, as scheduling and management information is transmitted individually to associated stations.

3.1.6 IEEE 802.11ad Medium Access Control Layer

In contrast to legacy Wi-Fi, IEEE 802.11ad uses a hybrid MAC approach to address its various use cases [39], [13]. The standard supports contention based access, scheduled channel time allocation and dynamic channel time allocation. The latter two schemes correspond to TDMA and polling mechanisms. The polling based access shares similarities with the IEEE 802.11 point coordination function (PCF) mode (see Section 1.3.2.1), but is adapted to directional transmissions and provides a higher flexibility when it comes to distribution of resources among the nodes. The scheduled allocation mechanism extends the traffic stream concept known from the IEEE 802.11 HCF (see Section 1.3.1) to request time shares of the DTI for TDMA like medium access. Next, the three methods are described.

3.1.6.1 Contention Based Medium Access

Medium access in CBAPs follows IEEE 802.11 enhanced distributed channel access (EDCA), including traffic categories to support quality of service, frame aggregation and block acknowledgments. However, when using contention based access with directional antennas, the problem of deafness arises. A deaf node does not receive directionally transmitted information due to misaligned antenna patterns. A detailed description of the effect can be found in [10]. While the beam training process in IEEE 802.11ad prevents deafness for intended transmissions, it poses a problem for carrier sensing during contention based access and can lead to increased collisions. A further problem for contention based access is that a receiver typically does not know where a signal comes from. Thus, usage of quasi-omni-directional beam patterns is necessary, which reduces link budget and throughput.

IEEE 802.11ad EDCA equals the basic DCF access, described in Section 1.3.1.1 in many aspects. In general, stations start (or resume) a random back off counter a DIFS interval after the end of the acknowledgment of a data frame. The backoff counter decreases at each slot which

equals 5μs. Once a backoff counter reaches zero, the corresponding station wins a Transmit Opportunity (TXOP), where it can exclusively transmit one or more frames to another station. This mechanism is not present in the basic DCF description, but was inherited form the IEEE 802.11e enhancement [35]. Further, in accordance with legacy DCF, stations overhearing ongoing frames, track their duration to maintain a Network Allocation Vector (NAV) and defer from decreasing their backoff counter. If a station senses the channel to be busy (either by virtual or physical sensing see Section 1.3.1.1) or a frame transmission fails, it doubles its contention window until the maximum contention window size of 1023 slots is reached. After successfully accessing the channel, a station resets its maximum contention window to the minimum value of 15 slots.

IEEE 802.11ad adapts the CSMA/CA mechanism to directional medium usage. Idle stations generally listen with a quasi-omni-directional receive pattern as the direction of the next incoming transmission is unknown. Thus, directional antenna gain is only achieved at the transmitter side, requiring a robust modulation coding scheme. Therefore, the first frames exchanged are a directional RTS/CTS pair at the most robust coding modulation scheme. The RTS/CTS exchange further increases the chance of main interferers within the antenna's boresight to sense the ongoing transmission and refrain from interfering. Further, support for multiple NAV timers (one per peer station) is supported. This allows a transmission to be initiated to a peer device where the NAV for that device is zero, even though the NAV for another peer device might be nonzero. Additional, details about 802.11 EDCA and its use in 802.11ad can be found in [39], [38].

IEEE 802.11ad enables spatial sharing during CBAPs by modifying the deferral behavior. Instead of deferring whenever a frame is overheard, a station might still initiate transmission when the receiver is known to be idle. This leads to multiple transmissions at the same time, when multiple pairs of stations intend to transmit at the same time.

3.1.6.2 Dynamic Channel Time Allocation

IEEE 802.11ad defines a dynamic channel time allocation mechanism that implements polling based channel access. Dynamic channel time allocation is an extension of the IEEE 802.11 PCF mode. It provides higher flexibility in resource allocation (polled stations request channel time instead of just transmitting one frame) and adaptation to directional communication. Polling based channel access brings several advantages for mm-wave communication. First, due to the centralized approach with a PCP/AP, stations are aware of the direction of incoming signals. Thus, the deafness problem that affects contention based access is prevented and quasi-omni directional receive patterns can be avoided. Second, centralized scheduling at a PCP/AP also helps to efficiently react to bursty downstream traffic, as dynamic scheduling can be adapted over the course of a BI. In contrast, pseudo-static scheduling described in the following section can only announce modified allocation parameters with the beginning of every BI. When applying the dynamic allocation mechanism, the medium access during DTI is organized as follows. The PCP/AP acquires the medium and sends a series of polling frames to associated stations. This is answered with a block of Service Period Requests (SPRs) used by the polled stations to request channel time.

The PCP/AP allocates the available channel time according to these requests, announcing each allocation with a separate grant period, consisting of individual grant frames for the stations involved in the allocation. IEEE 802.11ad allows integration of the dynamic allocation mechanism into both CBAPs and SPs. When integrated in a CBAP, associated stations try to acquire the medium and may interfere with the dynamic allocations. To prevent this, the PCP/AP makes use of prioritized medium access using the short PIFS inter frame spacing and the channel is protected by extension of the frame duration fields. This extension causes nodes that overhear a frame to assume the channel to be occupied until the time specified in the duration field. This mechanism is used, such that Polling and SPR frames protect the polling phase, while every dynamic allocation is protected by its preceding grant frames. To simplify the scheduling mechanism and reduce implementation complexity, dynamic allocations are scheduled back to back, with every allocation immediately following its grant period. To reliably reach the nodes that are involved in an allocation, individual directional frames are transmitted during the grant period. In case of an allocation between PCP/AP and a station, only one grant frame is sent to the non-PCP/AP station. When not all available channel time is allocated dynamically, the PCP/AP can repeat the entire polling process. In case of integration into a CBAP, remaining channel time can also be used for CSMA/CA access. An example for three polled stations is shown in Figure 3.4. The PCP/AP commences a polling phase at the beginning of the DTI, transmitting a polling frame for every associated station, which is answered with a series of three SPRs by the stations. The second station requests communication with another non-PCP/AP station while stations one and three intend to communicate with the AP. The resulting allocations are scheduled back to back; each proceeded by a grant period. In case of communication with the AP, the grant period consists of one frame, otherwise of two. The time until which preceding frames protect the channel is indicated by separating lines.

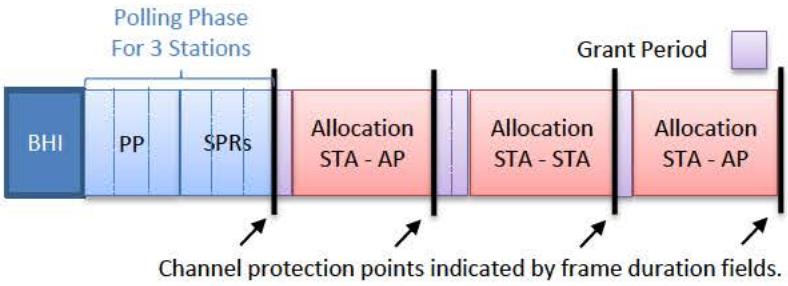

Figure 3.4: Dynamic channel allocation example.

3.1.6.3 Pseudo-Static TDMA Channel Time Allocation

During pseudo-static channel time allocation, SPs that reoccur every beacon interval are dedicated exclusively to a pair of communicating nodes. Accessing the channel using this TDMA mechanism provides reliability and is the best way to comply with quality of service demands.

Further, the schedule of SPs is propagated by the PCP/AP to all associated stations. Thus, every node that is not communicating during a SP can go into sleep mode, which allows for efficient power saving. For pseudo-static medium allocation, the concept of traffic streams for IEEE 802.11 HCF, as described in [38], is extended. A traffic stream is defined as a flow of MAC service data units that is to be delivered subject to certain quality-of-service parameters, characterized by a traffic specification. The IEEE 802.11ad amendment defines stations to use traffic specifications to request scheduling of pseudo-static channel allocations at the PCP/AP. A requesting station defines the properties of its traffic demand in terms of allocation duration and isochronous or asynchronous traffic characteristic. Calculating the allocation duration requires a completely beam-trained link with known rate between source and destination. Otherwise, the traffic specification has to be modified after beam training when the link's throughput rate is known. An isochronous traffic stream results in pseudo static SP allocations that satisfy a constant rate of reoccurring payload (typical, e.g., for wireless display applications) with certain latency demands. Asynchronous traffic streams, in contrast, satisfy non reoccurring payload demand. A typical example application are rapid file downloads. The actual schedule that includes the requested allocations is broadcasted by the PCP/AP in an extended schedule element in the next BTI or ATI.

3.1.7 Beamforming Concept

Beamforming training determines the appropriate receive and transmit antenna sectors for a pair of stations. This is achieved by transmission of a bidirectional training frame sequence. Throughout the training process, transmission with quasi-omni directional beam patterns at receiver and transmitter are avoided as they are severely limited in range. The beamforming phase is split into two sub-phases. First, during the Sector Level Sweep (SLS) an initial coarse-grain antenna sector configuration is determined. This information is used in a subsequent optional Beam Refinement Protocol (BRP), which fine-tunes the selected sectors. During SLS, each of the two stations either trains its transmit antenna sector or the receive antenna sector. When devices are equipped with antenna arrays capable of reasonable transmit antenna gain, the most common choice is to train only transmit sectors during SLS and derive receive antenna configuration during a following BRP. Fully refined transmit and receive sectors at both sides of a link allow to reach multi-Gbps speeds over ranges of up to 10 m. This section explains the general approach to beamforming introduced in the IEEE 802.11ad amendment. The beamforming concept allows a significant amount of implementation dependent customization and has a variety of optional features. Therefore, we first focus on the mandatory SLS phase followed by a description of the mandatory parts of the BRP.

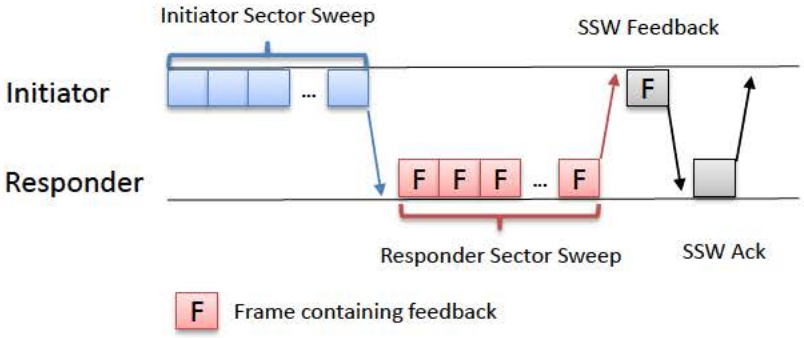

Figure 3.5: Sector level sweep structure.

Figure 3.6: Transmit and receive sector training.

3.1.7.1 SLS - Sector Level Sweep Phase

During the SLS, a pair of stations exchanges a series of Sector Sweep (SSW) frames (or beacons in case of transmit sector training at the PCP/AP) over different antenna sectors to find the one providing highest signal quality. During the SLS, each station acts once as a transmitter and once as a receiver of a sweep as shown in Figure 3.5. The station that transmits first is called the initiator, the second the responder. Both, initiator and responder sweep can be used in two different ways as depicted in Figures 3.6. During a Transmit Sector Sweep (TXSS) shown in the left part of the figure, frames are transmitted on different sectors while the pairing node receives with a quasi-omni directional pattern. To identify the strongest transmit sector, the transmitter marks every frame with an identifier for the used antenna and sector. During a Receive Sector Sweep (RXSS) shown in the right part of Figures 3.6, transmission on the same sector (best known sector) allows to test for the optimum receive sector at the pairing node. Overall, there are four possible sweep combinations for a SLS: transmit sector sweeps at both initiator and responder, receive sector sweeps at both stations, initiator RXSS and responder TXSS, and initiator TXSS and responder RXSS. The achieved optimum SNR and in case of a TXSS the sector and antenna identifier are reported to the pairing node. SLS feedback follows the structure described in Figure 3.5. Feedback for the initiator is carried by every frame of the responder sector sweep, which

ensures reception under still unknown optimum antenna configuration. The feedback for the responder is transmitted with a single SSW feedback frame, on the determined optimum antenna configuration. Finally, the SSW feedback frame is acknowledged with an SSW-ACK by the responder. The last frame is further used to negotiate the details of a following BRP. In case two stations have sufficient transmit antenna gain, their SLS phase can be realized as pure transmit sector training, with the receive sector training postponed to a following BRP. Devices with few antenna elements have to add antenna gain at the receiver side in order to achieve sufficient link budget to establish a link. Thus, these devices are likely to include a receive sector sweep in their part of the SLS. The initiator can request the responder to do a receive sector sweep by specifying the number of receive sectors to train during the initiator sweep. When the initiator sweep is a receive sector training, additional signaling has to precede the SLS as will be described in Section 3.1.8.

3.1.7.2 BRP - Beam Refinement Protocol Phase

The BRP refines the sectors found in the SLS phase. These sectors are determined using inhomogeneous quasi-omni directional receive antenna patterns and may have sub-optimal signal quality. Further, the BRP foresees optimization of antenna weight vectors, independent of the pre-defined sector patterns, for phased antenna arrays. This can yield additional throughput gains, while increasing the beam training search space. Even though free variation of the antenna weight vectors can result in arbitrary antenna patterns, the directional focus remains for antenna configurations that yield high throughput. Thus, the training process for pre-defined directional sectors and antenna weight vectors optimization remains the same. Finally, the BRP is used to train receive antenna configurations in case this was not part of the preceding SLS. Multiple optional pattern refinement mechanisms are defined for the BRP and are out of scope of this background chapter. We focus on the mandatory beam refinement transactions, an iterative process in which both initiator and responder can request training for receive or transmit antenna patterns. A BRP transaction evaluates a set of directional transmit or receive patterns against the best known directional configuration at the pairing node. Thus, the imperfection of quasi-omni-directional patterns is avoided. As the BRP relies on a preceding SLS phase, a reliable frame exchange is ensured and different antenna configurations can be tested throughout the same frame. This severely reduces transmission overhead in contrast to the SLS, where a full frame is necessary to test a sector. To sweep antenna configurations throughout a frame, transmit and receive training fields (TRN-T/R) are appended to the frames exchanged during BRP transactions (see Section 3.1.4). Each field is transmitted or received with an antenna configuration that is to be tested for its signal quality. The remaining portion of the frame is transmitted and received with the best known antenna configuration.

BRP receive antenna training is requested by specifying the number of configurations to be tested in a frame's L-RX header field. The pairing node will append the according number of TRN-R fields to its next frame. A transmit training is requested by setting the TX-TRN-REQ

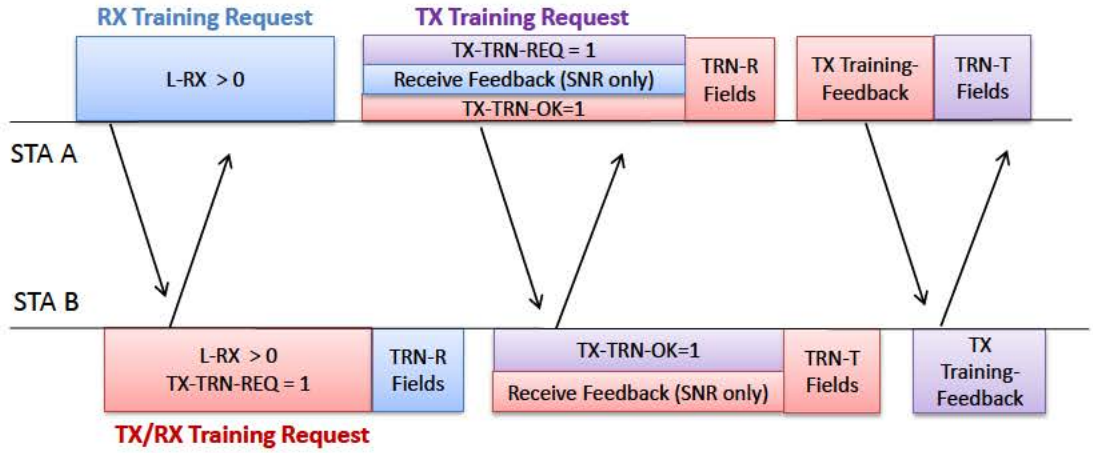

Figure 3.7: Beam refinement transactions.

header field and appending TRN-T fields to the same BRP frame. Optionally, no training fields are attached and an acknowledgment frame with the TX-TRN-OK field set is transmitted by the recipient before the requester appends the TRN-T fields to its following frame. Equal to the SLS, BRP feedback is given in form of SNR for the best found configuration and the best configuration ID in case of a transmit training. Figure 3.7 shows a BRP transaction, that first trains the receive configuration between two stations, followed by additional transmit training refinement. Note that station B combines the request for transmit and receive training in one frame using the request variation explained above. Station A, in contrast, uses two frames to request the two transmit directions. The frames and training fields belonging to one of the different training request are marked in the same color. A BRP phase can immediately follow the SLS, using the SSW ACK frame for parameter exchange. Alternatively, it can be initiated by a special BRP setup sub-phase, consisting of training field free BRP frames. In either case, L-RX and TX-TRN-REQ fields are used to exchange the BRP parameters.

3.1.8 Beamforming Protocol

The general beamforming concept described in Section 3.1.7 integrates into the different IEEE 802.11ad medium access schemes and the association process. Before association, stations use an adapted version of the beamforming process to connect with the PCP/AP without preceding coordination. This training is further realized in a way that allows the PCP/AP to do sector training to all stations at the same time rather than separately. This section explains the association beamforming training, followed by a description of beam training between non-PCP/AP stations in accordance with the three different MAC schemes.

3.1.8.1 Association Beamforming Training

Beamforming training between the PCP/AP and an unassociated station cannot rely on coordination preceding to the beam training. To overcome the challenges of directional link setup, the PCP/AP uses its beacon sweep during the BTI, as an initiator sector sweep for all stations. To this aim, SSW frame specific control fields are added to the beacon frame. To allow multiple stations to respond to a beacon sweep without coordination, the A-BFT interval implements a contention based response period. The A-BFT reserves channel time for multiple responder sector sweeps (A-BFT slots) from the stations. An overview for the association beamforming training during BTI and A-BFT is shown in the upper left part of Figure 3.8. Each A-BFT slot consists of a fixed time allocation for a number of SSW frames (transmitted by the connecting station) and one SSW feedback frame sent by the PCP/AP as depicted in the lower part of Figure 3.8. Contending stations randomly select which slot to access.

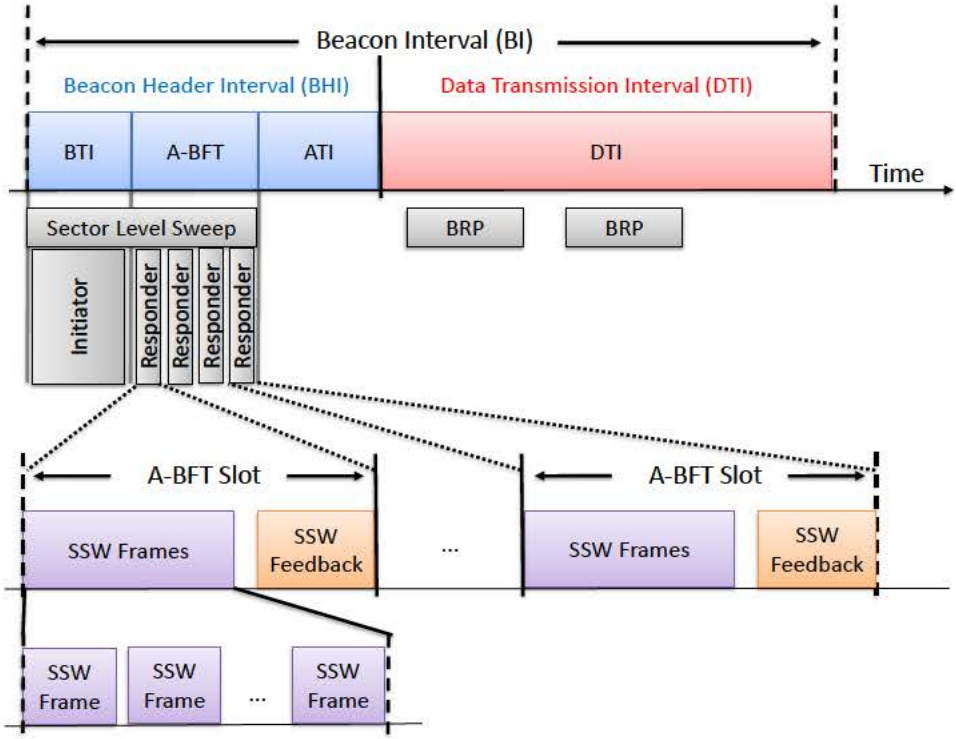

Figure 3.8: Association beamforming training.

The contention process during an A-BFT does not apply carrier sensing. Instead, a collision is detected by a missing SSW Feedback frame from the PCP/AP. In addition, a station might be unable to finish its sweep because its sectors exceed the number of SSW frames per slot. To handle such cases, several measures can be taken. First, the PCP/AP can answer an incomplete sweep with a SSW Feedback frame, forcing the selection of a potentially sub-optimal transmit sector. Second, a station might contend for further slots during the A-BFT in the same or a

following BI. To resolve congestion of the association beamforming training interval, a station has to wait for an additional number of back off slots when its retries exceed a given limit. Also, the beam training can be moved into a dedicated SP by the PCP/AP, according to the procedures described in Section 3.1.8.2. BRPs for the links between the PCP/AP and stations are scheduled in the DTI, as indicated in the upper right part of Figure 3.8. A PCP/AP can announce an A-BFT for receive sector training. Hereby, the slot size indicates the number of receive sectors that the PCP/AP trains and associating stations transmit the according number of SSW frames.

3.1.8.2 Beam Training in the Data Transmission Interval

Beamforming training during the DTI can be initialized following two different methods. First, the initiator can directly begin a sector level sweep when it gains control over the channel. This method is required during CSMA/CA access. Second, the PCP/AP can convey beam training parameters between two nodes, during dynamic or pseudo-static channel allocation. Using the second mechanism, the PCP/AP learns about the pending beam training and can integrate that information into the scheduling process. For direct beam training initialization, a station that seized the channel initiates the beamforming process with a transmit sector sweep to the responder. However, if the initiator intends to start a receive antenna training, additional signaling is necessary. In that case, the initiator inquires the number of receive sectors at the responder via the PCP/AP or higher level protocols. Then, to initialize the SLS, a Grant/Grant-ACK exchange is used to request a receive sector sweep. Following that, both nodes start the training after the Grant-ACK frame. During contention based access, short inter frame spacing between beamforming frames ensures no other node wins a transmit opportunity and causes interference. Beam training via the PCP/AP during pseudo static channel allocation is requested with the initial traffic specification that is transmitted. The beam training parameters are included by the PCP/AP in the extended schedule element that announces the first allocation, which causes both nodes of a traffic stream to commence training at the beginning of their first allocation. To initiate beam training via the PCP/AP during dynamic channel allocation, a node requests an allocation to the beam training partner. In its corresponding SPR frame, the initiator indicates the parameters for the intended training. When granting the corresponding allocation request, the PCP/AP includes the beam training parameters into the Grant frames sent to both stations involved in the allocation. Beam refinement during the DTI typically follows immediately after a SLS. The initiator uses the SSW ACK frame to request transmit or receive training as described in Section 3.1.7.2. A station that seized the channel can also initiate a standalone BRP using a BRP setup phase. To request mandatory beam refinement transactions only, the setup phase comprises a single BRP frame initiating the refinement sequence.

3.2 Performance Analysis of Millimeter Wave Networks

Consumer-grade devices for millimeter wave wireless networks require significant technological advances compared to 802.11n/ac networks operating in the traditional 2.4 and 5 GHz ranges. Devices based on the recent 802.11ad amendment [39] for operation in the unlicensed 60 GHz band must be able to handle 2.16 GHz wide channels and use directional beamforming antennas to overcome the increased attenuation at these frequencies. With the central role of directional communication in millimeter wave systems, the ability to steer its directional beams becomes essential. As the size of antennas scales with the wave length, millimeter wave systems can integrate antenna arrays with a high number of elements even into small handheld devices. Theses antenna arrays allow electronic configuration of the antennas' beam direction and provide very high directional gain. In contrast to lower frequency beamforming mechanisms, millimeter wave systems usually rely on beam steering via codebooks of predefined beam patterns that implement different directions, which reduces the complexity of transceivers and of the beam training process.

As at the moment no 802.11ad compliant devices are comercially available, it is unclear to which degree such systems will cope with the challenges implied by millimeter wave communication. This especially applies to the beamforming capabilities of millimeter wave antenna arrays. While arrays with a modest number of elements have been in use since first generation devices, little is known about their impact on system level network performance. That is, while the transmitters use directional beam patterns, they might not fully achieve the 60 GHz vision of extreme pencil-beam focusing. Thus, it is unclear to what degree practical millimeter wave systems will be able to satisfy the high expectations towards millimeter wave communications. Among these expectations, particularly the vision of high spatial reuse and imperceptible interference (see Section 3.1) is of high interest.

In this section, we investigate the practical limitations of millimeter wave devices to gain insights on challanges and perspectives of IEEE 802.11ad communication. To this aim, first generation millimeter wave devices are analyzed. These systems target mainly static or pseudo static application scenarios like backhaul links (for example the HXI Gigalink 6451 system used in [107]) or transmission of uncompressed high definition video data [90]. With formation of the WiGig Alliance [26], the latter use case broadened to docking station applications and finally incorporated general Wi-Fi use cases when, in 2012, WiGig was merged into the IEEE 802.11ad amendment. Our analysis focuses on devices compliant with the WiHD [12] and WiGig [26] standard. Thus, as the tested systems are based on predecessor standards to the IEEE 802.11ad [59], the presented results are expected to also hold for upcoming 802.11ad devices.

Existing work studied several *individual factors* that millimeter wave system address regarding both the characteristics of 60 GHz communication—fading [54], reflections [100], frequency selectivity [103], and multipath effects [106, 108]—as well as the design of hardware such as phased antenna arrays [8, 28, 48, 104]. However, little is known about the performance of entire millimeter wave networks with electronic beam steering. Available literature is basically lim-

ited to anlysis of consumer-grade 60 GHz devices in terms of impact of human blockage [90] and transmission range [107]. Thus, many open questions remain, with the following being of particular interest for the 60 GHz vision:

A. **Directional communication.** How directional are consumer-grade phased antenna arrays? How large is the actual impact of side lobes?

B. **High spatial reuse.** How close can devices operate without experiencing collisions? How strong is the impact of interfering reflections?

C. **High data rates.** Which coding and modulation schemes are feasible? How efficient is aggregation?

In the following, we provide answers to these central questions. To this end, we use a down-converter to overhear and analyze the communication of 60 GHz devices. This gives us unprecedented insights into link utilization, beam patterns, and frame level operation. Otherwise such details are unavailable since existing devices behave as black box devices.

The remainder of this section is structured as follows. First, details on the tested devices and our measurement setup are provided. Then the details of our measurement campaign are presentend together with the obtained results. Finally, a discussion about the findings relates them to the millimeter wave vision and presents expected challenges and trends for IEEE 802.11 networks.

3.2.1 Measurement Setup

In this section we present details of the evaluated 60 GHz systems and our measurement equipment. Further, we describe the setups for the frame level analysis, beamforming, reflection and interference measurements.

3.2.1.1 Devices and Measurement Equipment

We evaluate two different millimeter wave systems in order to analyze their behavior and performance in real-world settings and investigate inter-system interference. At the time of writing, none of the off-the-shelf 60 GHz system allows access to any significant MAC or PHY level information. Hence, we use a 60 GHz down-converter together with an oscilloscope to overhear the communication.

Devices Under Test. Our first device under test is the Dell D5000 wireless docking station, which follows the WiGig standard. The docking station allows connections by Dell notebooks equipped with a compatible WiGig network card and antenna module. We use Latitude E7440 notebooks as remote stations. The system can connect multiple USB3 devices using the wireless bus extension (WBE) protocol, as well as multiple monitors. The serviced area with best reception is in a cone of 120 degree width in front of the docking station. In indoor environments, over short link distances,

and with reflecting obstacles, we found it, however, to perform over a much wider angular range. The maximum achievable distance depends on the environment and fluctuates between 12 and 18 meters. During disassembly, we found that both docking station and notebook module are manufactured by Wilocity. Both, receiver and transmitter comprise a baseband processing chip connected to a 2x8 element antenna array that itself is directly connected to another chip, which is most probably responsible for PHY processing. The docking station comes with an application that provides limited configurability (e.g., channel selection) as well as PHY data rate readings.

The second evaluated system is a WiHD-compatible DVDO Air-3c system for the transmission of High-Definition Multimedia Interface (HDMI) data streams. The system has transmitter and receiver modules that do not allow for any configuration and do not provide link state information. When testing the transmission range and link stability, we found that it performs much better than the D5000 docking station. In an indoor environment, we could transmit video over a distance of 20 meters, with a 90 degree misalignment and blockage on the direct path. Upon disassembly, we found on both sides of the link a 24 element antenna array with irregular alignment in rectangular shape.

Measurement Equipment. To collect data for frame level analysis and received signal power measurements, we use a Vubiq 60 GHz development system in conjunction with an Agilent MSO-X 3034A oscilloscope. We use this setup to obtain traces of the analog I/Q output of the Vubiq receiver. These traces allow us to extract the timing and amplitude of different frames. The frontend supports down conversion of 1.8 GHz modulated bandwidth at the common IEEE 802.11ad/aj frequencies [67]. Different horn antennas can be attached to the WR-15 wave guide connector of the Vubiq system to achieve different levels of directivity compared to the wide beam pattern of the system when used with an open wave guide. While we use the open wave guide for protocol analysis, for beam pattern measurements we use a 25 dBi standard gain horn antenna.

3.2.1.2 Measurement Setup

In the following, we explain the setup of the four measurement studies that we present in this chapter, namely, the analysis of the frame level protocol operation, beam patterns, interference, and reflections.

Frame Level Protocol Analysis. In order to gain insights into the protocol operation of the devices under test, we down-convert their signals to base-band frequencies and analyze them in Matlab. To this end, we use the wide reception pattern of the open wave-guide of the Vubiq system. This allows us to overhear the frames of both the transmitter and the receiver.

For the Dell D5000 case, we use the laptop as the transmitter and the docking station as the receiver. To identify which frames come from which device, we place the Vubiq down-converter behind the docking station and point it towards the notebook's lid. As a result, the down-converter receives the frames of the notebook via a direct path, and the frames of the docking station via a reflection from the notebook's lid. Thus, the average amplitude of the notebook frames is larger

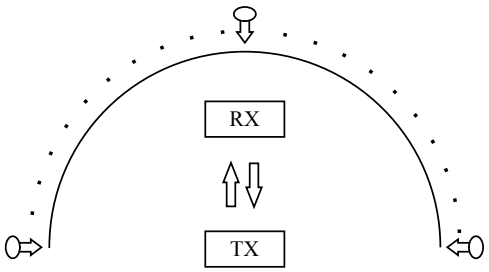

Figure 3.9: Beam pattern analysis setup.

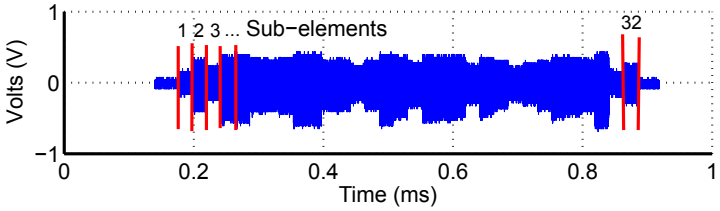

Figure 3.10: Dell D5000 device discovery frame.

than the one of the docking station frames, and we can easily separate them. We use Iperf[1] to generate Transmit Control Protocol (TCP) traffic on the WiGig link that connects the laptop with the Ethernet adapter at the docking station. We run the Iperf server on the laptop and the Iperf client on a second system connected via Ethernet to the docking station.

For the wireless HDMI case, we place the Vubiq down-converter close to the transmitter. No reflector setup is needed since the frames of the receiver inherently have a larger amplitude. Again, we post-process the collected signal traces in Matlab to analyze their structure. We carry out most of the trace analysis using automated algorithms. However, we also use manual inspection to draw some of our conclusions in Section 3.2.2.1.

Beam Pattern Analysis. To analyze the directivity and side lobes of the antenna patterns, we use the Vubiq system with a highly directional horn antenna as described in Section 3.2.1.1. By aligning this setup to the device under test, the impact of the second device in an active link is almost imperceptible, which allows for accurate beam pattern measurement. As beam patterns change once data transmission starts after link initialization, we also measure the patterns of trained links.

We measure the beam pattern in the azimuthal plane on 100 equally spaced positions on a semicircle with radius 3.2 m. To this aim, we rotate the complete measurement setup, which consists of the Vubiq frontend and the oscilloscope, along all measurement locations, and collect signal traces at each position. Figure 3.9 shows our setup. We place the device under test in the center of the semicircle, and ensure a clear line of sight between transmitter and receiver throughout the experiment to prevent unwanted beam training. Due to the high directivity of the

[1] https://iperf.fr/

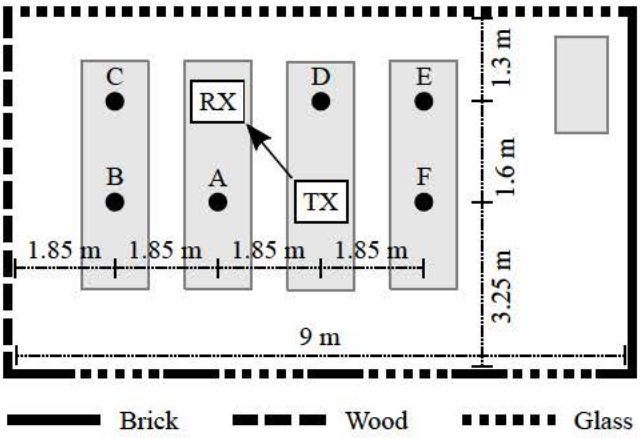

Figure 3.11: Reflection analysis setup.

horn antenna that we use, we found that the most powerful data frames always belong to the device under test. When processing the frame traces, we further ensure that we extract signal strength from data frames only and discard the periodic control frames (which are transmitted with higher power and with wider antenna patterns). The signal strength in every location is then averaged over the filtered frames recorded over the span of one minute.

Further, we analyze the device discovery behavior of the Dell D5000 docking station. When disconnected, the system frequently emits a device discovery frame that is transmitted over multiple antenna patterns to cover an area as large as possible. An example for this frame type is shown in Figure 3.10. It can be seen that the frame consists of 32 sub-elements, each with relatively constant amplitude. Each of these sub-elements is transmitted with a different antenna configuration. As the pattern sequence of the sub-elements is the same for all frames, we can measure them using the same averaging approach as for active data transmissions. We then split the frame into its sub-elements during post processing to find the beam pattern of each sub-element.

Reflection Analysis. Next, we analyze the impact of reflections in a realistic wireless setting. This addresses the common assumption that 60 GHz reflections are very limited compared to the 2.4/5 GHz case, and result from quasi-optical propagation in the direction of transmission. To this end, we set up a single 60 GHz link in an empty conference room, either using the D5000 or the WiHD system. We then measure the energy received from all possible directions at six different locations $\{A \dots F\}$ in the room, as shown in Figure 3.11. If no reflections occur, we expect to receive energy only from the direction in which the transmitter is located. For instance, at location A in Figure 3.11, we should only observe energy coming horizontally from the right. Additional lobes in the corresponding angular profile indicate reflections. To analyze the impact of different materials, we perform the experiments in a room which has brick, glass, and wood walls. Figure 3.11 shows the material layout. To measure the angular profile at each location, we mount the Vubiq receiver on a programmable rotation device and place it at each of the six locations in Figure 3.11. Moreover, we attach a highly directional horn antenna to the receiver.

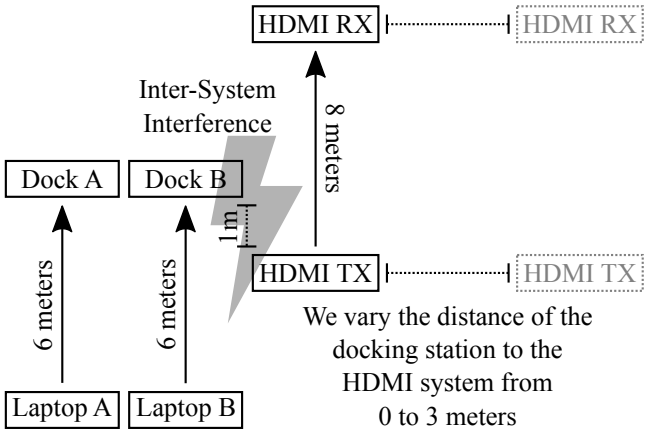

Figure 3.12: Interference analysis setup.

At each location, we then measure the incident signal strength in each direction and assemble the result to an angular profile.

Interference Analysis. To analyze how interference affects 60 GHz communication, we operate multiple 60 GHz systems in parallel on the same channel. In particular, we use two pairs of notebooks connected to D5000 docking stations and the DVDO Air-3c WiHD system, as shown in Figure 3.12. The Dell D5000 systems do not interfere with each other since they use CSMA/CA to share the medium. However, we use two of them in parallel to increase wireless medium utilization, and thus raise the probability of observing interference with the WiHD system. Since the WiHD system does not use CSMA/CA, it blindly transmits data causing collisions and retransmissions at the D5000 systems. That is, the inter-system interference in Figure 3.12 is due to the impact of the "HDMI TX" on "Dock A" and "Dock B". We set the distance between the WiHD transmitter and receiver to eight meters to ensure that the transmitter transmits frames with sufficiently high power. A scenario comparable to this setup could be caused for example by two close-by mm-wave systems connected to different access points in a multi-AP network. Further, we vary the horizontal distance between the D5000 and the WiHD system in the range from 0 to 3 meters to analyze the impact of the interference incident angle. As we found that the WiHD system transmits with a much wider antenna pattern than the D5000, this procedure creates interference whenever a side lobe of the D5000 system matches the interferers direction. To measure the effect of interference we measure link utilization, reported link rate and the time of transmission of a file with a size of 1 GB. To obtain link utilization measurements we collect seven minutes of channel traces and use a threshold based detection approach to calculate the ratio of idle channel time. While the formerly described reflection analysis allows us to assess the existence and strength of reflections, we use a second setup to determine the impact of those reflections on data transmissions. In particular, we set up two geometrically non-interfering 60 GHz links close to a metal reflector, as shown in Figure 3.13. To eliminate the influence of side lobes on the measurement, we position shielding elements close to the WiGig devices. Further, we make sure that we

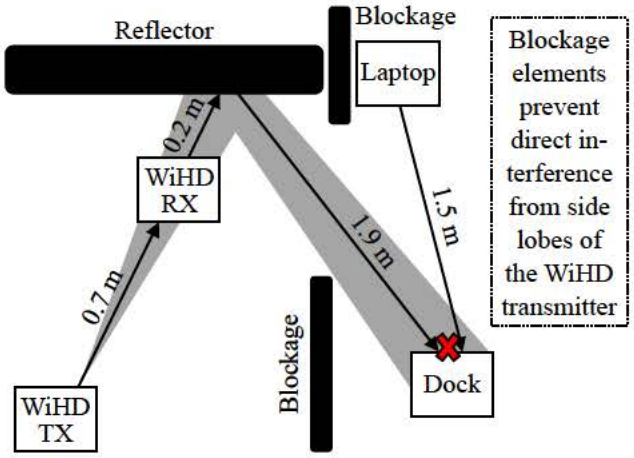

Figure 3.13: Reflected interference: Measurement setup.

do not block the reflected signal resulting from the metallic surface behind the WiHD receiver. We then analyze the coverage area of this reflection using the Vubiq transceiver to ensure that the docking station is located inside. Finally, we perform a TCP throughput measurement, with frame flow from the laptop to the docking station. By powering on and off the WiHD devices, we can evaluate the impact of the reflected signal on the WiGig TCP connection.

3.2.2 Results

In this section we present the results of our measurements using the setups described in Section 3.2.1. We first present our findings on protocol operation and data aggregation. Second, we analyze the beamforming capabilities of the D5000. Third, we investigate the impact of reflections. Finally, we evaluate the interference between WiGig and WiHD, including reflections.

3.2.2.1 Protocol Analysis

We study the flow of frames between the devices under test using the Vubiq receiver. In particular, we analyze the frame structure of both the D5000 and the WiHD system, as well as the frame length and the burst length of the D5000. The latter allows us to get insights on the impact of data aggregation.

Dell D5000. The Dell D5000 follows the WiGig standard. This is particularly interesting since the later versions of the standard are closely related to the IEEE 802.11ad amendment. Hence, the behavior of existing consumer-grade WiGig devices reveals the issues that future devices based on IEEE 802.11ad will face. The WiGig protocol description is not freely available, but we observe that it consists of three phases, namely, device discovery, link setup, and data transmission. In the first stage, the docking station emits a characteristic device discovery frame that is transmitted over several quasi omni-directional beam patterns shown in Figure 3.10. The frequency of these beam sweep frames is given in Table 3.2. A detailed beam pattern analysis of this frame follows

Frame type	Frequency
D5000 Device Discovery Frame	102.4 ms
D5000 Beacon Frame	1.1 ms
WiHD Device Discovery Frame	20 ms
WiHD Beacon Frame	0.224 ms

Table 3.2: D5000 and WiHD frame periodicity.

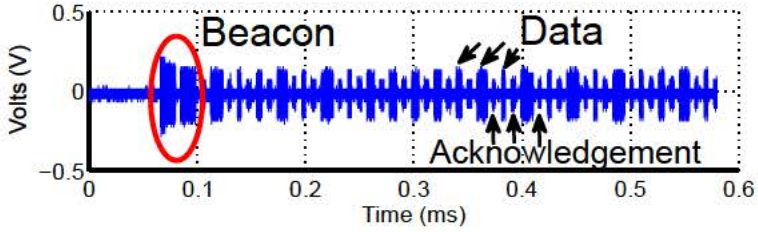

Figure 3.14: Dell D5000 frame flow.

in Section 3.2.2.2. At the second stage, a complex association and beamforming process between dock and remote station takes place. Finally, when the link is set up completely, data transmission begins.

Our frame level analysis shows that the data transmission phase contains bursts, similarly to the IEEE 802.11ad EDCA TXOP (see Section 3.1.6.1). The maximum length of such bursts is 2 ms. Each burst begins with two control frames, which have a different amplitude than the subsequent series of data and acknowledgment frames, as shown in Figure 3.14. These control frames are likely an RTS/CTS exchange, which is crucial due to the deafness effects resulting from the directional transmission (see Sections 1.3.2 and 3.1.6.1). Outside the bursts, the channel is idle except for a regular beacon exchange between the docking station and the notebook. The transmission frequency of these beacons is given in Table 3.2.

To study data aggregation, we measure the length of data frames for different TCP throughput values. We control the TCP throughput by adjusting its window size in Iperf. Figure 3.15 depicts the Cumulative Distribution Function (CDF) of the frame lengths for each throughput value. The CDF reveals that frames are either short (around 5 μs) or long (15 to 20 μs). The length of long frames varies more than the length of short frames, which may be due to different levels of aggregation. The highest level we observed corresponds to a frame duration of 25 μs. Further, the amount of long frames *increases* with throughput—the higher the traffic load, the more data aggregation. This matches Figure 3.16, which shows the fraction of long frames, i.e., longer than $\approx$ 5 μs, for increasing throughput values. Further, we investigate the level of medium usage for increasing throughput values. Surprisingly, Figure 3.17 shows that, beyond a relatively low throughput value, all oscilloscope traces contained data frames. That is, the transmitter transmitted *continuously*. Hence, the throughput increase is not due to a higher medium usage but either due to a higher MCS, or a higher level of data aggregation. Figure 3.18 answers this question—it

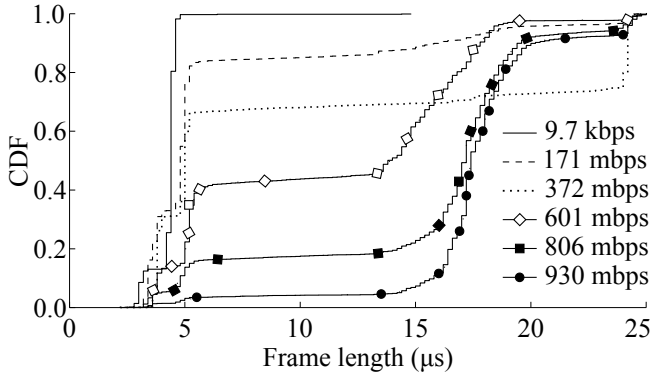

Figure 3.15: WiGig data frame length.

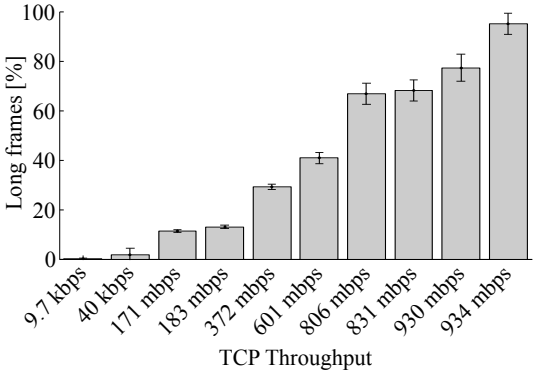

Figure 3.16: Percentage of long frames in WiGig.

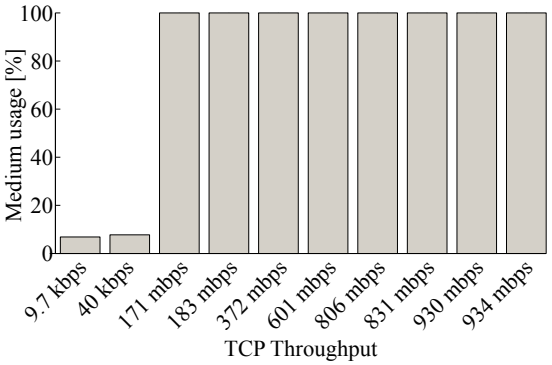

Figure 3.17: WiGig medium usage.

shows the raw physical layer data rate reported by the D5000 driver over a timespan of ten minutes. For short links, Figure 3.18 shows that WiGig uses a very high MCS. This explains the low link usage for 9.7 and 40 kbps in Figure 3.17, which were also measured at a short distance. Further, it suggests that the MCS is not adapted to the link load. Hence, it is most likely that high throughput values are achieved exclusively by means of data aggregation, as the MCS only depends on the signal strength. At the same time, this comes at the expense of continuously using the medium even for medium throughput values as aggregation is only increased under heavy load. We expect the reason for this behavior to be to limit delay for the higher level protocols. Especially, as TCP is sensitive to long transmission delays, excessive aggregation of frames might reduces TCP performance. Further, as described in Section 1.3.3 frame aggregation increases chances for bit errors in long frames and can cause significant retransmission overhead. Adapting the amount of frame aggregation to the link load, is thus an important measure to balance 60 GHz communication between throughput and reliability. Figure 3.18 also shows the impact of the link length on the physical layer rate. As expected, the longer the link, the lower and unstable the data rate. Unless indicated otherwise, we carry out all of our experiments for links below two meters. Interestingly, the rate reported by the WiGig driver matches the MCS levels defined in

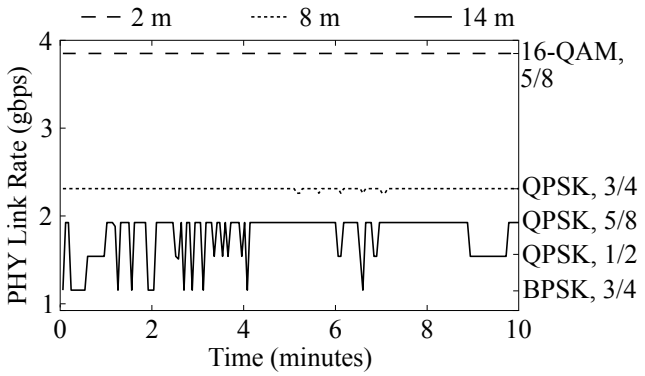

Figure 3.18: MCS with low traffic.

the standard for single-carrier mode (see [26] and Section 3.1.4), which suggests a direct relation. Figure 3.18 includes the MCS that corresponds to each of the rates we measure. While we reach 16-QAM with 5/8 coding—the second highest MCS in the standard—we never observed the highest MCS. We measure the rates in Figure 3.18 in a stable environment without mobility. Naturally, our results are mostly constant for short link lengths. Still, Figure 3.18 only shows a relatively short time interval. Figure 3.19 depicts the rate and amplitude under similar conditions for roughly one hour. In this case, we observe that the link rate varies occasionally. Moreover, this occurs precisely when the signal amplitude changes. Since the environment is constant, such amplitude variations are most probably due to a beam pattern realignment. This suggests that rate adaptation and beam pattern selection are implemented as a joint process in the Dell D5000 system.

DVDO Air-3c. Next, we analyze the frame flow for the DVDO Air-3c WiHD system. We observe the same communication stages as for the Dell D5000 system. The frequency of device discovery frames transmitted by the WiHD devices is given in Table 3.2. When analyzing the data transmission stage, we found the beacon frame frequency to be much higher than for the D5000 system. Also the data transmission process significantly differs. Figure 3.20 shows an example frame flow for the WiHD system. In contrast to the D5000, there is no clear data/acknowledgement frame exchange. Instead, the transmitting device emits data frames of variable length following periodic beacons of the receiver. Whenever no data is queued for transmission, we only observe beacon frames. The trace shows the transition from an active video data transmission period to an idle period. The WiHD system does not seem to perform channel sensing, which has a significant impact regarding interference (c.f. Sections 3.2.2.3 and 3.2.2.4).

Our results show that data aggregation is key for 60 GHz communication. In particular, we observe that aggregation improves throughput from 170 *mbps to* 930 *mbps, i.e., a* $5.4\times$ *gain. Our measurements also suggest that links become unstable and often break before the transmitter switches to the lower MCSs defined in the standard. Finally, link rates may fluctuate even in static scenarios due to beam pattern realignments.*

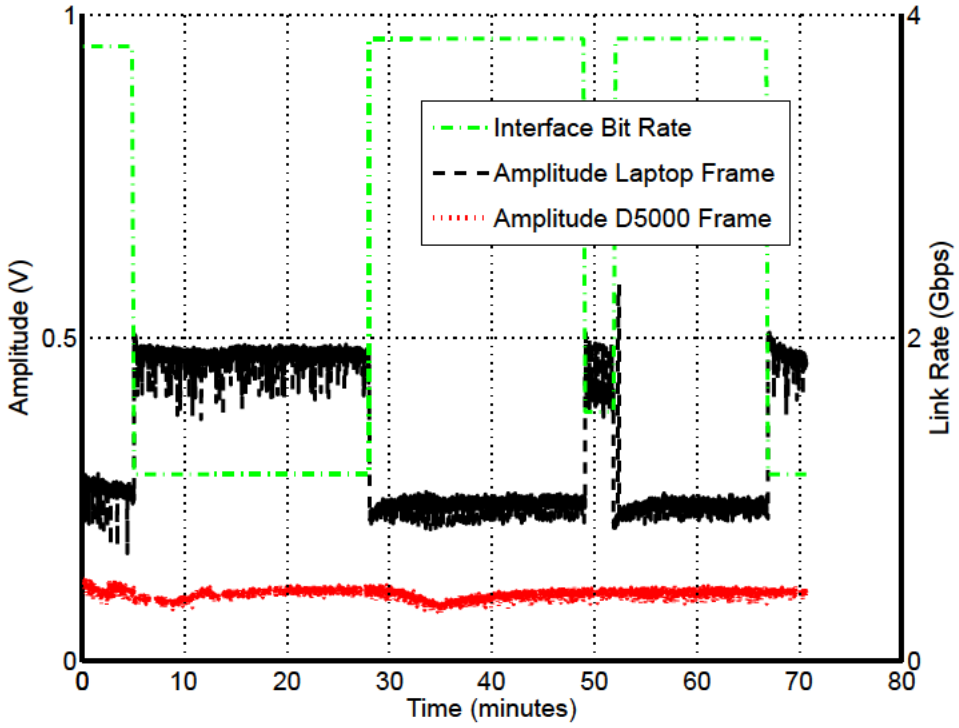

Figure 3.19: Dell D5000 frame amplitudes and rate.

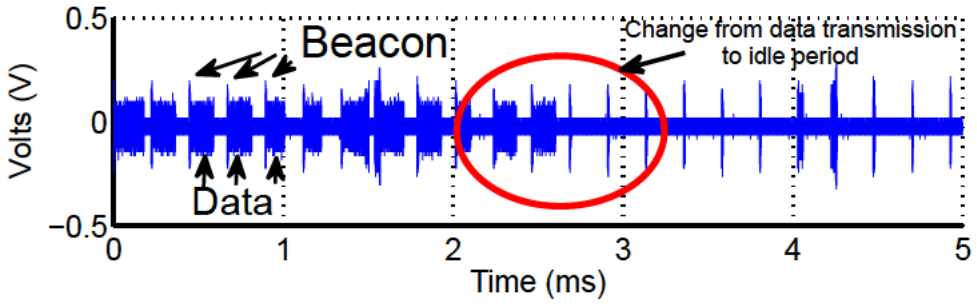

Figure 3.20: DVDO Air-3c WiHD frame flow.

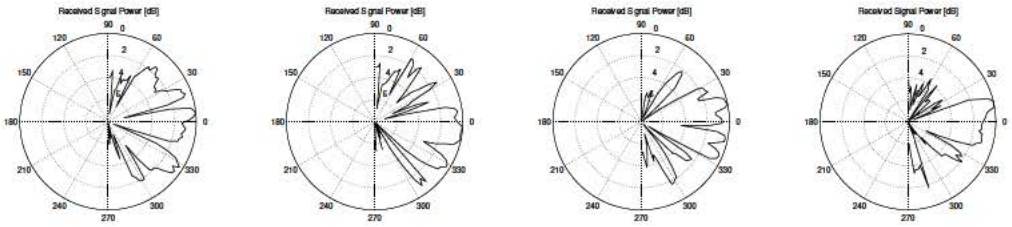

Figure 3.21: Quasi omni-directional beam patterns swept by the Dell D5000.

3.2.2.2 Beam Patterns

Next we present the measured antenna patterns for the D5000 system. First, we discuss our findings on quasi omni-directional communication during device discovery. After that, we analyze the highly directional patterns used during the data transmission stage.

Quasi Omni-directional Search. Implementation of omni-directional antenna patterns is a major challenge for millimeter wave communication [28]. However, this kind of pattern is needed for device discovery and beam training, see Sections 3.1.5.1 and 3.1.7. The Dell D5000 system sweeps 32 different quasi omni-directional patterns during its remote station search before the link setup. Each of these patterns is used during a sub-element of the device discovery frame. The device discovery frame is continuously repeated by the D5000 until a connection is established.

Figure 3.21 shows four out of the 32 different antenna patterns that the D5000 sweeps during link establishment. While the Half Power Beam Width (HPBW) (angular width before the signal strength is reduced by 3 dB) can be as wide as 60 degrees, each pattern contains several deep gaps that may prevent communication with devices at this specific angle. The remaining 28 patterns are comparable in terms of directional focus and received signal power. The device discovery frame of the WiHD system also sweeps several quasi omni-directional beam patterns. However, their order changes with every transmitted device discovery frame. Hence, measuring the beam patterns with our setup is not practicable. *Device discovery in 60 GHz systems proves to be a challenging process. We find that the two systems that we test repeatedly sweep multiple quasi omni-directional beam patterns to reliable reach a pairing device. In particular, one of the systems sweeps as many as 32 different quasi omni-directional patterns.* **Directional Transmission and Side Lobes.** Next we evaluate the beam pattern used by the D5000 system during the data transmission stage. There, in contrast to the device discovery frames during the link setup, highly directional antenna configurations are used. Figure 3.22 shows the measured transmit patterns of a Dell E7440 notebook and the D5000 docking station. The patterns are of highly directional nature with a HPBW below 20 degree. Despite the strong signal focus, significant signal energy is measured from side lobes. These side lobes can have a transmit power in the range of -4 to -6 dB compared to the main lobe, and thus can cause major interference effects. The asymmetry of the pattern—especially for the notebook—results from the antenna being placed at the side of the notebook's lid.

In a second measurement we introduce a misalignment of 70 degrees between docking station

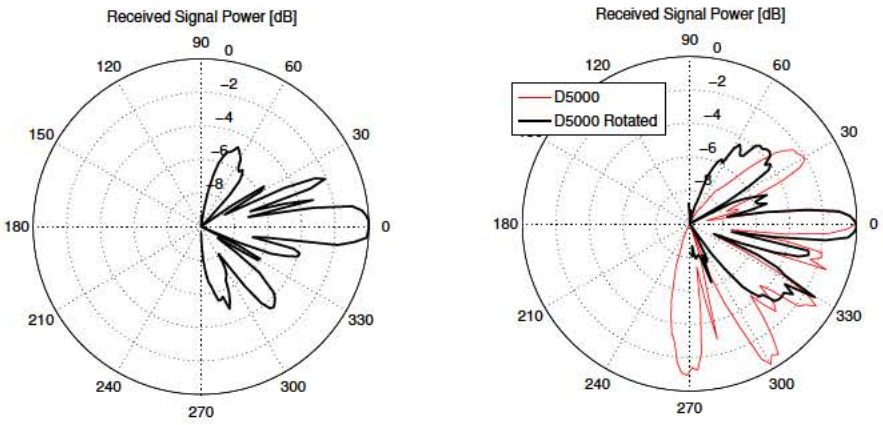

Figure 3.22: Laptop (left) and D5000 (right) beam patterns. Main lobe points always to 0 degrees.

and notebook. Figure 3.22 shows the resulting docking station beam pattern as an overlay. While measuring this pattern, we had to increase the receiver gain by 10 dB. That is, beamforming towards the boundary transmission area of the antenna array significantly reduces link gain. Also, we observe a much higher number of side lobes as strong as -1 dB with respect to the main lobe.

While antennas are already highly directional for first generation 60 GHz devices, strong side lobes exist. Further, the specific placement of the antenna inside a device has a noticeable impact on the antenna pattern. When beamforming close to the outer limit of an array's transmission area, directionality is reduced and the number of strong side lobes increases significantly.

3.2.2.3 Reflections

In the following, we present our reflection results for the setup shown in Figure 3.11. Figures 3.23 and 3.24 depict the angular profiles that we measure for the D5000 and the WiHD system, respectively. In both cases, most angular patterns have at least two clearly identifiable lobes—one pointing to the transmitter and one pointing to the receiver. The reason for the latter is that the receiver not only receives data frames but also transmits the corresponding acknowledgments. However, a significant number of angular patterns features additional lobes that do not point to any of the devices in the room. This is a clear indication of reflections off the walls. In contrast to common assumptions regarding 60 GHz communications, the lobes show a significant amount of incident energy. For instance, the angular pattern at position F in Figure 3.23 has a lobe directly pointing to the lower wall. Geometrically following the reflection of the signal off the nearby window suggests that this lobe is due to the transmitter. Further, the angular pattern at position B features a lobe pointing towards the wooden wall. However, this lobe can only arise from a *second order* reflection originating at the receiver, and bouncing off both the glass wall as well as the wooden wall. In comparison to the D5000, the WiHD system results in similar effects. However, the angular patterns in Figure 3.24 feature more and larger lobes than in Figures 3.23. This suggests that the WiHD system is less directional than the D5000, and thus results in sig-

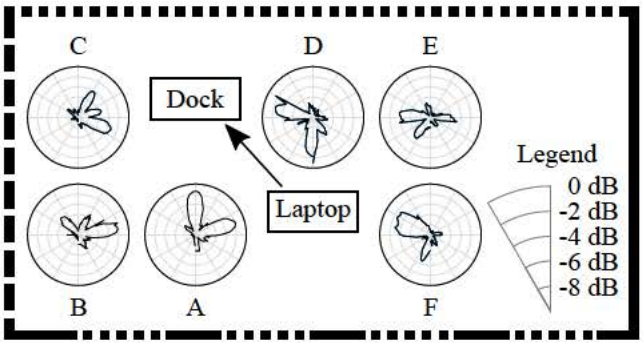

Figure 3.23: Reflections for Dell D5000.

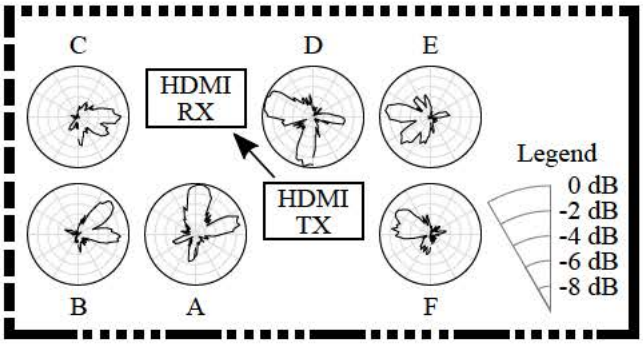

Figure 3.24: Reflections for DVDO Air-3c WiHD.

nificantly more reflections. As a result, the impact on spatial reuse is even higher. This matches earlier observations throughout our measurement campaign. In Section 3.2.2.4, we analyze this effect in detail.

Reflections are strong and may thus undermine the alleged spatial reuse of 60 *Ghz systems. Moreover, second order reflections occur and may have a large impact.*

3.2.2.4 Interference

In this section, we analyze the cross platform interference between the WiGig compliant Dell D5000 docking solution and the WiHD system. Both systems are forced to operate on the same channel, leading to imperfect channel usage coordination and interference. While the directionality of 60 GHz communication is supposed to severely limit interference we analyze two aspects of electronically steered indoor systems that can break this assumption. First, interference caused by the severe side lobes identified in Section 3.2.2.2 is analyzed by a setup with WiGig and WiHD devices operating in parallel. Second, we investigate the effect that can be caused by strong reflections as described in Section 3.2.2.3. To this aim, a combined setup of WiGig and WiHD devices is used, where the direct path between the two device classes is shielded. The measurement setups for both experiments are described in Section 3.2.1.2. We begin this section with the description

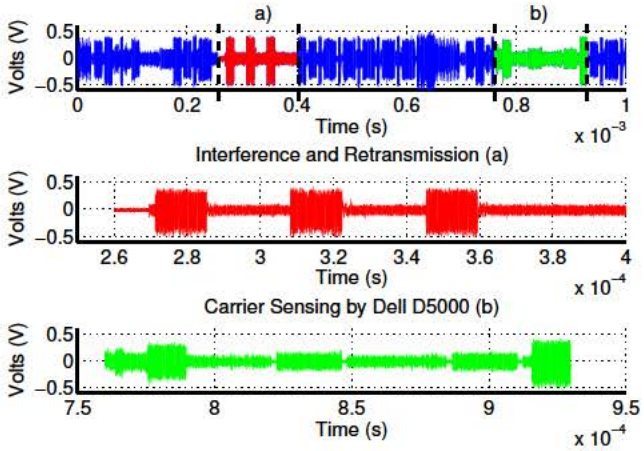

Figure 3.25: Inter system interference effects.

of frame level effects observed for the interfering links which are the same for both setups. Then, details on the impact of link performance are given.

Effects observed in frame level analysis. From a frame level analysis of the traffic flow between two interfering links, which follow different communication standards, we distinguish the following four different cases. First, data transmission of one system may occur during an idle period of the other system. In this case, there is a minor impact from the beacon frames transmitted by the interfering system, but we do not observe frame retransmissions or increased link utilization. Second, due to highly directional beam patterns, data streams may coexist without provoking retransmissions on the Dell D5000 link. Third, when links are close by, the D5000 shows enlarged data transmission gaps that are occupied by frames of the WiHD system. We assume this to be caused by a carrier sensing feature integrated in the Dell D5000. The same effect was found when two docking station links coexist. Finally, for close by links and overlapping transmissions, the D5000 shows missing acknowledgments and delays in the data frame flow. This indicates frame loss and retransmissions. In the latter two cases we also observe increased link utilization.

Figure 3.25 shows an example where both systems operate in parallel. Here, a typical D5000 data frame flow is interrupted by frames from the WiHD system. In particular, we observe collisions between 0.25 and 0.35 ms (first enlarged interval in Figure 3.25). The elevated noise floor indicates the presence of a weakly received WiHD frame, while at the same time D5000 data frames are transmitted. As the acknowledgments for these frames are missing, it is very likely that the three frames are retransmissions due to corrupted packet reception. Further, between 0.76 and 0.95 ms a dense series of WiHD data frames can be found (second enlarged interval in Figure 3.25). This series interrupts the usual D5000 data flow and does not suffer interference from the D5000 for a substantial time period. We attribute this behavior to the aforementioned carrier sensing of the D5000.

Side Lobe Interference Impact. We now discuss the performance impact observed from side lobes for links in a parallel setup (compare Section 3.2.1.2), suffering from inter-system interfer-

ence. The impact is evaluated in terms of observed link utilization, time for transmission of a file on the Dell 5000 system and the link rate reported by the D5000 WiGig driver application.

Figure 3.26 depicts the results for two setups: 1) an aligned D5000 link interfering with the WiHD system and 2) the same setup with the docking station misaligned by 70 degrees (denoted by 'rotated'). In the second setup, the docking station is beam-forming towards the outer limit of its serviceable transmission area and beam-forming performance is significantly worse as shown in Section 3.2.2.2. When comparing link utilization percentages, we find them to be significantly increased in both interference scenarios. We measure the interference free link utilization to be 38% and 42% in the aligned and rotated setup, respectively. Thus, we find a maximum link utilization increase of 62% and 58% for the two interference scenarios, which is significantly higher than the link utilization of the WiHD link alone, that we found to be 46%. The additional increase results from the frame collisions and retransmissions as described earlier in this section.

Even though we use two parallel Dell D5000 docking station links, the link utilization never saturates the channel. Thus, the measured transmission time stayed approximately constant despite retransmissions and carrier sensing induced delays. Therefore, we rely on the link utilization to asses the impact of interference. For higher network densities that saturate the channel and/or higher rate requirements of the wireless applications, interference is expected to have a significant impact on the throughput rate.

The difference of link utilization over the measured interference distances reveals a high interference regime for distances of up to two meters. When further increasing the distance of the second link, utilization reduces but only reaches interference free levels at distances beyond 5 meters. In the high interference regime, link utilization in the misaligned docking station setup is higher by around 10% compared to the between aligned setup. At some measurement locations it reaches values of up to 100% and also shows a strongly varying pattern. For the aligned link we find a strong utilization increase to 97% at an interferer distance of 1.6 meters. We conjecture that this behavior is due to the side lobes that we observe for the data transmission antenna patterns of the D5000 link (compare Section 3.2.2.2). The fluctuating link utilization in the high interference regime for the misaligned link correlates well with its measured beam pattern that shows many strong side lobes. Unfortunately, we can not directly compare measured side lobes to the interference impact as it is not possible to measure receive antenna patterns. Also, since we cannot influence the selection of antenna patterns, it is not possible to ensure that the docking station uses the same pattern for both measurements.

From the reported link rates it can be clearly seen that the misaligned link performs worse due to the reduced beamforming capability at the limit of the antenna arrays transmission area, as explained in Section 3.2.2.2. Further, in the high interference regime below two meters link distance, an inverse correlation between link rate and link utilization is found. We assume the docking station link to adjust the link rate according to Signal to Interference and Noise Ration (SINR) measurements and packet loss statistics, thus the rate decreases under high link utilization that leads to an increase in collisions.

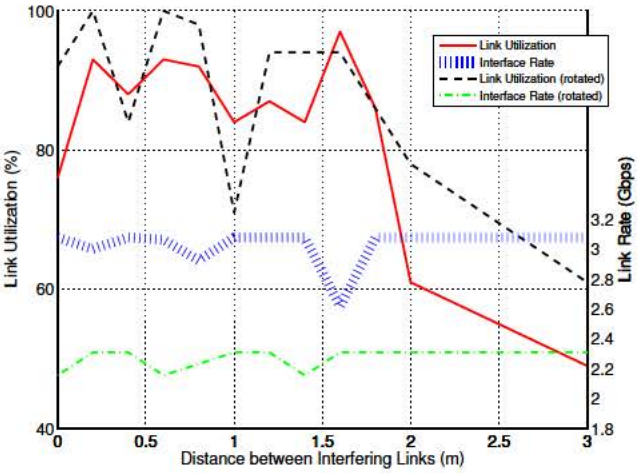

Figure 3.26: Side lobe interference impact.

We find significant impact of inter-system interference on link utilization, especially when interferers with wide antenna patterns are as close as two meters. However, as current millimeter wave links are far from saturating the wireless link, there is little impact on the overall throughput achieved by the end systems. As rate requirements and number of communicating devices increase, we expect to see a significant impact on throughput. We further find increased interference for antenna arrays focusing their beam close to the transmission area boundaries since patterns are less directional. The interference that we observe correlates well with the strong side lobes of the antenna patterns in Section 3.2.2.2.

Reflection Interference Impact. In this section we discuss TCP throughput measurements for a setup of WiGig and WiHD devices suffering inter-system interference via reflected paths. To this aim, we use a setup with a strong reflector. We shield the line-of-sight path between the links to protect from direct path and side lobe interference. The setup is described in Section 3.2.1.2.

The Iperf server used a 250 KByte TCP window and was configured to fully load the underlying Ethernet link, which was tunneled over the 60 GHz wireless link. While the WiGig tunneling managed to provide full gigabit speed for the Ethernet link, we found that it almost completely saturated the link. Most probably, this is because the D5000 system tries to minimize the Ethernet delay. Instead of aggregating data to reduce the medium usage, the transmitter sends a larger number of packets, as discussed in Section 3.2.2.1. Because of this high medium usage, we expect the TCP link to be very sensitive to interference effects. Figure 3.27 shows the Iperf TCP throughput results for our reflection measurement. We observe that the TCP throughput increases after about 90 seconds, which is when we power off the WiHD link. The performance degradation due to the WiHD reflection is about 200 mbps compared to the interference-free transmission. The strongest throughput loss occurs about 20 seconds after the start of the measurement—at that point, the throughput drops by almost 300 mbps. Further, we observe that the throughput fluctuates strongly under interference. Most probably, these variations result from the change of idle and data transmission periods at the WiHD link (c.f. Section 3.2.2.1).

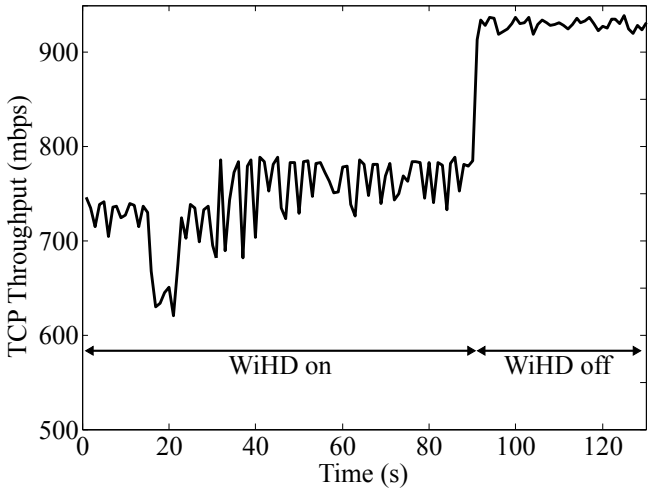

Figure 3.27: Reflection interference impact.

When analyzing the effect of reflections on 60 GHz communication, we find that, apart from an increase of the coverage area, also interference increases. For an isolated experiment setup with direct path blockage between links we find a severe impact on TCP throughput due to inter-system interference. The average throughput reduction was about 20%*, and reached up to* 33%*.*

3.2.3 Discussion

In Section 3.2, we formulated a number of unanswered questions regarding the performance of consumer-grade 60 GHz devices. Our measurements in Section 3.2.2 provide insights which we now use to answer those questions.

3.2.3.1 Findings on First Generation Millimeter Wave Networks

Directional Communication. *How directional are consumer-grade phased antenna arrays?* We show that such antennas suffer from significant side lobes. This means that MAC protocols for 60 GHz networks can not rely on pencil-beam focusing—the actual behavior lies somewhere between a wide and a highly directional pattern. This is challenging, since we can neither resort to existing protocols designed for omni-directional communication nor can we assume that no interference occurs as long as links are not aligned. This hinders protocol designs that would only use location information to determine whether a node can transmit. *How large is the actual impact of side lobes?* Our measurements show that side lobes can be as strong as -1 dB compared to the main lobe for certain beamforming directions. This worsens the above impact on MAC protocol design. In particular, the MAC protocol may need to adapt its operation to the intended beamforming direction. In some cases, a node may even need to switch to a different MAC protocol.

High Spatial Reuse. *How close can devices operate without experiencing collisions?* The minimum distance for our test devices was two meters. Shorter distances are feasible but require

precise receiver positioning between the side lobes of potential interferers, or a MAC protocol that allows nodes to perform TDMA. In other words, the vision of extremely dense networks where nodes can communicate without interference is not feasible with current off-the-shelf devices. To enable this, better consumer-grade antenna arrays are needed. *How strong is the impact of interfering reflections?* We measured up to a 33% TCP throughput loss due to interfering reflections. While this shows the strong detrimental effects, it also hints at the underlying potential. For instance, a network layer protocol may exploit such reflectors in a multi-hop scenario in order to adapt the connectivity graph to the network load. Further, passive reflectors deployed in an indoor environment could help nodes to establish reflected beams that circumvent obstacles. This highlights the importance of 60 GHz protocols being aware of their physical environment.

High Data Rates. *Which coding/modulation schemes are feasible?* We observe physical layer rates up to 3850 mbps, which corresponds to 16-QAM with 5/8 coding. In contrast, 802.11n/ac supports up to 256-QAM. Most probably, this limitation is due to physical layer challenges such as synchronization, which may lead to significant phase noise. *How efficient is aggregation?* Our results show that aggregation is highly efficient, achieving up to a $5.4\times$ gain. While our test device only aggregates data if needed to minimize delay, a better approach may be to vary the level of aggregation depending on the individual requirements of each connection. This would reduce medium usage and thus ease medium access for other devices potentially following a different standard based on a different MAC protocol.

3.2.3.2 Challenges for Future Millimeter Wave Systems

Section 3.2.3.1 discusses our findings on first generation millimeter wave networks and concludes that the visions of pencil-beam communication and extreme spatial reuse as presented in Section 3.1 does not hold without further technological advances. These advances are particularly required at the level of millimeter wave antenna arrays, which still come with a modest number of antenna elements. This results in imperfect beam patterns, which suffer from side lobes and significantly increased interference effects compared to the envisioned millimeter wave scenarios. However, as a side effect, these imperfections result in an expansion of the reception area, which benefits first generation low complexity devices in several ways. First, setup of directional communication between two nodes becomes significantly easier, as initial probing frames have higher chances to reach the pairing devices. In addition to reception over the main lobe, this can happen via a matching side lobe in direction of the receiver or through a reflected paths. Second, due to increased reception area, CSMA/CA mechanisms suffer significantly less from deafness, and can operate close to the behavior of legacy 802.11 networks. As a draw back, parallel transmissions are only possible with widely separated transceiver pairs.

To effectively enable the millimeter wave vision, more advanced antenna arrays are needed which will change the communication conditions in the following ways. Directional patterns will get even narrower and strength of side lobes will be further reduced. While this reduces direct interference effects between devices, it will also further reduce the number of reflections

that are created as byproduct of directional transmissions. Because of this, the coexistence of parallel non interfering wireless links is boosted even for close by devices. Unfortunately, this will remove the earlier mentioned coordination benefits resulting from an increased coverage area which complicates millimeter wave protocol design. From our findings on first generation devices, we identify two key challenges that need to be addressed, namely the *setup of directional links* and *the impact of deafness on the CSMA/CA mechanism*.

Setup of Highly Directional Links. Stronger directional focus is required to reach the 60 GHz vision of extreme spatial reuse. This will result in increased beam training overhead as first generation devices rely on beam pattern imperfections and reflections to increase the chances of probing frame reception. For next generation millimeter wave networks with highly directional focus, establishment of directional communication links will become more challenging. This will manifest in two ways. First, due to higher directionality, more virtual antenna sectors will have to be defined to cover the entire service area of an antenna array. Each of theses sectors needs to be probed during the link setup phase causing increased signaling overhead. While defining wider patterns could be an alternative for initial link setup, this will later on require increased refinement overhead. Also, wider patterns will not bring sufficient antenna gain to reach distant devices. Second, the increased beam training messaging creates higher interference impact on parallel transmissions. This intensifies, when less reflections and side lobes of highly directional networks reduce link stability in mobile networks and require constant retraining.

CSMA/CA Deafness Effects. Higher directional focus will significantly increase the deafness effect on CSMA/CA coordinated millimeter wave networks. While this is required to increase the number of parallel operating stations in a network, particular attention has to be taken to maintain operability of the most popular medium access scheme for Wi-Fi communication. Our study shows that side lobes and reflections play an important role for first generation millimeter wave networks. These effects lead to significant interference problems but also increase the reception area of frames outside the expected main beam areas of directional links. With the evolution of millimeter wave antenna arrays this behavior will change towards the envisioned pencil-beam communication paradigm. This severely impacts the performance of CSMA/CA networks, as deafness increases. As has been shown for lower frequency communication [10], deafness causes significant problems for CSMA/CA networks, including excessive backoff behavior. Together with the effects of frame aggregation, which we found to play a central role for millimeter wave networks (see Section 3.2.2.1), we expect significant modifications required to efficiently enable CSMA/CA communication in future highly directional millimeter wave networks.

3.3 Conclusion

In this section we provide in-depth information on the IEEE 802.11ad amendment, which is supposed to become the de facto standard for consumer grade mm-wave networks, which will operate at multiple frequency bands. We highlighted the amendment's hybrid MAC-layer de-

sign that defines three different medium access schemes, CSMA/CA, Polling and TDMA. Each scheme addresses different aspects of mm-wave communication and supports varying quality of service mechanisms, making it suitable for different IEEE 802.11ad use cases. Further, we addressed the elaborate beam training protocol, which enables highly directional communication. The association beamforming training and two level beam training are the fundamental elements of this protocol. First, the association beam training aligns antenna beams between a station and a central network controller when the direction between the two devices is unknown. Second, the two level training reduces the beam training search space using its primary coarse-grained training stage that relies on predetermined virtual antenna sectors. Its second stage further refines the found antenna configuration, varying from predefined sectors and also addresses the challenges of imperfect omni-directional antenna patterns. With fully trained transmit and receive antenna configurations, IEEE 802.11ad reaches its maximum throughput of up to 7 Gbps. In addition, the beamforming protocol supports a training procedure for low antenna gain devices and can convey training parameters to a central network coordinator for channel access scheduling. The combination of the hybrid MAC-layer and the novel beam training protocol is key to satisfying new IEEE 802.11ad use cases and addressing specific device and millimeter wave propagation characteristics.

The newly introduced IEEE 802.11ad mechanisms aim towards a novel communication paradigm for wireless communication. That is, due to high directionality and the adverse propagation effects at 60 GHz significant reduction of interference can be achieved. Under this assumption increased aggregated network throughput can be achieved by parallel transmission with non interfering pencil-beam antenna patterns. In order to compare this vision to current millimeter wave networks the second part of this section presented an in depth study of first generation off-the shelf millimeter wave devices. This identifies challenges for next generation devices and future protocol design. To this aim we focus particularly on frame level protocol analysis, beam pattern measurements and interference studies. Using a 60 GHz down converter we retrieved baseband traces of black box millimeter wave systems that were used to gain insights about the used protocol. This also allowed us to observe frame level effects caused by interference and infer the beam patterns used for several protocol features. Further, we found that the beam patterns applied by the tested devices change significantly throughout the different states of communication. The observed beam patterns reveal three challenges for current millimeter wave communication. First, during the device discovery several quasi omni-directional antenna patterns have to be used, transmitted repeatedly in probing frames. Otherwise reception in the entire transmission area can not be ensured as these patterns suffer from deep gaps in the antenna gain. Second, we find that during highly directional data transmission the antenna patterns include side lobes as strong as -4 dB compared to the main beam. These patterns enable reception in more than just the intended communication direction and increase susceptibility to interference. Last, we found reduced directionality and increased amounts of strong side lobes when focusing the antenna beam at the boundary of the transmission area of an antenna array. These effects, were also confirmed by

measurements to analyze the impact from an interferer using a wide communication pattern.

We conclude that next generation devices will need advanced antenna arrays, to reduce side lobes and reflections, which have an intensified impact due to imperfect beam patterns. Only by these measures, the pencil-beam 60 GHz vision that achieves increased aggregated network throughput by spatial reuse can be realised. Unfortunately, this will come at the cost of a significantly reduced reception area for directional beam patterns. While current systems exploit this effect for stable communication links and reliable coordination message exchange, future systems will not be able to benefit from them. In the discussion in Section 3.2.3.2 we identify two main aspects of 60 GHz communication where this change will have its main impact, the *directional link setup* and *performance of the CSMA/CA access scheme.*

Chapter 4

Multi-Frequency Band Beam Steering

The IEEE 802.11ad millimeter-wave Wi-Fi amendmend promises data rates of up to 7 Gbps via high gain antenna arrays used to overcome the increased attenuation of 20-40 dB at the mm-wave band (see [15, 39, 61] and Section 3.1). In order to achieve the millimeter wave vision of parallel interference free transmissions, extreme antenna directionality is required, as our measurement campaign in Section 3.2 revealed. Thus, in next generation networks, sender and receiver must match the potentially narrow directions of their respective beams. Hereby, IEEE 802.11ad discretizes the search space and divides the antenna radiation sphere into as many as 128 virtual sectors supporting beamwidths of less than 3 degrees. A two stage process is used to select the best sector: first, an exhaustive search to select the best transmit sector is performed by both transmitter and receiver. This first stage is required to established a low throughput but robust link between the pairing devices which is used for further coordination message exchange. As described in Section 3.2.3.2, current millimeter wave devices use relatively wide beam patterns and rely on side lobes and reflections to facilitate the inital link establishment. Future devices however have to remedy these reception area increasing effects as they stand in direct opposition to interference free communication. Instead, the maximum amount of directional sectors has to be probed to ensure connectivity in all possible transmit directions at high distances. Second, after an initial connection has been established between pairing devices, directionality gain is increased by fine-tuning antenna settings at both the transmitter and receiver as described in Section 3.1.7.

The search space and overhead of the beam training process directly scales with the product of the number of nodes and their transmit and receive sectors. While this is acceptable for mm-wave use cases like wireless HDMI with mostly static transmitters, the next generation of mm-wave systems targets the mobile device [39, 53, 107]. Device mobility breaks the beam adjustment and requires constant retraining, significantly increasing the beamforming overhead. This holds especially for device rotation. From experiments with a 7 degree beam width system we found that a mere misalignment of 18 degree reduces the link budget by around 17 dB. According to IEEE 802.11ad coding sensitivities [39], this drop can reduce the maximum throughput by up to 6 Gbps or break the link entirely. This misalignment is easily reached multiple times per second

by a user holding the device, causing substantial beam training overhead to enable multi-Gbps throughput for mm-wave Wi-Fi.

This chapter, presents design, implementation, and experimental evaluation of **B**lind **B**eam **S**teering (BBS), a system to steer mm-wave beams by replacing in-band trial-and-error testing of virtual sector pairs with "blind" out-of-band direction acquisition. BBS thus provides a novel approach to reduce beamforming training overhead for highly directional future millimeter wave networks, bringing the millimeter wave vision into reach. BBS exploits diverse propagation characteristics of the accessible frequency bands of devices compliant with the IEEE 802.11ad amendmend. To this aim, it utilizes legacy 2.4/5 GHz bands to estimate the direction for pairing nodes from passively overheard frames, which does not incur any additional protocol overhead or signaling. BBS uses out-of-band direction interference mechanisms that list received signal energy over an azimuthal receive spectrum. A history of these direction estimates is maintained for every potential pairing device in the network. Whenever a link is to be beam trained, the history is queried first for a valid direction estimate that can replace in-band training.

However, the direction information derived from the legacy band does not always correspond to the best mm-wave band direction due to multipath and noise effects. Further, frequency dependent transmission coefficients may lead to direction estimates that steer the beam into an obstacle, causing high mm-wave attenuation. BBS evaluates the ratio of multipath reflections observed in the out-of-band direction information to prevent erroneous mappings. Further, BBS aggregates the direction estimates retrieved from frames under small scale mobility. As reflections fluctuate under small movements [97, 98] while the direct path does not, this improves the direction mapping precision. BBS further extracts the angular spread of the direct path estimate from the aggregated information. This gives an indicator for the estimation precision and whether multiple mm-wave antenna sectors come into consideration for mapping. If this is the case, a highly efficient refinement process that uses the already obtained coarse grained direction estimate, determines the optimum sector. This refinement further probes antenna configurations with directivity close to the LOS path. Interference in other directions is thus prevented as no sweeping probes are emitted. The BBS mechanism combines the above techniques to transfer precise and reliable direction estimates to a mm-wave interface to reduce and in many cases eliminate in-band beam training overhead.

We implement the key components of BBS on a multi-band testbed that combines 2.4 GHz direction inference based on the software defined radio platform WARP [56] and a mechanically steerable 60 GHz RF-frontend used to obtain signal strength measurements. Our evaluation targets three key aspects of BBS. First, combining out-of-band direction inference results and mm-wave received signal strength analysis, we evaluate mapping precision for multiple locations. We find BBS achieves excellent direction estimation accuracy for short range line-of-sight links that are typical for IEEE 802.11ad. Second, we evaluate the suitability of the multipath reflection ratio to predict a reflected or blocked path and find that it is a very good indicator for both adverse conditions. Lastly, we analyze the trade-off between overhead reduction and achievable

maximum receive power for BBS trained directional links. Our analysis shows that while achieving optimum sector selection, BBS eliminates more than 80% of IEEE 802.11ad beamforming overhead.

4.1 System Architecture

In this section, we describe the BBS architecture, its integration with IEEE 802.11ad and the specific mm-wave characteristics addressed by BBS. Particularly, the BBS architecture that combines multiple radio interfaces at different frequencies for out-of-band direction inference is introduced.

4.1.1 IEEE 802.11ad and mm-Wave Wi-Fi

Directional Communication. To reach the necessary link budget for Gbps throughput mm-wave communication requires high-gain directional antenna arrays or switched directional antennas (see Section 3.2). In contrast to 2.4/5 GHz frequencies, a higher number of mm-wave antenna elements fits into the same space due to the smaller wave length, which yields higher directional gain [61, 66]. Usage of directional antenna solutions however requires transmitter and receiver to be aligned [15, 61]. In case of mm-wave communication the propagation behavior is quasi-optical, due to high free space attenuation and strong first order reflections [101]. For extremely directional future millimeter wave networks, with limited impact of antenna side lobes, alignment of antenna patterns equals a geometrical matching of transmit and receive focus on the direct path. To this aim, IEEE 802.11ad implements code books of predefined beam patterns, with each pattern focusing signal energy into a specific azimuthal direction.

The establishment of directional links or Beam Forming (BF) training in IEEE 802.11ad is a two stage process [39, 62]. During the first stage, the Sector Level Sweep (SLS) stations train their transmit patterns by probing every possible predefined beam pattern for its signal quality (see Section 3.1.7.1). The SLS phase is a high overhead procedure, where a complete frame has to be transmitted at each sector at the lowest PHY rate. BBS completely removes the SLS phase from directional link establishment. Instead of performing exhaustive sector search, our system utilizes out-of-band direction information to select appropriate antenna sectors.

In the BRP phase, antenna settings found during SLS using quasi-omni reception are fine-tuned. Also, receive antenna training is added to achieve highest directional gain and multi-Gbps throughput as described in Section 3.1.7.2. In contrast to the SLS, the BRP phase can already rely on an established directional link and probing of antenna configurations close to the initially found direction can happen throughout one frame. Thus, a BRP refinement adds significantly less overhead to the beam training than a SLS. The BRP phase can be a complementary procedure to BBS when the provided direction information by BBS needs further refinement. However, as shown in our evaluation (Section 4.3.5) our system reduces the BRP search space and further reduces overhead.

For first generation devices we still find moderate numbers of antenna elements (between 16-24, see Section 3.2.1.1), which show significant beam pattern imperfections. Thus, for devices enabling the parallel interference free high throughput transmission a higher number of sectors close to the maximum of 128 sectors per device as allowed by the IEEE 802.11ad amendment [39] will be required. However, with a higher number of antenna elements, higher gain and sharper focus of sectors are implied, which requires to probe more sectors to cover the full azimuth. Thus, future devices will operate close to the maximum overhead that the IEEE 802.11ad amendment allows for. Further, the number of sender-receiver sector pairs that needs to be matched multiplied by the number directional links to be trained in a network defines the amount of necessary beam training in a directional network.

60 GHz for Mobile Devices. Due to sensitivity to blockage and directional antenna misalignment, as well as high attenuation, first generation commercial mm-wave systems targeted short-range ($< 10m$) quasi-static scenarios, such as HDMI cable replacement. The recently ratified amendment IEEE 802.11ad goes the next step and targets mobile devices in a Wi-Fi like application scenario [39, 53]. Also, recent works claim that ten times the distance of current systems is achievable and even propose mm-wave cellular systems [107]. However, mobility still poses a problem, as overhead for directional link setup is amplified due to beam readjustment. We found for a beam width of 7 degree that a mismatch of 18 degree reduces signal strength by 17 dB. Comparing to the IEEE 802.11ad modulation sensitivities [39], it is likely that a link breaks if rate adaptation and beam recovery mechanism do not react quickly. Considering a walking user 5 meters away from an access point, who moves a mobile device with 70 degree per second, such a mismatch occurs roughly 5 times a second. BBS specifically targets applications with mobile devices and proposes a novel device architecture to obtain target device bearing without in-band overhead cost.

4.1.2 Node and System Architecture

Node Architecture. The BBS node architecture is based on a multi-band capable device design where mm-wave and IEEE 802.11ac/n interfaces are combined. We expect IEEE 802.11ad devices to comply with this design as the amendment defines a session transfer feature between mm-wave and legacy bands [39]. Further, with the recent acquisition of Wilocity by Qualcomm, we see chip vendors trending towards multi-band chipsets (2.4/5/60 GHz) [6]. For the BBS system design we assume a mm-wave interface that comprises an antenna array with predefined highly directional sectors patterns that cover an 360° azimuth. We refer to the mm-wave system as the *Application Band*, where the antenna pattern is steered according to BBS information to achieve multi-Gbps directional transmissions. We further assume an IEEE 802.11ac/n interface that has a N-antenna omni-directional array usable for inference of bearing to a pairing node. We refer to this frequency band (802.11ac/n platform) as the *Detection Band*.

Devices applying high directional gain require more precise direction estimation for antenna sector selection. However, even devices with few detection band antennas can help to guide

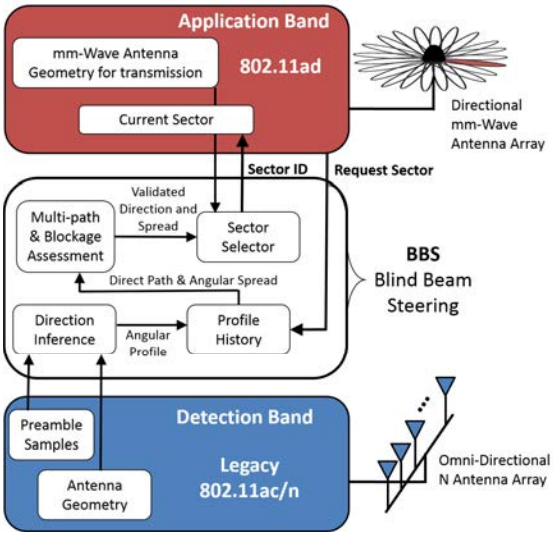

Figure 4.1: BBS system architecture.

high gain application bands. BBS applies a final sector refinement when the direction inference is not accurate enough. A low number of detection band antennas increases the search space for this refinement but still prevents the high overhead sector level sweep phase. Even when equipped with a single antenna in the detection band, a device can still be traced by a multi-antenna BBS detection device, increasing the link training efficiency at one side of the link.

System Architecture. Figure 4.1 depicts the BBS system architecture. The IEEE 802.11ad compliant *application band* is on the top part of Figure 4.1. At the application band, beamforming overhead is removed by applying direction estimates provided by BBS , shown in the middle block. BBS obtains preamble sample frames from the *detection band* (depicted in the bottom block). It infers the pairing node's bearing from frames received at lower frequencies (2.4/5 GHz), taking into consideration the antenna geometry of the detection band.

BBS runs a background process that infers other devices' direction by passively overhearing detection band frames. This comes without further overhead and does not require any changes to the detection band protocol. As discussed in section 4.3.6, even idle nodes generate sufficient traffic (e.g. through power management or AP roaming) for at least coarse grained direction inference. While BBS is independent of the technique used to infer a pairing device's bearing, it requires information about the received signal strength in relation to the azimuthal incidence angle θ. We refer to this information as an angular profile $P(\theta)$. These angular profiles are further analyzed to ensure robustness to mobility, multipath and signal blockage, to then perform reliable mm-wave sector selection. An example for angular profiles can be found in Section 4.2.3. The BBS architecture gathers angular profiles in a history, that is queried whenever a beam training request occurs.

4.2 Mechanism

BBS integrates into an IEEE 802.11ad implementation at the point of beam training. Both, link initialization as well as link retraining profit from BBS sector selection. The mechanism in Algorithm 1 ensures that BBS delivers reliable direction information from the detection to the application band. Starting from a beam training request, the angular profile collecting background process (see Section 4.2.1) is queried (line 1). If available, a profile history from frames received under differing multipath conditions is returned for the beam training partner. Profiles are combined to increase resilience against multipath (line 3). The aggregated profile is further analyzed for a blocked direct path or remaining multipath effects (line 4). If neither are detected (line 5), the strongest incidence angle is assumed to match the direct path to the training partner and is mapped to application band sectors. As direction estimation uncertainty due to noise is taken into consideration, it is possible that multiple sectors fall into the range of the estimated direct path. To select among these, a low overhead stand-alone BRP is performed (see line 9). The selected sector is then returned to the IEEE 802.11ad implementation. In case BBS can not provide a sector estimation, legacy beam training is initiated. The remainder of this section explains the details of Algorithm 1.

Algorithm 1: BBS Sector Selection

Input: beam training request to pairing node d
Result: application band sector at θ^*

1 $H(d) = \{P_t(\theta) | s(P_t(\theta)) = d\}\ \forall P_t, P_v \in H(d) : P_t \neq P_v, |t - v| > T_c$
2 **if** $|H(d)| > 0$ **then**
3 $\quad A_d(\theta) = \frac{\sum_{P \in H(d)} P(\theta)}{|H(d)|}$
4 $\quad \Psi(A_d) = \frac{\max_\theta(A_d(\theta))}{\frac{1}{|A_d|}\sum_{\phi=0}^{2\pi} A_d(\phi)}$
5 $\quad$ **if** $\Psi(A_d) > T_\Psi$ **then**
6 $\quad\quad \theta^* = \text{argmax}_\theta(A_d(\theta))$
7 $\quad\quad W_{\theta^*} = \text{argmin}_x \left(\frac{A_d(\theta^* \pm x)}{A_d(\theta^*)} \leq T_{\text{peak}} \right)$
8 $\quad\quad$ **if** $2 \cdot W_{\theta^*} > W_s$ **then**
9 $\quad\quad\quad \text{BRP}(\theta^* \pm W_{\theta^*})$
10 $\quad\quad$ **end**
11 $\quad$ **else**
12 $\quad\quad \theta^* =$ legacy beam training
13 $\quad$ **end**
14 **else**
15 $\quad \theta^* =$ legacy beam training
16 **end**

4.2.1 Out-of-Band Sector Inference and Profile History

BBS performs out-of-band direction inference, using passively overheard detection band frames to calculate angular profiles $P(\theta)$. A profile specifies received signal energy with respect to the azimuthal incidence angel θ (see Section 4.1.2). The retrieved profiles are organized in a history for every overheard device d as defined in Eq. 4.1. Hereby, $P_t(\theta)$ is an angular profile obtained from a frame overheard at time t and $s(P)$ denotes the node id for the device that transmitted the frame. Each pair of profiles in $H(d)$ is spaced by more than the channel coherence time T_c. This ensures the multipath characteristics vary between all profiles. Without this additional constraint, the frame aggregation process described in the following subsection could be biased negatively towards a certain reflected path.

$$\begin{aligned} H(d) &= \{P_t(\theta) | s(P_t(\theta)) = d\} \\ \forall P_t, P_v \in H(d) : P_t \neq P_v, |t - v| &> T_c \end{aligned} \tag{4.1}$$

Further, the background process ensures that outdated profiles, retrieved from obsolete transmitter positions are removed from the history in a first in first out buffer like process. To this aim, a time weighted average over the profile's main direction component can be used to identify the last accurate frame and crop the history accordingly. Weighting by time prioritizes newer frames as they are more likely to reflect the current position of the target. We find from our experiments, that a small number of frame preamble samples is sufficient to generate a reliable profile. Thus, even acknowledgment or null data frames can be used to retrieve profiles.

4.2.2 Profile History Aggregation

When receiving a beam training request, BBS queries the profile history $H(d)$ matching the beam training target d. This history contains profiles obtained under varying multipath conditions and from the latest known position of the pairing node, as described in Section 4.2.1. For the history we found the following two conditions to hold:

- An unblocked LOS path is reflected in every profile by a peak at the same angle.
- Peaks resulting from reflections vary among profiles.

We exploit this by averaging the profiles of the history and define the aggregated angle profile as follows.

$$A_d(\theta) = \frac{\sum_{P \in H(d)} P(\theta)}{|H(d)|} \tag{4.2}$$

By aggregating over measurements taken under varying multipath conditions, alternating reflection peaks are attenuated and the remaining strongest peak likely corresponds to the direct path. A second effect that we observe is that noise and multipath affected frames slightly deviate the direct path angle. Thus, spectra aggregation spreads the direct path peak according to the amount of noise. The spreading gives an estimate of the uncertainty for the direct path estimate.

4.2.3 Line-Of Sight Inference and Reflected Path Rejection

When applying direction estimates from the detection band to the application band we have to deal with two major obstacles. First, mm-wave communication suffers extreme signal attenuation from direct path blockage [101]. This poses a problem when the detection band uses lower frequencies that are less prone to blockage. In this case mapping a direction estimate can steer the application band antenna focus into an obstacle, severely impacting link quality and throughput. Second, multipath can induce destructive interference to the direct path signal, in case reflected and direct path signal can not be resolved with sufficient precision. For systems with limited detection band resources, this can result in reflected signal strength to be higher than that of the direct path, and the direction estimate to deviate from the direct path. By averaging over multiple profiles as described in Section 4.2.2, this effect can be mitigated but not fully prevented.

Reflected mm-wave paths impose additional attenuation [101] and reflections on the detection band do not necessarily coincide with those on the application band. We therefore do not use reflection based direction estimates for BBS and the system reverts to the high overhead but more resilient legacy beam training method. The same accounts for direct path blockage. To identify these conditions, passively collected detection band information is used and thus no further protocol overhead is imposed.

Peak to Average Ratio. The basic indicator for reflected and blocked path rejection is the ratio of the highest signal strength component to the average received signal energy of an aggregated profile.

$$\Psi(A_d) = \frac{\max_\theta(A_d(\theta))}{\frac{1}{|A_d|}\sum_{\phi=0}^{2\pi} A_d(\phi)} \tag{4.3}$$

Strong multipath spreads the incidence energy over a wide range of the angular receive profile and thus increases the denominator of the fraction. A reflection-less direct path on the other hand results in a sharp peak at its incidence angle and increases the ratio. We experimentally find direction blockage to cause the same effect. As the direct path peak looses magnitude by blockage, the numerator of the ratio shrinks while the average energy received through reflections remains. Figures 4.2 and 4.3 show examples for high and low peak-to-average ratios. We experimentally evaluate a threshold T_Ψ for the peak to average ratio that allows reflected path and blocked line-of sight rejection at the same time. If the ratio for a direction estimate is below this threshold, BBS proceeds with the legacy IEEE 802.11ad beam training method.

4.2.4 Sector Mapping

To relate a direct path estimate from the detection band to the application band, we determine the strongest signal peak identified by its azimuthal angle $\theta^* = \mathrm{argmax}_\theta(A_d(\theta))$ from the aggregated profile for the pairing node d. BBS translates θ^* to the application band sector that matches the direct path between two nodes and provides the highest signal quality. Due to quasi-optical propagation behavior and strong directional focus of the targeted future generation devices, a

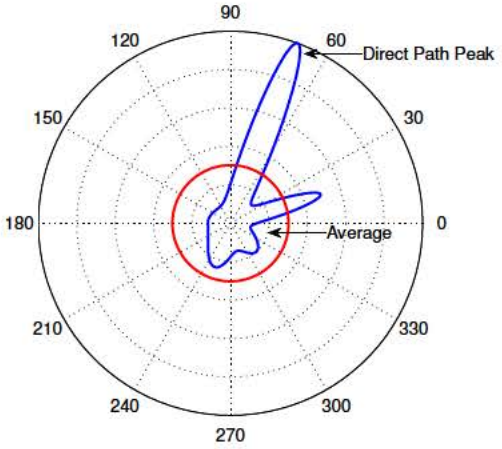

Figure 4.2: Angular profile: Unobstructed direct path.

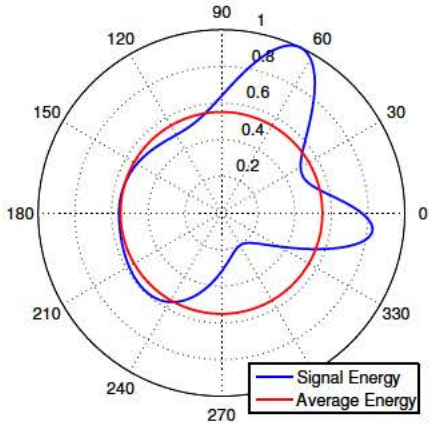

Figure 4.3: Angular profile: Multipath and blockage.

mapping is a straight forward geometrical matching. Even for lower complexity devices with imperfect beam patterns, highest throughput is expected from focusing on the line of sight. If transmit and receive antenna geometry differ, geometrical matching can be done separately.

4.2.5 Optional Sector Refinement

Due to remaining noise and multipath effects, the strongest peak θ^* can slightly deviate from the direct path to the target node. Thus, we extract the peak width around θ^* as it gives insight about the angular range that the direct path can reside in. We define the width of the strongest peak as the minimum angular range around θ^* before it drops below a relative attenuation threshold T_{peak}. The width of the strongest peak W_{θ^*} is defined by Eq. 4.4.

$$W_{\theta^*} = \text{argmin}_x \left(\frac{A_d(\theta^* \pm x)}{A_d(\theta^*)} \leq T_{\text{peak}} \right) \tag{4.4}$$

Choosing a low value for T_{peak} extends the angular region around θ^* and increases the chance for the direct path to lie within it. On the other hand, chances for mapping of the estimate to a single application band sector decrease with the size of the considered region. We evaluate the impact of T_{peak} by measurements on our BBS prototype, applying both, a conservative strategy maximizing the likelihood of choosing the optimum sector and an overhead minimizing strategy.

When the angular spread exceeds the width of an application band antenna sector W_s, additional in-band refinement is triggered with the aim of finding the optimum sector in the indicated set. As a rough estimate for the direction is given by BBS , the IEEE 802.11ad SLS can be skipped and efficient refinement in form of a stand alone BRP phase is carried out. In contrast to the SLS phase that transmits one frame per sector, during BRP a set of sectors is swept with one frame that has a matching number of training fields appended (compare Figure 3.7). Thus, the set of sectors reported by BBS can be refined with just one additional in-band frame that sweeps all of them.

We experimentally evaluate the overhead reduction achieved by BBS , finding that applying a standalone BRPis a highly efficient method to refine the remaining set of antenna sectors.

4.3 Implementation and Evaluation

In this section we describe our implementation, the testbed setup, and the performance evaluation of the BBS system.

4.3.1 Blind Beam Steering (BBS) Prototype

We prototype BBS using the FPGA-based software defined radio platform WARP for direction inference in the detection band at 2.4 GHz, and combine this system with a Vubiq 60 GHz waveguide development system [67] for directional communication in the application band.

4.3.1.1 Implementation of the Detection Band

For our experiments, we use WARPLab [56], a programming environment capable of prototyping physical layer algorithms in MATLAB that permits over-the air channel characterization with WARP nodes. For out-of-band sector inference, we use eigenvector analysis based on the MUSIC algorithm [80]. To collect data for the calculation of angular profiles, we use two WARP boards with 8 transceiver chains with synchronized baseband and radio clocks. The setup is shown in Figure 4.5. We implement a linear array geometry and refine angle profiles by applying the spatial smoothing and antenna sub-grouping mechanisms proposed in [98] with grouping factor $N_G = 2$. Through spatial smoothing, the angular profiles are averaged over multiple antenna sub-groups. This further reduces the likelihood of destructive interference on the direct path through adverse multipath conditions in certain locations. As sub-dividing a 4 antenna configuration leaves our profile calculation with 3 sample streams a maximum of two reflections can be resolved. Thus, to evaluate the performance for devices with few detection band antennas we disable the spatial smoothing mechanism. Further, the spectrum history length is fixed to a value of 50 IEEE 802.11 frames. All angular profiles obtained for one location comply with the requirements for the profile history described in 4.2.1. To generate the angular profile, for every frame three short preamble sequences (corresponding to 192 samples) are averaged. Further, the direct path estimate for every receiver location and its mean error are averaged over 500 histories with 50 frames each. The tracked device is a WARP board with one radio interface.

4.3.1.2 Implementation of the Application Band

We implement the application band for directional multi-Gbps data transmission using a mm-wave development platform from Vubiq [67]. This platform consists of transmitter and receiver waveguide modules that provide 1.8 GHz modulation bandwidth in the 58 to 64 GHz unlicensed bands. We feed a 16-QAM modulated multi-tone baseband signal with 15 MHz bandwidth from

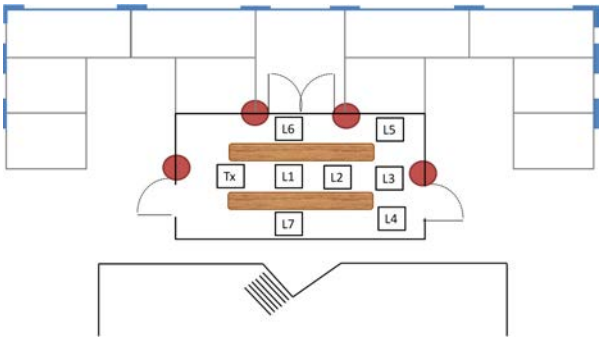

Figure 4.4: BBS measurement floor plan.

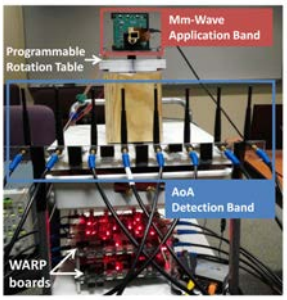

Figure 4.5: BBS prototype platform.

an Agilent E4432B signal generator to the mm-wave transmitter. We analyze the received signal strength with a Tektronix TDS7054 oscilloscope measuring the IQ baseband amplitude provided by the mm-wave receiver. To evaluate different sector patterns we utilize four types of antennas: three horn antennas with beamwidths of 7, 20 and 80 degrees, and an omni-directional antenna. We implement an IEEE 802.11ad like sector sweep through a programmable rotating table that emulates fixed sector positions. The implementation of the mm-wave application band is shown in Figure 4.5.

4.3.1.3 Experimental Setup

We conduct our experiments in an indoor setting. To match the targeted mm-wave Wi-Fi scenario, we perform single-room experiments. Our experiments are conducted under static channel conditions in a room of 15x8 meters, where we perform measurements in 7 locations as shown in Figure 4.5. All transceivers are placed at a height of 1-1.5 meters and non-obstructed direct path conditions are ensured, except for the experiments analyzing blockage. We take a series of frame preamble snapshots for the 2.4 GHz tracking target capturing 0.4 ms of the transmitted signal, while the delay between snapshots is approximately 2 seconds. We infer direction on different subsets of this data to evaluate the performance of 4, 5, 6, 7, and 8 detection band antennas. As our static measurement environment experiences long channel coherence times we place the tracking target on a rotation device. This induces small position changes that do not significantly change the angle between nodes but alter multipath reflection characteristics.

4.3.2 Direct Path Detection Accuracy

The key requirement to achieve multi-Gbps rates with mm-wave communication is a non-obstructed direct path between transmitter and receiver. It is vital that the sector inferred from the 2.4 GHz detection band corresponds to this direct path, but effects such as reflections and scattering at the 2.4 GHz band affect the detection accuracy. In this section, we evaluate BBS accuracy to infer the direction to a pairing node and select the correct sector for directional communication.

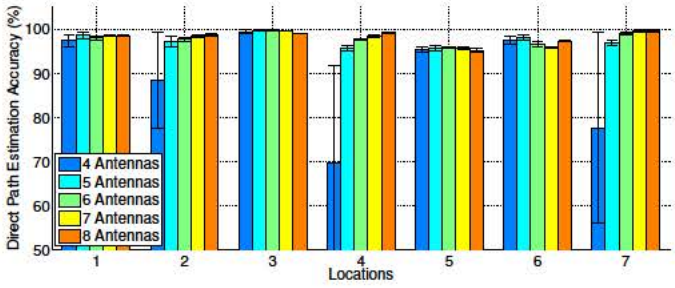

Figure 4.6: Detection accuracy of direct path for 8 to 4 detection antennas in 7 evaluated locations.

We determine the detection accuracy for every measured location as the ratio of angular mismatch against the maximum mismatch of 180 degree. The angular mismatch is determined from 60 GHz signal strength measurements and the 2.4 GHz direction estimation results. It is defined as the absolute difference between the direct path's center peak on 2.4 GHz and the center angle of the strongest 7 degree beamwidth antenna sector on 60 GHz. Figure 4.6 shows the detection accuracy (Y-axis) for all 7 transmitter locations (X-axis) sub-divided by the number of used detection band antennas.

The detection accuracy results show excellent direct path estimation accuracy with an average precision of 97.8% over all locations when using at least 5 detection band antennas. Accuracy varies slightly over locations indicating varying multipath severeness for different transmitter positions. The number of detection band antennas shows no significant impact on direct path estimation accuracy except for a 4 antenna detection band configuration, for which the direct path prediction accuracy drops to 89%, 67%, and 78% at locations 2, 4 and 7, respectively. The increased sensitivity to multipath for the 4 antenna configuration results from deactivating spatial smoothing as described in section 4.3.1.1. *We find that on average, BBS achieves 97.8% (corresponding to 4 degrees) accuracy in mapping 2.4 GHz direction estimates to mm-wave antenna sectors with beam widths as low as 7 degrees when using at least 5 detection band antennas.*

4.3.3 Robustness to Multipath and Signal Blockage

Blocked direct paths can severely reduce the received signal of mm-wave links, rendering communication impossible. Furthermore, as discussed in Section 4.3.2, multipath introduces inaccuracies in direct path detection, and might cause the direction estimation to lock onto a reflected path. The following two experiments evaluate BBS 's ability to identify these conditions.

Detection of Severe Multipath. In order to analyze the effect of multipath, we evaluate the peak to average ratio as defined in Section 4.2.3. A high ratio indicates little impact by multipath and vice versa. Thus, we compare the accuracy results of 4.3.2 to the ratio to verify that it can be used as an indicator for the accuracy of BBS estimates. Figure 4.7 depicts the relation of the direction estimation accuracy achieved by an angular profile to its peak to average ratio. The data points are aggregated over locations and number of detection band antennas. From the graph we

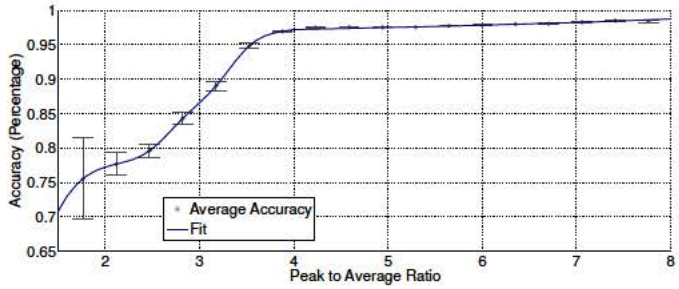

Figure 4.7: BBS: Peak to average ratio in relation to accuracy.

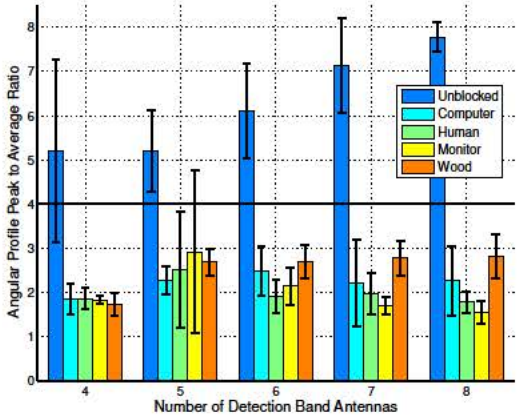

Figure 4.8: BBS: Effect of blocking obstacles on the mean peak to average ratio of aggregated angular profiles for 7 evaluated locations.

observe a clear correlation between high peak to average ratio and accuracy. For values below 4, the accuracy decreases significantly with the ratio. Further, the mean error increases with decreasing accuracy which indicates that the error results from locking onto reflection peaks with equal magnitude as the direct path.

We thus define a peak to average threshold T_Ψ of 4 and reject aggregated profiles with a ratio below. We evaluate over all locations and antenna configurations the number of false positives and negatives, where a threshold based decision wrongly turns off BBS or uses a highly inaccurate estimate with accuracy below 90%. *We observe that a threshold based decision strategy can successfully detect strong multipath and prevent erroneous mapping with a success rate of 94%*

Detection of Blocked LOS Path. Our third experiment evaluates the impact of LOS blockage on the spectrum peak to average ratio. This experiment was performed in locations 1 and 3, which have a receiver-transmitter distance of 2 meters and 9 meters respectively. The results are averaged over these locations. The blockage material applied to the direct path is typical to an office environment, i.e, a desktop PC, a monitor, plywood with a width of 1.8 cm, and human blockage. In Figure 4.8 we observe the effect of blocking obstacles in the aggregated angular profile peak to average ratio. The Y-axis depicts the peak to average ratio and the X-axis depicts the number of detection band antennas. The results show that for all types of blocking objects,

the peak to average ratios do not exceed a value of 3. When choosing a peak to average ratio threshold of 4 (as proposed from the multipath analysis), we assure with 96.5% certainty that the obtained direction estimate refers to a non-obstructed LOS path. *BBS reliably distinguishes between unblocked and blocked paths by a threshold based evaluation of the peak to average ratio.*

4.3.4 Training Overhead

BBS maps the estimated direct path to mm-wave antenna sectors under consideration of the angular spread detected for the direct path peak. When multiple mm-wave sectors fall into this region, a standalone IEEE 802.11ad BRP selects the optimum among them. The angular spread depends on the relative signal attenuation threshold T_{peak} that sets the boundaries of the peak. Low values for T_{peak} increase the search space and thus the likelihood to identify the best sector, but also increase training overhead.

With higher device complexity, detection and application band antenna orders increase. For example an AP has more 2.4/5 GHz antennas as a smart phone and also implements stronger directional focus on the mm-wave band. Thus, we assume a correlation between the antenna order on both bands and analyze the behavior of three device classes: 4, 6, and 8 detection band antennas with 80, 20, and 7 degree sector beamwidth in the application band, respectively.

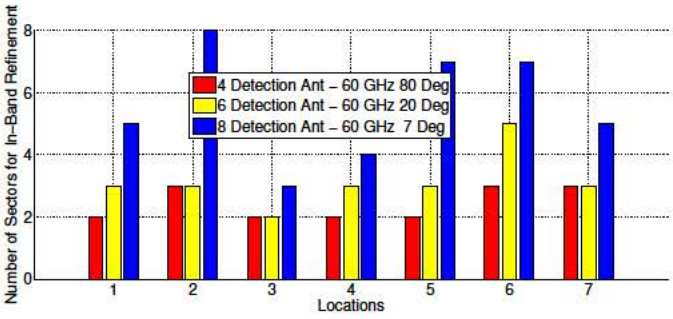

Figure 4.9: Remaining refinement sectors for optimal sector selection with $T_{\text{peak}} = 0.3$.

Optimum Sector Selection. For our measurement campaign, we find $T_{\text{peak}} = 0.3$ to be the threshold that always includes the optimum sector while having the narrowest possible refinement search space. Thus, BBS always finds the optimum sector and reaches the maximum achievable received power under this parameterization. In this experiment, we evaluate the number of mm-wave sectors necessary for BRP in-band refinement for this optimum sector selection strategy. We obtain these numbers from the average angular spread $W_{\theta^\star}$ of each location mapped to the sector width of the three device classes. Figure 4.9 depicts on the Y-axis the amount of sectors considered for BRP refinement. The X-axis shows the transmitter locations sub-grouped by BBS antenna configurations. We observe that the BRP search space is increased for complex antenna systems, i.e., 8 detection antennas with 7 degree 60 GHz sectors. A maximum in-band overhead of 7 sectors for such a 52 sector system is required at location 2 which corresponds to

In-Band Sector Refinement	7 Degrees IEEE 802.11ad SLS+BRP time = 1.54 ms			20 Degrees IEEE 802.11ad SLS+BRP time = 0.88 ms			80 Degrees IEEE 802.11ad SLS+BRP time = 0.63 ms		
	BBS (ms)	Time Savings (ms)	% Reduction	BBS (ms)	Time Savings (ms)	% Reduction	BBS (ms)	Time Savings (ms)	% Reduction
0	0	1.54	100	0	0.88	100	**0**	**0.63**	**100**
2	0.28	1.26	81.42	**0.28**	**0.6**	**67.55**	0.28	0.35	54.66
4	**0.29**	**1.25**	**81.03**	0.29	0.59	67.21	0.29	0.34	53.72
10	0.31	1.23	79.87	0.31	0.57	64.85		-	
20	0.34	1.20	77.94		-			-	

Table 4.1: BBS and IEEE 802.11ad time comparison for directional link establishment.

13% of the maximum possible search space. The smallest amount of required in-band refinement can be found in location 3 where only 2 sectors are required for a 52 sector system and no overhead is imposed for the other two antenna configurations. These findings correlate with the high detection accuracy found in 4.3.2. *BBS can achieve perfect sector selection with only 0 to 13% remaining in-band training.*

4.3.5 Time of Directional Link Establishment

As shown in Section 4.3.4, BBS provides perfect sector matching, and thus optimum link budget. In order to achieve a perfect sector matching, there are cases in which BBS requires beam-refinement for a small number of sectors. Nevertheless, BBS removes the IEEE 802.11ad sector level sweep phase and reduces the BRP search space, thus significantly reducing the amount of time required to establish directional links. This directly leads to an increase in spectrum efficiency by allowing more time for data transmissions. Also, wide spread probing frames to cover all necessary directions can be avoided, which otherwise can act as omni-directional interference signal, hindering parallel transmission. In this experiment we evaluate the BBS overhead reduction by comparing the link setup time of IEEE 802.11ad to our proposed method. Specifically, we compare the time BBS takes to perform a standalone BRP on the remaining sector set after out-of-band direction inference compared to the full IEEE 802.11ad legacy beamforming training procedure comprising SLS and BRP.

In case the BBS refinement sector set is determined by the method described in Section 4.2.4, we assume the search space for the legacy method to be fixed to one fourth of the total number of sectors. For the BRP procedure, we assume a three step message exchange for both BBS and IEEE 802.11ad. During the BRP, first initiator and receiver realize a receive training transmitting one frame with the number of requested training fields. Second, two interleaved receive and transmit BRP transactions are performed which include feedback for identified strongest sectors. For all calculations a pairing node with 16 sectors is assumed.

Table 4.1 lists the BBS and IEEE 802.11ad time comparison for directional link establishment for the evaluated antenna configuration of BBS. We extract the average BRP search space size for the three antenna configurations from Figure 4.9 (0 sectors, 2 sectors and 4 sectors) and evaluate the corresponding training time reduction. We find that the BBS guided beamforming training achieves an average channel usage reduction of 1.24 ms, 0.59 ms and 0.35 ms per link setup for sector widths of 7, 20 and 80 degrees respectively. The corresponding values are highlighted in Table 4.1. This performance increase scales with the number of nodes in a network and link re-

training caused by device mobility. Further, for highly directional systems a notable setup delay reduction is achieved by BBS. For example, to set up a link that needs in-band refinement of 4 sectors, only 0.29 ms are required compared to 1.54 ms for a 7 degree beam width system. *Summing up, BBS achieves perfect sector selection, while reducing beamforming training overhead for every link setup by up to 1.24 ms (81%) for highly directional systems with sector widths as narrow as 7 degrees.*

4.3.6 Direct Path Detection under Mobility

Due to the lack of commercially available mm-wave antenna arrays that support controllable real-time beam steering, it is difficult to directly evaluate BBS under mobility. Nonetheless, by reducing the frame history length in our static setup we can deduce the behavior for mobile nodes, where direction information becomes obsolete fast. We observe that the high average accuracy above 95% can be maintained for frame histories as small as 8 frames, when at least 5 detection band antennas are available. Further, we measured the number of frames transmitted by a range of different idle IEEE 802.11n/ac devices (notebooks and smartphones). We found a substantial amount of null data frames to be transmitted and their number to increase with the expected device mobility. This renders coarse-grained direction estimation under mobility possible, given BBS small frame history length requirements. Null data frames serve for several implementation dependent features, e.g., power management, channel scanning, keep alive mechanisms and AP roaming.

Additionally, IEEE 802.11ad defines a seamless session transfer from mm-wave to legacy frequencies in case of link breakage at the mm-wave band. This feature creates traffic on the lower frequency band, which allows BBS to derive a high accuracy direction estimate and reestablish the link.

4.4 Related Work

Prior work on 60 GHz communication mainly focused on channel measurements and modeling, as well as hardware design. To the best of our knowledge, BBS is the first work to introduce multi-band coupling to remove overhead for beam-training in directional mm-wave communication. However, there exists complementary work on the key components of our system: multi-band coupling and direction inference.

Multi-band Systems. Various previous systems and hardware architectures concurrently use multiple bands for purposes other than directional link establishment. For example, Wake on Wireless [84] uses multiple interfaces on battery operated devices to save energy. It puts devices on standby mode and utilizes a second very low-power radio on a different frequency band to wake up the primary device when required. Other works combine 3G, WiMAX and Wi-Fi radios to increase capacity or offload traffic [29, 42]. Protocols for opportunistic usage of multi-band spectrum were studied in [79]. The 802.11ad amendment [39] itself supports seamless integration

with 802.11a/b/g/n/ac, through a mechanism called transparent Fast Session Transfer (FST). This mechanism allows real-time transition of communication from any band/channel to any other band/channel. As a consequence, we expect a large fraction of IEEE 802.11ad transceivers to operate on multiple bands and thus directly support our BBS mechanism.

Direction Inference. The techniques utilized for out-of-band detection inference in this chapter are based on [21,97,98]. These mechanisms have primarily evolved from MUSIC [80], which was the first work to analyze incident waveforms: quantity, direction of arrival, strength and cross correlation among them. Direction inference in combination with various multi-antenna or MIMO techniques and channel impulse response measurements is often used for indoor localization [21, 95, 97, 98]. Incidence angle based localization techniques have further been used in ad-hoc mesh networks [60], CDMA mobile cellular systems [11, 99] and in combination with ToA using antenna arrays and interference cancellation for LOS environments and wide-band CDMA [11]. In contrast, BBS utilizes bearing inference in a multi-band system with the purpose of guiding 60 GHz directional communication.

60 GHz Beamforming Overhead. In [49] beam training is considered as optimization of a 2-D signal strength function defined over finite codebooks of transmit and receive antenna sectors. The proposed algorithm, based on a numerical Rosenbrock search, probes a reduced number of sector combinations compared to the exhaustive searches that are currently state of the art. However, probing specific sector pairs requires coordination between the involved nodes and reliable communication on untrained links is not possible in IEEE 802.11ad networks. Thus, the method proposed in [49] is not applicable to this type of network. In contrast, the IEEE 802.11ad amendment [39] uses a sector level sweep to find antenna sectors for initial communication and BBS efficiently solves the problem by out-of-band direction inference.

4.5 Conclusion

In this section, we presented the design and experimental evaluation of a novel architecture and framework for mm-wave directional communication, named *Blind Beam Steering (BBS)*. BBS addresses the overhead and interference problem for directional mm-wave link establishment. As described in Section 3.2.3.2 beam training for future highly directional mm-wave networks becomes significantly more complex, posing a limit to mm-wave's very high throughput capabilities and beam-width scalability. Further, due to its probing frame transmission in a sweeping manner (see Section 3.1.7), interference unaligned with established transmissions, is created that hinders the millimeter wave vision of parallel high throughput transmissions. We further highlighted the fact that mobile network scenarios, like IEEE 802.11 communication, increase the problem as frequent beam readjustment is required.

The proposed system architecture couples 60 GHz mm-wave with legacy 2.4/5 GHz bands to exploit the propagation properties of each. We infer the line-of-sight direction between the communicating devices from omni-directional transmissions at low frequencies in the *Detection*

Band. The information is further processed to ensure robustness to multipath and signal blockage, to then perform mm-wave sector selection. The sector selected by the BBS framework is passed to the *Application Band* which implements IEEE 802.11ad compliant mm-wave directional communication.

Thus, by exploiting the multi-band architecture of upcoming IEEE 802.11ad devices, BBS removes significant amounts of mm-wave in-band probing. The aforementioned drawbacks for future mm-wave networks are thus alleviated, allowing robust link setup with reduced overhead and interference. Our experimental evaluation demonstrates that BBS achieves on average 97.8% accuracy for direction estimation when 5 or more antennas are used at the detection band. This accuracy in direction estimation results in IEEE 802.11ad beamforming training overhead reduced by 81% for a highly directional transceiver with 7 degree beam width. Further, in our typical office-style testbed environment BBS successfully detects unblocked direct path conditions for highest throughput mm-wave transmissions with a rate of 96.5%.

Chapter 5

Multi-Frequency Band MAC Enhancements for Fairness and Efficiency

Communication in the 60 GHz band is a promising next step for the evolution of high speed Wi-Fi and is considered a key technology for 5G networks. Beside the vast amount of spectrum (7 GHz available bandwidth for unlicensed use in the 60 GHz band), its potential for high spatial reuse of frequency resources makes it very attractive for future dense networks. This is due to the envisioned highly directional pencil-beam antenna patterns which reduce interference between devices to a minimum and also contribute to overcome the high free space attenuation found at mm-wave frequencies (see Section 1.1.1 and 3.1.3). As we describe in Chapter 3.2, currently available millimeter wave devices still apply imperfect beam patterns, due to deficiencies in available consumer-class antenna technology. This leads to increased interference through antenna side lobes but also expands the reception area of transmissions. As a result current devices still can utilize established medium access schemes and communication protocols without experiencing too much impact from directionality. This however will change when future devices improve their beamforming capabilities (see Section 3.2.3.2). The resulting reduction in signal reception area will raise new challenges for the MAC-layer design of future Wi-Fi systems. In particular, the deafness problem – stations that are located outside of the transmitter antenna's boresight cannot overhear or sense the transmission – has to be considered for protocol design. As we show in this chapter this problem impacts mm-wave CSMA/CA mechanisms, which experience reduced efficiency and fairness.

Figure 5.1 depicts an RTS collision caused by two stations being deaf towards each other given their beams directed towards the AP. In Figure 5.2, an RTS is lost because the AP focuses its receive beam away from the deaf station, towards a data transmission.

The IEEE 802.11ad amendment for 60 GHz Wi-Fi [39] addresses these challenges by defining a hybrid medium access mechanism. This includes polling and TDMA as well as the well known

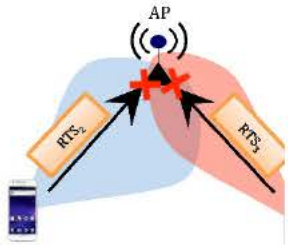

Figure 5.1: RTS collision due dire
mit focus on AP.

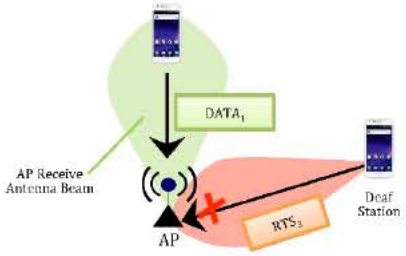

Figure 5.2: Missed RTS due to receive sector misalignment.

IEEE 802.11 carrier sense multiple access with collision avoidance (CSMA/CA) as described in Section 3.1.6. However, polling introduces overhead at all stations independent of whether they are communicating or not. Also, TDMA requires additional coordination and communication to determine the schedule. In contrast, CSMA/CA is very efficient in handling unpredictable burst traffic, such as the request/response type traffic generated by web browsing. Hence, adaptation of the CSMA/CA scheme to the constraints imposed by mm-wave communication is of high interest.

In its basic form, CSMA/CA suffers from several drawbacks when applied to directional communication systems, the main challenge being incomplete carrier sensing. Further, erratic deferral behavior and increased collisions lead to reduced fairness in terms of channel access. While long term fairness is still achieved, a group of active nodes may dominate the channel whereas long time inactive users have a low probability of successfully accessing the medium.

Even though several works have addressed the deafness problem in WLAN and Wireless Personal Area Network (WPAN) [105], most solutions are designed for lower frequency communication where omni-directional transmission and reception is feasible and can be used for coordination purposes. At mm-wave frequencies, however, increased attenuation requires directional antennas at least at one side of a communication link (see Section 3.1.7). The most suitable adaptations of CSMA/CA for mm-wave frequencies are proposed by the IEEE 802.11ad amendment [39] and work by Gong *et al.* [23]. IEEE 802.11ad modifies the CSMA/CA mechanism to protect a data exchange between two nodes with a directional RTS/CTS exchange, which prevents stations with an antenna beam aligned with the transmissions from creating interference. However, as messages are likely to not be overheard by deaf nodes with antenna beams in other directions, these do not defer during ongoing transmissions but unsuccessfully try to access the channel and then excessively increase their contention window. This leads to a fairness problem as stations that successfully access the channel have a substantially higher chance to subsequently win the contention again.

A different approach is proposed in [23], where CTS messages are broadcasted by a central controller. To achieve sufficient link budget to receive the omni-directional CTS messages, every station by default directs its receive beam towards the AP. Unfortunately, this approach still suffers from colliding directional RTS messages, which lowers the effectiveness of the deferral process and results in reduced fairness.

Efficiency and fair channel access, i.e., low per packet delay and high throughput, play a major role for a satisfying user experience and current state of the art CSMA/CA schemes exhibit rather suboptimal performance in this respect.

In this chapter, we address the deafness problem for uplink channels, while maintaining high fairness through a combination of 60 GHz communication with control messages on legacy Wi-Fi frequencies. Thus, the benefits of multi-band capable devices are exploited, to leverage from the difference in propagation behavior between 60 GHz frequencies and legacy Wi-Fi bands at 2.4/5 GHz. When contending for the channel, stations exchange omni-directional RTS/CTS messages on the lower frequency band to set up a data transmission. The source and destination stations then exchange data frames on the 60 GHz band. The advantage of the presented approach is twofold. First, control message exchange on frequencies of 2.4 or 5 GHz is highly reliable over the typically short IEEE 802.11ad communication distances. Thus, every station overhears the control messages, and can correctly defer, avoiding the IEEE 802.11ad unfairness problem. Second, by parallelizing control and data transmission, we free resources on the 60 GHz band for high speed data transmission. Thus, the dual frequency approach enhances throughput and MAC efficiency. Further, the number of RTS messages sent in vain to already transmitting devices is reduced. This prevents interference into random directions, different from already established links. Last, as the IEEE 802.11ad amendment foresees transition between the two bands for seamless failover (so called Fast Session Transfer) and range extension [39], we expect most IEEE 802.11ad devices to be suitable for the dual band approach.

The contributions presented in this chapter are as follows. First, we analyze the deafness problem in 60 GHz CSMA/CA networks and propose a dual-band solution to it. This approach couples interfaces on the 60 GHz band with the ones on legacy Wi-Fi frequencies. Second, our mechanism shifts control messages onto a legacy IEEE 802.11 channel with lower bandwidth, freeing up channel time for high throughput transmissions on 60 GHz. By this, we achieve a throughput increase of up to 65.3% over *IEEE 802.11ad* CSMA/CA. Last, exploiting omni-directional transmissions on legacy Wi-Fi frequencies we solve the deafness problem and increase MAC fairness by up to 42.8% compared to *IEEE 802.11ad*.

The chapter is structured as follows: Sections 5.5 and 5.1 present the past proposals on solving the deafness problem, as well as a description of 60 GHz CSMA/CA impairments due to the deafness problem. Our dual-band CSMA/CA approach is described in Section 5.2. Section 5.3 provides the channel and transmission model used to simulate the numerical results shown in Section 5.4. Section 5.6 concludes the presented work on fairness in IEEE 802.11ad networks.

5.1 Fairness Impairments in Directional CSMA/CA

This section describes the impact of deafness on the two most relevant CSMA/CA mechanisms for directional networks, IEEE 802.11ad and the centralized approaches proposed in [22, 23].

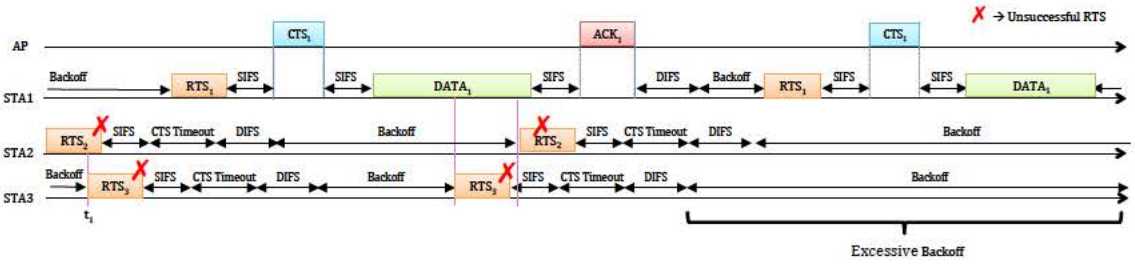

Figure 5.3: Excessive backoff behavior of CSMA/CA in IEEE802.11ad

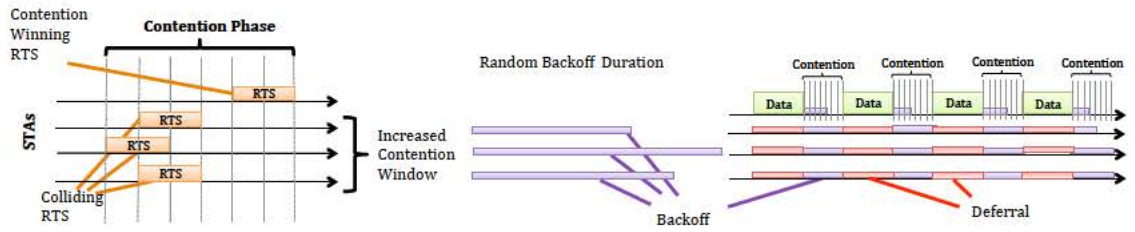

Figure 5.4: Excessive deferral with colliding RTS messages in CSMA/CA with broadcast CTS

5.1.1 IEEE 802.11ad CSMA/CA

The deafness problem entails that in many cases other stations will neither overhear frames nor sense that the carrier is busy when two stations are communicating. This causes two important performance impairments described in detail below.

Excessive Backoff. Due to limited (or lacking) carrier sensing, the frame collision probability during contention increases. Especially in dense networks, this significantly increases the average contention window. Furthermore, as frames (including RTS/CTS exchanges) are transmitted directionally, stations outside the transmit beam will not overhear the ongoing communications and thus will not defer. Instead, a deaf station may try to transmit to an already communicating station, which has its receive antenna beam steered into another direction. While this may not disrupt the ongoing communication, the deaf station will assume a failed transmission and increase its contention window. Figure 5.3 depicts this excessive backoff problem. Stations two and three initially collide with their RTS messages, resulting in increased contention windows compared to station 1. Both have reduced chances to 'hit' the following contention windows. Their next RTS messages will be lost as the AP directs its receive beam away from them due to an ongoing data transmission. Stations two and three further increase their backoff and station one dominates the medium access.

Unbalanced Contention. Stations suffering excessive back-off have a low probability to win contention, which favors recently active stations with smaller contention windows. While this effect is also present in conventional IEEE 802.11, in IEEE 802.11ad it is vastly exacerbated by the fact that contending stations do not know when an ongoing frame ends, i.e., when to resume contention. This in turn increases the probability that the same active station transmits a high number of frames consecutively, before other stations happen to win the contention for medium

access. This effect primarily impacts short term fairness and over longer time scales, the identity of the active station changes sufficiently often to achieve some level of fairness.

5.1.2 Centralized CSMA/CA

The centralized CSMA/CA schemes [22, 23] partially solves the aforementioned problems through an omni-directional CTS sent by the AP.

However, an omni-directional CTS only ensures correct deferral of overhearing stations in the subsequent data transmission phase. The increased RTS collisions rate due to lack of carrier sensing and the resulting long backoff times remain.

As the duration of an RTS comprises 2 slots, chances for collision are very high especially at network initialization when stations use the minimum contention window of 15 slots. Even for moderate network densities, it is not uncommon that multiple RTS messages collide, resulting in more than two stations increasing their backoff windows in the same contention phase. Interestingly, here IEEE 802.11ad benefits from a significantly lower RTS to RTS collision rate, since RTS messages are often uselessly sent during an ongoing data transmission rather than during the contention phase.

The high RTS collision probability may lead to a rapid increase of the contention windows after network initialization. At the same time, in a highly loaded network, the contention period is relatively small (drawn from the 15 slot minimum contention window). As all stations freeze their contention timer during deferral, a high back off counter needs a significant amount of contention periods to reach 0. This again gives an unfair advantage to currently active nodes with small contention windows to win channel contention. As for networks with deaf stations, it is likely that a small set of active nodes alternately uses the channel, while other stations remain in long periods of repeated maximum backoff. The effect is shown in Figure 5.4. Due to an overlapping RTS collision, three stations will increase their contention windows. During the following data transmission the collided stations correctly defer. As a result, their large backoff time is reduced only slowly over the coming short contention intervals (the active station draws its backoff time from the minimum contention window). The active station thus dominates the channel access for a long period. This effect is more pronounced than for IEEE 802.11ad, as with IEEE 802.11ad even stations with a small contention window are likely to uselessly transmit an RTS during an ongoing data phase and then increase their contention window.

5.2 Dual-Band CSMA/CA

In this section, we propose a dual-band CSMA/CA scheme that mitigates the deafness problem for uplink communication while achieving low overhead and high fairness. Our approach leverages omni-directional transmissions on legacy Wi-Fi frequencies to coordinate high throughput transmissions in the 60 GHz band. As control messages are received by all stations, our approach ensures correct deferral behavior and a low frame collision probability.

We assume an IEEE 802.11ad compatible transceiver design and an infrastructure based network architecture with AP. Further, we require all stations to be able to communicate over a 60 GHz interface as well as over a legacy Wi-Fi interface. This type of transceiver architecture is very likely, as IEEE 802.11ad makes use of a multi-band fast session transfer for range extension and seamless failover in case of link breaks. Thus, we expect typical IEEE 802.11ad devices to be compliant with the requirements of our dual-band CSMA/CA scheme. For simplicity we omit details about beam training on the directional 60 GHz interface and assume pre-trained directional links for all stations to the AP. In general, this assumption is satisfied by the association beam training process described in Section 3.1.7. Dual-band CSMA/CA access can then be enabled as an addition to the IEEE 802.11ad hybrid MAC architecture of Section 3.1.6.

5.2.1 Dual-Band CSMA/CA Protocol

Our dual band CSMA/CA protocol follows the basic IEEE 802.11 scheme, including random backoff and deferral mechanism, as well as RTS/CTS exchanges as defined for IEEE 802.11ad (compare Section 3.1.6.1). However, the contention mechanism together with the RTS/CTS exchange are realized on omni-directional legacy Wi-Fi bands. The IEEE 802.11ad interface of the dual-band devices is exclusively used for data transmission (and acknowledgments).

When applying the contention mechanism on legacy Wi-Fi interfaces, only one message can be exchanged over the medium at a time. Thus, for our approach, it is essential to have data frame sizes that exceed the duration of the RTS/CTS exchange consumed on the lower frequency. Otherwise, the data transmission would be delayed by the exchange of control frames. This is especially important considering that lower frequency IEEE 802.11 has longer frame duration of RTS/CTS control messages compared to the 60 GHz band. In addition, since the duration of a data frame is known, it is possible to use in-band RTS/CTS as in conventional IEEE 802.11ad for small data frames for which dual-band RTS/CTS creates too much overhead.

When frames are transmitted according to the dual-band mechanism, stations need to sense the lower frequency band to be idle for at least a DIFS time before starting the contention mechanism. The transmitted RTS frame will reference the end of the latest known transmission on the 60 GHz band plus a SIFS interval. Receiving RTS and CTS messages omni-directionally ensures that the latest transmission is known to everybody. Note that the RTS/CTS exchange can already occur during the transmission of some previous data frame on the 60 GHz band to avoid unnecessary delay.

Figure 5.5 shows an example frame flow for our dual-band approach. Three stations (distinguishable by the subscript in frame descriptions) intend to transmit a frame to the AP at the same time. In contrast to deaf IEEE 802.11ad CSMA/CA, backoff happens on the legacy frequency band and the RTS/CTS messages are overheard. As can be seen from frames $Data_1$ and RTS_2, data frame transmission and backoff procedure happen in parallel on two bands.

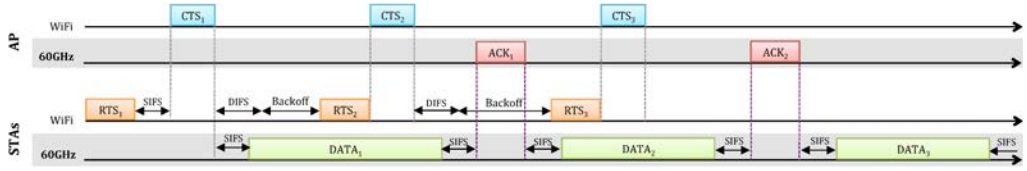

Figure 5.5: Channel access mechanism of the dual-band approach.

5.2.2 Fairness and Throughput

A fundamental advantage of our dual-band approach is that all stations can overhear the RTS/CTS exchange on lower omni-directional frequencies, thus solving the deafness problem. As a result, dual-band CSMA/CA does not suffer from the impairments described in Section 5.1. Our approach achieves a flawless deferral behavior, avoids excessive contention windows, and increases the fairness of medium access.

A second benefit results from the parallelization of RTS/CTS exchanges and data transmissions on two separate frequency bands. This removes idle time and RTS/CTS transmissions from the 60 GHz frequency band. As RTS/CTS exchanges are transmitted with the most robust and thus lowest rate coding and modulation scheme, inefficient use of the 60 GHz channel is avoided. Instead, all available channel time with only a SIFS interval between data frames (and acknowledgements) can be utilized for very high throughput transmissions on the 60 GHz channel. Sacrificing transmission time on the legacy Wi-Fi band for control traffic improves efficiency as the band supports much lower transmit rates compared to the 60 GHz band.

5.3 Simulation Models

This section elaborates the simulation models that are used to produce the numerical results in Section 5.4. We consider an indoor wireless network with a single AP and a set of $\mathbf{S}$ non-AP stations that are randomly distributed within a cell area. The total number of stations is $|\mathbf{S}| = N_s$. Let $\{s, d\}$ represent a transmission pair. We denote the source station as s and the destination station as d.

Channel model. The received power at d when receiving from s is

$$\mathrm{P}_r(s,d)(\mathrm{dBm}) = \mathrm{P_t}(\mathrm{dBm}) + \mathrm{G}_s(\mathrm{dBi}) + \mathrm{G}_d(\mathrm{dBi}) - \mathrm{PL}(l_{s,d}), \tag{5.1}$$

where G_s and G_d are the antenna gains at station s and station d, respectively. The path loss $\mathrm{PL}(l_{s,d})$ including oxygen absorption of stations that are $l_{s,d}$ apart is

$$\mathrm{PL}(l_{s,d}) = 20\log_{10}\frac{4\pi l_{s,d}(\mathrm{m})}{\lambda} + \alpha l_{s,d} \quad (\mathrm{dB})$$

as presented by Zhu *et al.* [107] (compare also Sections 1.1.1 and 1.1.2). The oxygen absorption is $\alpha = 0.02$dB/m and the wavelength λ at 60 GHz frequency band is 5mm. P_t is the transmit power

a
n
is
I
n
b
F
o

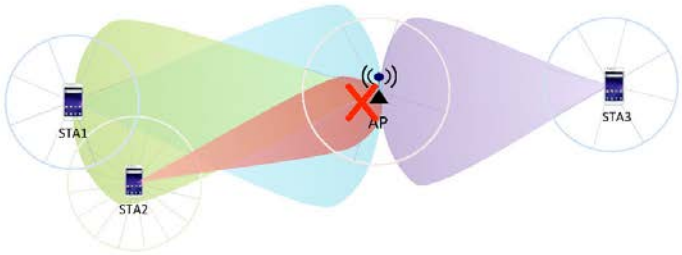

Figure 5.6: Interference in a directional transmission network.

In the presence of interference, the total interference power $P_{\text{int}}(s,d)$ at the a receiving station d is

$$\mathrm{P}_{\text{int}}(s,d) = \sum_{n \in \{\mathbf{S} \cup \mathrm{AP}, n \neq d, n \neq s\}} \mathrm{P}_r(n,d). \tag{5.2}$$

As mentioned, not all interference causes packet loss. A packet is only lost if the interference signal causes the resulting SINR degrades below the threshold needed to decode a message coded with a certain coding and modulation scheme. The corresponding thresholds are obtained from [39].

5.4 Results

This section evaluates the performance of our *Dual-band* scheme. We investigate the impact of the number of stations (N_s), time interval τ over which fairness is measured (called "fairness interval"), and frame size (f).

We consider an uplink scenario, where all stations contend for the channel to transmit data frames to the AP. Since all stations are attempting to transmit to the AP, their beams are always directed towards the AP. At a time instant, only one station can win a TXOP with the AP. Upon winning a TXOPs, a station transmits only one data frame and it needs to recontend for the channel to transmit another data frame.

Network topology and configuration. For all the scenarios, the stations are randomly distributed within a cell area with a radius of 23m. This range is the same as the maximum range we measured on first generation devices during our measurement campaign presented in section 3.2, a Dell E7440 laptop and D5000 docking system, operating at 60 GHz with 13° sector

width. The fairness intervals over which fairness is evaluated ($\tau = 5$ms and $\tau = 80$ms) are chosen to reflect short term and long term fairness, respectively. We also use different frame sizes $f = \{1.5, 15, 30, 45, 60, 75\}$KB to study the impact of different levels of frame aggregation on performance. For data frame transmission at 60 GHz, we consider the 12 single carrier MCSs defined in IEEE 802.11ad [39], with modulation schemes $\pi/2$-BPSK, $\pi/2$-QPSK, and $\pi/2$ 16-QAM. The corresponding transmit rate ranges from 389Mbps to 4620Mbps. The transmission rate of the control messages (MCS 0) depends on the band at which it is transmitted as shown in Table 5.1. Table 5.1 also shows the timing information for the key parameters used in the simulations.

Table 5.1: Dual-Band CSMA/CA: Parameters in 60 GHz and 5 GHz frequency bands.

Item	IEEE 802.11ad (60GHz)	IEEE 802.11ac (5 GHz, 80MHz bandwidth)
aDIFSTime	13μs	34μs
aSIFSTime	3μs	3μs
aSlotTime	5μs	9μs
MCS0	27.5Mbps	32.5Mbps
aRTSTime = aCTSTime	8.19μs	7.30μs

Performance metrics. Our main performance metrics are throughput, fairness, and delay. Throughput is the total amount of data bits successfully received at the destination station over the transmission time. To ensure fair comparison, we take into account the throughput loss on the lower frequency band that our scheme incurs, by summing up the throughput on both the low and high frequency band for all schemes. The achievable throughput on the lower band is set to 433Mbps, the maximum rate supported by IEEE 802.11ac devices without MIMO. Lastly, fairness is computed based on Jain's fairness index [41].

Performance comparison. We compare the performance of the proposed approach against two other schemes. The first approach, *IEEE 802.11ad*, resembles the IEEE 802.11ad amendment [39] where all messages are transmitted directionally between the source and the destination stations. The second scheme is the one proposed by Gong *et al.* in [23], where an RTS message is transmitted directionally from a source station to the central controller (i.e., AP), which broadcasts a CTS message to *all* stations in the system.[1] We denote this centrally coordinated scheme as *Central*.

5.4.1 Homogeneous scenario

Figure 5.7 illustrates the impact of increasing the number of stations N_s on the system throughput. As mentioned before, we also take into account the throughput obtained on the lower frequency band for all the schemes. As N_s increases, so does the probability of RTS frame collision, as shown in Figure 5.8. In the *Central* schemes, since all stations can overhear CTS messages broadcasted by the AP, this removes any collisions of frames with ongoing data trans-

[1] Note that this is in contrast to IEEE 802.11ad operation which only permits quasi-omni directional reception, but not transmission.

missions. However, during the contention phase, RTS frames are sent directionally. These frames are not overheard, thus stations may not sense the medium busy and multiple RTS packets may overlap, causing a collision. The number of collisions decreases when the Contention Window (CW) is larger and we observe that *Central* with $CW_{min} = 63$ (*Central*(CW_{min}) = 63) has a lower number of RTS collisions compared to that of *Central*(CW_{min}) = 31, which in turn has fewer collisions than *Central*(CW_{min}) = 15. *IEEE 802.11ad* (All Collision) in Figure 5.8 shows the total number of failed RTS messages due to RTS-RTS collision, RTS-CTS collision and RTS-Data collision. This number is significantly higher than RTS-RTS collisions only. In fact, the majority of the collisions in *IEEE 802.11ad* occur due to the transmission of RTS messages from the deaf stations while there is an ongoing data transmission (i.e., represented by RTS-Data collision) of another station with the AP. *Dual-band* has the lowest RTS-RTS collision rate since the first control message (i.e., RTS) is transmitted omni-directionally and thus stations defer access upon overhearing the transmission of the RTS frame. Collisions only occur if two RTS messages are transmitted in the exact same slot.

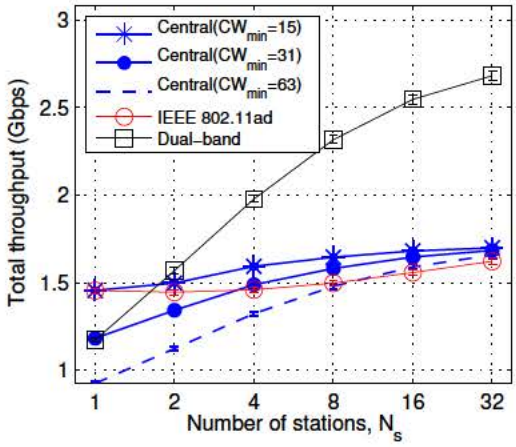

Figure 5.7: Total throughput on 60 GHz and 5 GHz band in the homogeneous sector scenario, $\tau = 80$ms, $f = 15$KB.

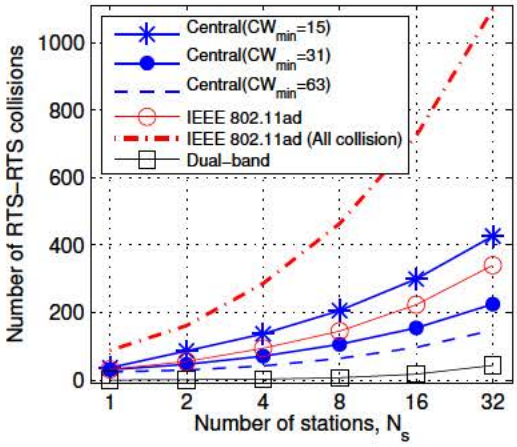

Figure 5.8: Number of RTS-RTS collision in the homogeneous sector scenario, $\tau = 80$ms, $f = 15$KB.

Although increasing N_s increases the number of frame collisions, it also increases the probability of a station contending for the channel. This reduces the time between two consecutive transmissions and as shown in Figure 5.7, throughput increases with N_s. While increasing CW_{min} reduces the probability of collision, it causes high throughput loss especially for small N_s. Having said that, scenarios with larger N_s should benefit from a larger CW. However, this is not reflected in the throughput performance in Figure 5.7 where *Central* with a larger CW_{min} performs worse than with a smaller CW_{min} for any $N_s < 32$. According to a detailed analysis on contention based access by Bianchi in [4], increasing the initial size of the CW (i.e., CW_{min}) has no significant impact on the system throughput in systems using the RTS/CTS mechanism. In fact using a large CW_{min} causes a higher throughput loss [4].

We also plot a bar graph to represent the amount of time used for data transmission, MAC overhead, idle time (the average time between two frames) and collision time as depicted in Figure 5.9. In comparison, the *Central* scheme with a higher CW_{min} incurs more idle time than that with lower CW_{min} for a given N_s. This shows that a higher CW_{min} causes a station to have the chance to draw a large backoff interval and thus causing an unnecessarily long waiting time. This is worse for a station with failed RTS as it needs to double its contention window before it attempts to access the channel again. In particular for larger N_s where many stations successfully contend for the channel, a station with failed RTS continues to defer its backoff process upon each successful contention and it takes a long time until its own backoff counter reaches zero and it is able to contend again for the channel. Consequently, a station with failed RTS suffers from excessively long deferral time (as illustrated in Figure 5.4).

Also *IEEE 802.11ad* suffers from excessively long backoff times due to the deafness problem. This causes a longer idle time as shown in Figure 5.9 compared to *Central*(CW_{min})= 15, especially when N_s is large. However, *IEEE 802.11ad* performs almost as well as *Central*. This is due to the fact that deaf stations continue reducing their backoff timer during ongoing packet transmissions and thus have a chance to access the channel upon the expiry of the backoff time even when their initial backoff time was very large. Figure 5.9 shows that, for $N_s = 16$, the idle time for *IEEE 802.11ad* is not significantly longer than that of *Central*.

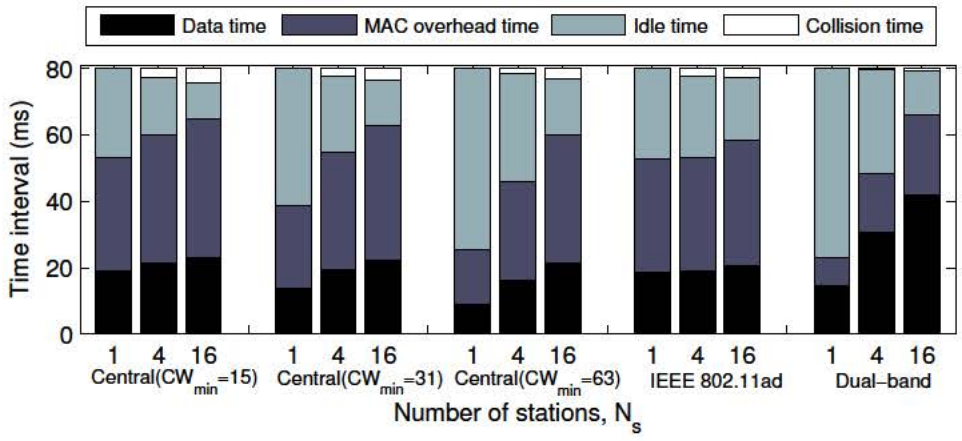

Figure 5.9: Time proportion for data transmission, MAC overhead, idle time and collision time for different $N_s = \{1, 4, 16\}$ in the homogeneous sector scenario. $\tau = 80$ms, $f = 15$KB.

In summary, the *Central* scheme lets all stations contend during the actual contention period which increases the RTS-RTS collision rate and thus the average backoff time, whereas with *IEEE 802.11ad* backoff timers are counting down also during ongoing transmissions and stations attempt to access the medium more often, but many times this is futile since the attempt is outside of the actual contention period of the AP.

In the *Dual-band* approach, stations defer once overhearing a control message. This enables

Dual-band to avoid most of the collisions caused by the large number of contending stations and it achieves a higher throughput than *IEEE 802.11ad* and *Central*. In addition, *Dual-band* transmission (as shown in Figure 5.5) aids in reducing the idle time between frames (see Figure 5.9). In Table 5.1, it is shown that *Dual-band* has a higher DIFS time and slot time on the lower frequency band. Therefore, for the same random backoff, the backoff interval time is 80% longer than that for *IEEE 802.11ad* and *Central*. This restricts the throughput gain of *Dual-band* especially for $N_s = 1$ which has negative gain. The impact of long slot time can also be observed from Figure 5.9 for $N_s = 1$ since a slot time of *Dual-band* (9μs) is longer than that of the other schemes (5μs). Note that disabling *Dual-band* in case it is not beneficial is a trivial extension. For higher numbers of stations, the benefits of *Dual-band* and its ability to mitigate the deafness problem outweigh increased inter-frame and slot times. *Dual-band* performs best for all other N_s and it achieves a throughput gain as high as 65.3% compared to *IEEE 802.11ad* and 57.9% compared to *Central*.

Figure 5.10 and Figure 5.11 show the fairness of the schemes when the time intervals over which the fairness is computed are $\tau = 5$ms (short term fairness) and $\tau = 80$ms (long term fairness), respectively. Fairness is higher for smaller N_s for the same fairness interval since with fewer stations, there is a higher probability that each station has a chance to contend for the channel within the fairness interval.

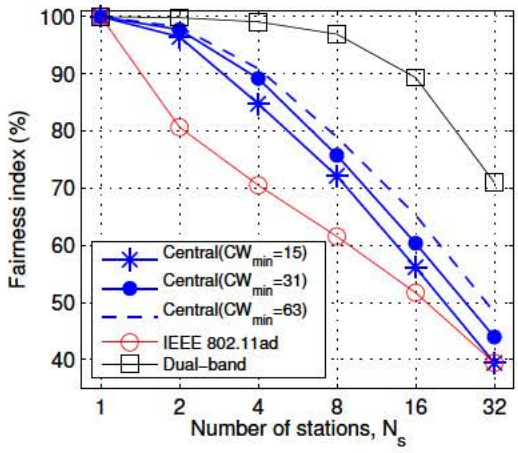

Figure 5.10: Short term fairness in the homogeneous sector scenario, $\tau = 5$ms, $f = 15$KB, $N_s = 16$.

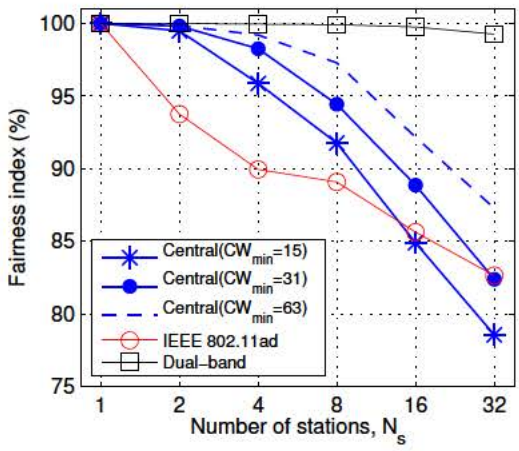

Figure 5.11: Long term fairness in the homogeneous sector scenario, $\tau = 80$ms, $f = 15$KB, $N_s = 16$.

As shown in Figure 5.10, *Central* and *IEEE 802.11ad* have significantly lower fairness than *Dual-band* since the stations that increase their CW (due to RTS collisions) have a very low chance of contending for the channel within a short time interval ($\tau = 5$ms). Although *Dual-band* faces the same problem, its lower RTS collision rate causes only a few stations to increase their CW while the others stay at CW_{min}. This allows it to achieve a higher fairness than *Central* and *IEEE 802.11ad*.

When τ increases, this also increases the chance for the stations with larger backoff interval to contend for the channel. While all stations defer access when a CTS is received in *Central*, only those within the boresight of the AP (that overhear the CTS) will defer backoff in *IEEE 802.11ad*. Thus, deaf stations in *IEEE 802.11ad* continue to reduce their backoff counter instead of deferring, and whether such a backoff counter happens to expire during the actual contention period is relatively independent of the randomly chosen backoff value. Therefore, *IEEE 802.11ad* outperforms *Central* for $N_s \geq 32$ (see Figure 5.11) when $\tau = 80$ms.

However, delay critical applications require fairness (and predictable short packet delays) on short time scales. Figure 5.12 and Figure 5.13 show the histogram of the maximum per frame delay for $N_s = 4$ and $N_s = 16$, respectively from 200 simulation runs. The delay duration is the time difference between the current data frame and the next data frame of a station (given that all stations are backlogged). When $N_s = 4$ (see Figure 5.12), *IEEE 802.11ad* has a higher number of frames with a long per frame delay than *Central*. This is because a station that successfully contends for the channel has a higher chance to recontend for the channel again since the deaf stations are, with high probability, transmitting their RTS during the data transmission phase and increase their CW. However, for $N_s = 16$, Figure 5.13 shows that the distribution of delay duration of *IEEE 802.11ad* and *Central* is similar. In fact, *IEEE 802.11ad* has a lower number of frames with long per frame delay compared to *Central*. As explained, this is due to the excessively long deferral time of a station with failed RTS transmission in *Central*. *Central* with higher $\mathrm{CW}_{\mathrm{min}}$ has a lower RTS collision rate and thus achieves higher fairness regardless of τ.

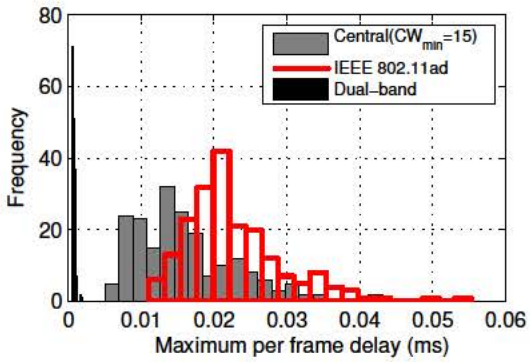

Figure 5.12: Maximum per frame delay in the homogeneous sector scenario, $F = 15$KB, $N_s = 4$, $\tau = 80$ms.

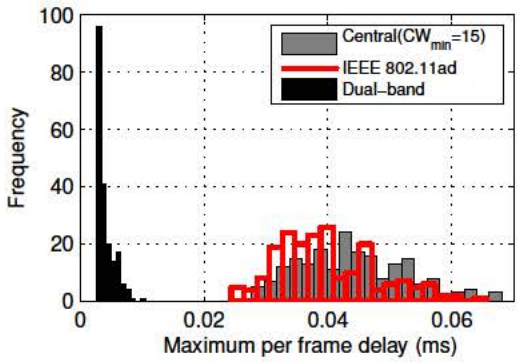

Figure 5.13: Maximum per frame delay duration in the homogeneous sector scenario, $F = 15$KB, $N_s = 16$, $\tau = 80$ms.

We further examine the impact of frame size f. Figure 5.14 and Figure 5.15 depict the impact of frame size for $\tau = 5$ms and $\tau = 80$ms, respectively. As larger frame size entails longer transmission time, multiple back-offs during one frame can occur for *IEEE 802.11ad*. Stations with multiple backoffs experience very long backoff intervals and have a lower chance to transmit within a short τ in Figure 5.14. This causes a decrease of *IEEE 802.11ad*'s fairness as f increases compared to *Central*. For *Central*, stations with failed RTS defer for a much longer time and the

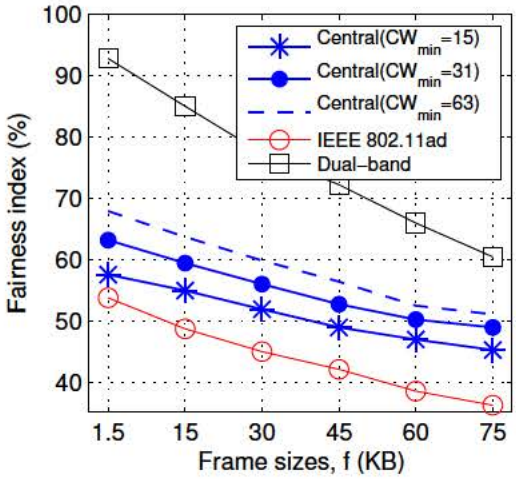

Figure 5.14: Impact of frame size on fairness in the homogeneous sector scenario, $\tau = 5$ms. $N_s = 16$

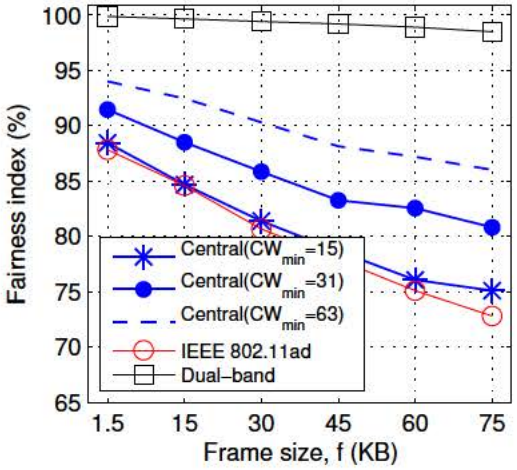

Figure 5.15: Impact of frame size on fairness in the homogeneous sector scenario, $\tau = 80$ms. $N_s = 16$

stations that draw a large backoff timer may not be able to transmit within $\tau = 5$ms. The drop in fairness is less significant than that of *IEEE 802.11ad* because the deferral at stations with failed RTS have the highest impact on the fairness. While a small portion of the stations that defer may have the chance to contend for the channel when f is small, these stations may not be able to do so when f is large. This explains the slight drop of fairness for *Central* as f increases. For all f, the fairness of the schemes improves when $\tau = 80$ms. *IEEE 802.11ad* performs well in Figure 5.15 for the same reason discussed before (i.e., stations that back off have almost an equal chance to transmit as the stations that defer backoff in *Central*). For *Dual-band*, transmitting a larger frame means more stations are loosing the chance to contend for the channel as they may have drawn a larger (random) backoff time especially when τ is low (see Figure 5.14) and this effect is less pronounced for $\tau = 80$ms in Figure 5.15. Nevertheless, *Dual-band* performs best for both $\tau = 5$ms and $\tau = 80$ms since it neither has excessive deferral time nor backoff time due to a high RTS collision rate.

5.4.2 Heterogeneous scenario.

We also simulate a heterogeneous scenario where stations have different sector widths, selected at random from the set $\{13°, 15°, 20°, 30°, 40°, 50°, 60°, 90°, 120°\}$. Since the performance is very similar to that shown in Section 5.4.1, we omit the discussion of the results for brevity.

5.5 Related Work

The deafness problem due to misaligned directional antennas was first addressed in the context of microwave communication (i.e., 2.4 GHz and 5 GHz frequency band) [1, 25, 46, 47, 57, 74, 89, 94]. [46] and [57] solve the deafness problem for CSMA/CA systems by omni-directionally transmitting control messages (i.e., RTS and CTS). However, by doing so all overhearing nodes will defer their transmission, preventing spatial reuse. In the same vein, Takai *et al.* [89] propose directional frame transmission while listening omni-directionally. This only partially solves the deafness problem as frames might not reach all receivers due to directionality of the transmission. Korakis *et al.* [47] propose a directional system that emulates omni-directional RTS transmission by sweeping transmit directions, i.e., transmitting an RTS in each possible direction. While this technique effectively deals with deaf stations, it has high overhead, especially for systems with many narrow directional sectors. The works in [1, 25] address the deafness problem by omni-directionally transmitting control messages but they require additional mechanisms to prevent interfering transmissions. Arora *et al.* [1] use separate channels to reduce collisions by adjusting the transmit power such that interference at the receiver is avoided. In [25], an additional GPS receiver is used to provide location information to create a coordination map to avoid interference.

Due to increased attenuation at the 60 GHz band, the gain resulting from a directional antenna is needed at least at one side of the wireless link (given the currently achievable receiver sensitivity and the regulatory transmit power limitations). For this reason, the aforementioned methods that rely on fully omni-directional communication may not work for 60 GHz. Only few works address the deafness problem while taking this additional challenge into consideration. Gong *et al.* [22, 23] use the Personal Network Coordinator (PNC) in a WPAN (i.e., similar to an AP in WLAN) to coordinate each transmission. Instead of exchanging RTS and CTS messages between the communicating devices, the source device transmits a directional RTS to the PNC. In response, the PNC broadcast the CTS message omni-directionally. All devices focus their receive antenna in the direction of the PNC and can thus receive the transmission. In case of an uplink channel, this results in a directional RTS transmitted by the station and the PNC broadcasting an omni-directional CTS. This technique partially solves the deafness problem (RTS messages can still collide), but may create a bottleneck at the central PNC. [55, 85, 86] highlight the importance of solving the deafness problem to avoid collisions in directional 60 GHz networks. However, their solutions are based on TDMA-like scheduling and do not support random access which this section focuses on. The IEEE 802.11ad amendment itself proposes a directional MAC-layer mechanism but does address the deafness problem. We discuss the details of this mechanism in Section 3.1.6.1 and Section 5.1.

Similar to our approach, [63, 64, 75] exploit the coexistence of a microwave interface. However, there the dual-band approach is used for neighbor discovery, as a fall-back mechanism for range extension, and for beamforming training optimization rather than solving the deafness problem.

5.6 Conclusion

In this section, we address the deafness problem that affects throughput and fairness for the next generation of highly directional 60 GHz transmissions with CSMA/CA channel access. To the best of our knowledge, our work is the first to design and analyze a multi-frequency band approach which leverages from varying propagation characteristics to mitigate the deafness problem. Our approach takes advantage of a coexisting 5 GHz band to coordinate the data transmission at 60 GHz. This is beneficial in two ways. First, due to omni-directional transmission on 5 GHz the deafness problem is solved for communication between stations and an AP, preventing fairness impairments. This scenario is the most relevant for Wi-Fi communication and predestined for application of CSMA/CA access. Second, moving robust low rate control messages to 5 GHz allows to use the 60 GHz band exclusively for high throughput data transmission.

Overall, the proposed scheme reduces the number of unnecessary transmitted frames, resulting from connection attempts to already receiving stations. This helps to realize the millimeter wave vision of parallel data streams, as unnecessary randomly directed interference outside the established directional beams is prevented. Further, usage of quasi-omni directional antenna patterns to listen for CSMA/CA transmission setup frames can be avoided. As shown in Section 3.2.2.2, these patterns suffer imperfections on first generation devices which can lead to deafness in certain directions. The proposed dual band scheme leverages from the difference in propagation characteristics of the targeted IEEE 802.11ad devices to use good omni-directionality at lower frequencies to overcome the limitations at the millimeter wave band. Thus, interference is reduced, throughput is boosted and connection reliability is increased to improve performance for future millimeter wave systems.

We analyze throughput and fairness of our proposed scheme through extensive simulations to compare it against *IEEE 802.11ad* and an alternative scheme that broadcasts CTS messages from a central controller. In terms of fairness, we improve by up to 42.8% over *IEEE 802.11ad* and 34.5% over the centralized scheme. Despite using air time on the 5 GHz band due to broadcasting of control messages, our approach still achieves significant overall throughput gain. Considering both bands jointly, we gain 65.3% and 61.8% over *IEEE 802.11ad*, respectively the centralized scheme.

Summary and Future Work

This thesis explores mechanisms to improve IEEE 802.11 communication that experiences varying propagation characteristics over the used frequency resources. These variations are addressed at two different levels. First, the intra-channel level is considered, i.e. differing behavior over a continuous frequency block used by a device for a cohesive transmission. While it is widely known that channel variations exist, current wireless systems apply rather basic equalization methods to remove these effects. In contrast, the presented work shows that differentiated adaptation can outperform these methods. Second, frequency varying behavior of the frequency bands accessible by multi-frequency band enabled IEEE 802.11ad devices is exploited. These devices combine interfaces for communication at millimeter wave frequencies with legacy Wi-Fi communication at 2.4 and 5 GHz. The resulting propagation differences are significantly more pronounced than at the intra-channel level and bear strong potential for entirely novel approaches to improve IEEE 802.11 networks.

The approach to investigate the potential of leveraging from frequency varying behavior evolved throughout the work on this thesis. First, investigation of intra-channel variations led to the recognition of the potential of the paradigm. With the rise of millimeter wave communication for commercial wireless systems, it became apparent that transfer of the principle to mm-wave systems bears high potential. Thus, an in-depth analysis of the IEEE 802.11ad amendment with focus on its beam forming capabilities is combined with a practical performance analysis of first generation mm-wave devices. This study identifies deficits of first generation systems, resulting in reduced directionality. However removal of these deficits will result in challenges for future systems' protocol design. While this study is a contribution on its own, it further identifies challenges for mm-wave communication that can be solved by methods exploiting the frequency variations of the accessible frequency resources.

Thus, this thesis presents three different methods that leverage frequency varying propagation behavior. First, Sub-Carrier Switch Off is an improvement to OFDM modulated IEEE 802.11 systems that utilizes a minimum feedback loop to decide which blocks of the frequency resources to use. SSO in practical networks requires to solve an optimization problem, namely how many of the available frequency blocks to use. Every excluded block potentially facilitates higher transmission rates at the remaining ones. At the same time redistribution of the payload of excluded blocks can lead to increased frame length. This work presents a threshold based solution to this

problem, derived from experiments conducted on a software defined radio testbed. Further, the solution is shown to achieve close to optimum behavior, significant throughput gains and extended transmission ranges.

Second, BBS is proposed, which is a mechanism to improve the beam training process of IEEE 802.11ad compliant millimeter wave communication. It leverages efficient direction inference at legacy Wi-Fi bands at 2.4 GHz, possible on future multi-band enabled devices. These inference methods are based on reliable omni-directional communication which is not feasible on the millimeter wave frequencies. BBS thus combines the strength of both bands. As a result, beam training overhead especially for mobile networks is reduced. In this type of network, beam training overhead occurs frequently, whenever the position between devices changes. Further, a reduction of interference from sweeping communication is achieved as the normal beam training has to cover all possible directions with probing frames to ensure connectivity. This process easily interferes with the principle of parallel directional transmissions that is envisioned for millimeter wave systems.

Last, a fairness and throughput improving adaptation for CSMA/CA channel access in IEEE 802.11ad networks is proposed. By means of simulation, directionality of millimeter wave communication is found to cause impairments to the carrier sensing mechanism, which is central to this access method. This phenomenon, also known as deafness problem, especially impacts fairness of CSMA/CA. The proposed method utilizes omni-directional transmission at legacy Wi-Fi bands at 2.4 or 5 GHz to exchange coordination messages for millimeter wave channel access. As a result, connection attempts to busy stations are prevented, as global knowledge about active transmissions is ensured. This reduces interference in directions not aligned with already established communication flows. Further, low throughput control messages are moved to legacy frequency bands and the millimeter wave link can be entirely used for high throughput communication, which leads to further throughput enhancements.

Future Work

Overall, this thesis shows, that adaptation to frequency varying behavior is a powerful approach that can be applied to improve several aspects of wireless communication. The SSO method presented in Chapter 2, applies said approach on an intra-channel level to early IEEE 802.11 systems. By enabling fine grained adaptation to frequency variations, modest performance gains are achieved. The offered potential of the method is expected to increase with every evolutionary step of wireless communication, as authors show in [73] by means of simulation. However, practical work that applies SSO to IEEE 802.11 standards with wider channel size is required to support theses claims. Also, a practical comparison of SSO to power loading and adaptive coding modulation could reveal trade-offs between complexity and benefits of the mechanisms. Last, several technical aspects of SSO deserve further investigation, e.g., hardware implementation of a real time feedback loop or application of SSO to the frame header.

While adaptation to intra-channel propagation variation still shows potential for future work it always comes at the price of increased transceiver and protocol complexity. In contrast, millimeter wave enabled multi-band systems can leverage frequency varying behavior more easily. Implementation of novel methods which improve several different communication aspects can be achieved due to communication over multiple wireless interfaces targeting different frequency bands. Several future application areas to leverage from frequency varying multi-band frequency resources can be envisioned.

Omni-directional legacy bands could be used to transmit other broadcast management frames apart from the RTS/CTS exchange proposed in Chapter 5. For example Address Resolution Protocol (ARP) requests, which are central to discover other devices in a network. These frames otherwise need to be replicated by a PCP/AP to reach all nodes in directly communicating millimeter wave networks. Further, IEEE 802.11ad multi-AP deployments, which are required in medium to large setups, could leverage lower frequency communication in several ways. Clients could use omni-directional legacy communication to identify the optimum AP without utilizing sweeping device discovery communication at the mm-wave band, thus avoiding interference in random directions. Further, hand-over of a station to another AP could be simplified, as no change of the receive direction on the 60 GHz interface is required to communicate with the new AP. Deafness towards one of the APs during hand-over can thus be prevented.

Also, the dual-band beam training method presented in Chapter 4, offers room for future work. First, in-depth analysis of integration into the IEEE 802.11ad amendment is of high interest. The amendment's highly flexible definition of the beam training protocol potentially allows backward compatibility with legacy, non-BBS enabled nodes. However, the complex IEEE 802.11ad Association Beamforming Training (A-BFT) makes this a non trivial challenge. Second, in contrast to using direction inference only, utilizing several APs that act as a localization system could significantly improve BBS behavior. When building a map of all clients, these could leverage direction information even when not equipped with legacy antenna arrays. Also, combining the directions inferred at multiple APs bears further potential to increase precision for multi-band beam steering.

References

[1] Aman Arora, Marwan Krunz, and Alaa Muqattash. Directional Medium Access Protocol (DMAP) with Power Control for Wireless Ad Hoc Networks. In *Proceedings of the IEEE Global Telecommunications Conference (GLOBECOM 04)*, Nov. 2004.

[2] Andre N. Barreto and Simeon F. Furrer. Adaptive Bit Loading for Wireless OFDM Systems. In *Proceedings of the 12th IEEE International Symposium on Personal, Indoor and Mobile Radio Communications (PIMRC 01)*, Sept./Oct. 2001.

[3] Oscar Bejarano, Edward W. Knightly, and Minyoung Park. IEEE 802.11ac: from Channelization to Multi-User MIMO. *IEEE Communications Magazine*, 51(10):84–90, Oct. 2013.

[4] Giuseppe Bianchi. Performance Analysis of the IEEE 802.11 Distributed Coordination Function. *IEEE Journal on Selected Areas in Communications*, 18(3):535–547, Mar. 2000.

[5] Helmut Bolcskei. MIMO-OFDM Wireless Systems: Basics, Perspectives, and Challenges. *IEEE Wireless Communications*, 13:31–37, Aug. 2006.

[6] Jon Brodkin. Tri-band Wi-Fi Chips for Multi-gigabit Streaming Coming from Qualcomm, July 2014. http://bit.ly/1QYQsCf.

[7] Joseph Camp and Edward Knightly. Modulation Rate Adaptation in Urban and Vehicular Environments: Cross-layer Implementation and Experimental Evaluation. In *Proceedings of the 14th ACM International Conference on Mobile Computing and Networking (MobiCom 08)*, New York, NY, USA, 2008. ACM.

[8] Xiao-Ping Chen, Ke Wu, Liang Han, and Fanfan He. Low-Cost High Gain Planar Antenna Array for 60-GHz Band Applications. *IEEE Transactions on Antennas and Propagation*, 58(6):2126–2129, June 2010.

[9] Sunghyun Choi. Emerging IEEE 802.11e WLAN for Quality-of-Service (QoS) Provisioning. *SK Telecom Telecommunications Review*, 12:894–906, 2002.

[10] Romit R. Choudhury and Nitin H. Vaidya. Deafness: A MAC Problem in Ad Hoc Networks when Using Directional Antennas. In *Proceedings of the 12th IEEE International Conference on Network Protocols (ICNP 2004)*, Oct. 2004.

[11] Li Cong and Weihua Zhuang. Hybrid TDOA/AOA Mobile User Location for Wideband CDMA Cellular Systems. *IEEE Transactions on Wireless Communications*, 1(3):439–447, July 2002.

[12] WirelessHD Consortium. WirelessHD The First 60 GHz Standard, Jan. 2008. http://www.wirelesshd.org/about/.

[13] Carlos Cordeiro. Evaluation of Medium Access Technologies for Next Generation Millimeter-Wave WLAN and WPAN. In *Proceedings of the IEEE International Conference on Communications Workshops (ICC Workshops 2009)*, June 2009.

[14] Inigo Cuinas and Manuel Garcia Sanchez. Permittivity and Conductivity Measurements of Building Materials at 5.8 GHz and 41.5 GHz. *Wireless Personal Communications*, 20:93–100, 2002.

[15] Robert C. Daniels and Robert W. Heath. 60 GHz Wireless Communications: Emerging Requirements and Design Recommendations. *IEEE Vehicular Technology Magazine*, 2(3):41–50, Sept. 2007.

[16] Davide Dardari and Velio Tralli. High-speed Indoor Wireless Communications at 60 GHz With Coded OFDM. *IEEE Transactions on Communications*, 47(11):1709–1721, Nov. 1999.

[17] Lara Deek, Eduard Garcia Villegas, Elizabeth Belding, Sung-Ju Lee, and Kevin Almeroth. The Impact of Channel Bonding on 802.11n Network Management. In *Proceedings of the Seventh ACM Conference on Emerging Networking Experiments and Technologies (CoNEXT 11)*, New York, NY, USA, 2011.

[18] Matthew S. Gast. *802.11 Wireless Networks: The Definitive Guide*. O'Reilly Media, Inc., 2nd edition, 2005.

[19] Matthew S. Gast. *802.11n: A Survival Guide*. O'Reilly Media, Inc., 2012.

[20] Matthew S. Gast. *802.11ac: A Survival Guide*. O'Reilly Media, Inc., 1st edition, 2013.

[21] Jon Gjengset, Jie Xiong, Graeme McPhillips, and Kyle Jamieson. Phaser: Enabling Phased Array Signal Processing on Commodity WiFi Access Points. In *Proceedings of the ACM Annual International Conference on Mobile Computing and Networks (Mobicom 2014)*, 2014.

[22] Michell Gong, Dmitry Akhmetov, Roy Want, and Shiwen Mao. Multi-User Operation in mmWave Wireless Networks. In *IEEE International Conference on Communications (ICC 2011)*, June 2011.

[23] Michell X. Gong, Robert Stacey, Dmitry Akhmetov, and Shiwen Mao. A Directional CSMA/CA Protocol for mmWave Wireless PANs. In *Proceedings of the IEEE Wireless Communications and Networking Confernce (WCNC 10)*, Apr. 2010.

[24] James Gross, Marc Emmelmann, Oscar Pu nal, and Adam Wolisz. Dynamic Single-User OFDM Adaptation for IEEE 802.11 Systems. In *Proceedings of the 10th ACM Symposium on Modeling, Analysis, and Simulation of Wireless and Mobile Systems (MSWiM 07)*, New York, NY, USA, 2007. ACM.

[25] DoHyung Han, JeongWoo Jwa, and HanIl Kim. A Dual-Channel MAC Protocol Using Directional Antennas in Location Aware Ad Hoc Networks. In *ICCSA Lecture Notes in Computer Science*, volume 3983, pages 594–602. Springer Berlin Heidelberg, Jan. 2006.

[26] Christopher J. Hansen. WiGiG: Multi-gigabit Wireless Communications in the 60 GHz Band. *IEEE Wireless Communications*, 18(6):6–7, Dec. 2011.

[27] Simon Haykin. *Communication Systems*. Wiley Publishing, 5th edition, 2009.

[28] Kenichi Hosoya, Narayan Prasad, Kishore Ramachandran, Naoyuki Orihashi, Shuya Kishimoto, Sampath Rangarajan, and Kenichi Maruhashi. Multiple Sector ID Capture (MIDC): A Novel Beamforming Technique for 60-GHz Band Multi-Gbps WLAN/PAN Systems. *IEEE Transactions on Antennas and Propagation*, 63(1):81–96, Jan. 2015.

[29] Xiaoxiao Hou, Pralhad Deshpande, and Samir R. Das. Moving Bits from 3G to Metro-scale WiFi for Vehicular Network Access: An Integrated Transport Layer Solution. In *Proceedings of the 19th IEEE International Conference on Network Protocols (ICNP 2011)*, 2011.

[30] Meng-Han Hsieh and Che-Ho Wei. Channel Estimation for OFDM Systems Based on Bomb-type Pilot Arrangement in Frequency Selective Fading Channels. *IEEE Transactions on Consumer Electronics*, 44(1):217–225, Feb. 1998.

[31] IEEE 802.11 Working Group. IEEE Standard for Information Technology – Telecommunications and Information Exchange Between Systems – Local and Metropolitan Area Networks – Specific Requirements – Part 11: Wireless LAN Medium Access Control (MAC) and Physical Layer (PHY) Specifications. *IEEE Std 802.11-1997*, 1997.

[32] IEEE 802.11 Working Group. IEEE Standard for Telecommunications and Information Exchange Between Systems – Local and Metropolitan Area Networks – Specific Requirements – Part 11: Wireless Medium Access Control (MAC) and Physical Layer (PHY) Specifications: High Speed Physical Layer in the 5 GHz band. *IEEE Std 802.11a-1999*, Dec. 1999.

[33] IEEE 802.11 Working Group. Supplement to IEEE Standard for Information Technology – Telecommunications and Information Exchange Between Systems – Local and Metropolitan Area Networks – Specific Requirements – Part 11: Wireless LAN Medium Access

Control (MAC) and Physical Layer (PHY) Specifications: Higher-Speed Physical Layer Extension in the 2.4 GHz Band. *IEEE Std 802.11b-1999*, 2000.

[34] IEEE 802.11 Working Group. IEEE Standard for Information Technology – Telecommunications and Information Exchange Between Systems – Local and Metropolitan Area Networks – Specific Requirements Part 11: Wireless LAN Medium Access Control (MAC) and Physical Layer (PHY) Specifications. *IEEE Std 802.11g-2003*, 2003.

[35] IEEE 802.11 Working Group. IEEE Standard for Information Technology – Telecommunications and Information Exchange Between Systems – Local and Metropolitan Area Networks – Specific Requirements – Part 11: Wireless LAN Medium Access Control (MAC) and Physical Layer (PHY) Specifications: Medium Access Control (MAC) Quality of Service Enhancements. *IEEE Std 802.11e-2005*, Nov. 2005.

[36] IEEE 802.11 Working Group. IEEE Standard for Information Technology – Telecommunications and Information Exchange Between Systems – Local and Metropolitan Area Networks – Specific Requirements – Part 11: Wireless LAN Medium Access Control (MAC) and Physical Layer (PHY) Specifications. *IEEE Std 802.11-2007*, June 2007.

[37] IEEE 802.11 Working Group. IEEE Standard for Information Technology – Telecommunications and Information Exchange Between Systems – Local and Metropolitan Area Networks – Specific Requirements – Part 11: Wireless LAN Medium Access Control (MAC) and Physical Layer (PHY) Specifications: Enhancements for Higher Throughput. *IEEE Std 802.11n-2009*, Oct. 2009.

[38] IEEE 802.11 Working Group. IEEE Standard for Information Technology – Telecommunications and Information Exchange Between Systems – Local and Metropolitan Area Networks – Specific Requirements – Part 11: Wireless LAN Medium Access Control (MAC) and Physical Layer (PHY) Specifications. *IEEE Std 802.11-2012*, Mar. 2012.

[39] IEEE 802.11 Working Group. IEEE Standard for Information Technology – Telecommunications and Information Exchange Between Systems – Local and Metropolitan Area Networks – Specific Requirements – Part 11: Wireless LAN Medium Access Control (MAC) and Physical Layer (PHY) Specifications: Enhancements for Very High Throughput in the 60 GHz Band. *IEEE Std 802.11ad-2012*, Dec. 2012.

[40] IEEE 802.11 Working Group. IEEE Standard for Information Technology – Telecommunications and Information Exchange Between Systems – Local and Metropolitan Area Networks – Specific Requirements – Part 11: Wireless LAN Medium Access Control (MAC) and Physical Layer (PHY) Specifications: Enhancements for Very High Throughput for Operation in Bands below 6 GHz. *IEEE Std 802.11ac-2013*, Dec. 2013.

[41] Raj Jain, Arjan Durresi, and Gojko Babic. Throughput Fairness Index: An Explanation. Technical report, Department of CIS, The Ohio State University, 1999.

[42] Shilpa Jindal, Alka Jindal, and Neena Gupta. Grouping WI-MAX, 3G and WI-FI for wireless broadband. In *Proceedings of IEEE and IFIP International Conference in Central Asia on Internet (ICI 2005)*, 2005.

[43] Leonard Cimini Jr. Analysis and Simulation of a Digital Mobile Channel Using Orthogonal Frequency Division Multiplexing. *IEEE Transactions on Communications*, 33(7):665 – 675, July 1985.

[44] Ad Kamerman and Leo Monteban. WaveLAN-II: a High-performance Wireless LAN for the Unlicensed Band. *Bell Labs Technical Journal*, 2(3):118–133, 1997.

[45] T. Keller and L. Hanzo. Sub-band Adaptive Pre-equalised OFDM Transmission. In *Proceedings of the IEEE Vehicular Technology Conference (VTC 99)*, 1999.

[46] Young-Bae Ko, Vinaychandra Shankarkumar, and Nitin H. Vaidya. Medium Access Control Protocols using Directional Antennas in Ad Hoc Networks. In *Proceedings of the IEEE Conference on Computer Communications (Infocom 2000)*, 2000.

[47] Thanasis Korakis, Gentian Jakllari, and Leandor Tassiulas. A MAC Protocol for Full Exploitation of Directional Antennas in Ad-Hoc Wireless Networks. In *Proceedings of the ACM International Symposium on Mobile Ad Hoc Networking and Computing (MobiHoc 03)*, New York, NY, USA, 2003.

[48] Antti E.I. Lamminen, Jussi Saily, and Antti R. Vimpari. 60-GHz Patch Antennas and Arrays on LTCC With Embedded-Cavity Substrates. *IEEE Transactions on Antennas and Propagation*, 56(9):2865–2874, Sept. 2008.

[49] Bin Li, Zheng Zhou, Haijun Zhang, and Arumugam Nallanathan. Efficient Beamforming Training for 60-GHz Millimeter-Wave Communications: A Novel Numerical Optimization Framework. *IEEE Transactions on Vehicular Technology*, 63(2):703–717, Feb. 2014.

[50] Yuxia Lin and Wong V.W.S. WSN01-1: Frame Aggregation and Optimal Frame Size Adaptation for IEEE 802.11n WLANs. In *Proceedings of the IEEE Global Telecommunications Conference (GLOBECOM 06)*, Nov. 2006.

[51] Hisham Mahmoud, Tevfik Yucek, and Huseyin Arslan. OFDM for Cognitive Radio: Merits and Challenges. *IEEE Wireless Communications*, 16(2):6–15, 2009.

[52] Stefan Mangold, Sunghyun Choi, Guido R. Hiertz, Ole Klein, and Bernhard Walke. Analysis of IEEE 802.11e for QoS Support in Wireless LANs. *IEEE Wireless Communications*, 10:40–50, Dec. 2003.

[53] Patrick Moorhead. Qualcomm Gets the Jump on WiGig 60 GHz Wireless with Wilocity Acquisition, July 2014. http://onforb.es/1iYWd2x.

[54] Nektarios Moraitis and Philip Constantinou. Indoor Channel Measurements and Characterization at 60 GHz for Wireless Local Area Network Applications. *IEEE Transactions on Antennas and Propagation*, 52(12):3180–3189, Dec. 2004.

[55] R. Mudumbai, S. Singh, and U. Madhow. Medium Access Control for 60 GHz Outdoor Mesh Networks with Highly Directional Links. In *Proceedings of the IEEE Conference on Computer Communications (Infocom 2009)*, Apr. 2009.

[56] Patrick Murphy, Chris Hunter, and Erik Welsh. Rice University WARP project. http://warp.rice.edu.

[57] A. Nasipuri, S. Ye, J. You, and R.E. Hiromoto. A MAC Protocol for Mobile Ad Hoc Networks Using Directional Antennas. In *Proceedings of the IEEE Wireless Communications and Networking Confernce (WCNC 2000)*, 2000.

[58] Richard Van Nee, V.K. Jones, Geert Awater, Allert Van Zelst, James Gardner, and Greg Steele. The 802.11n MIMO-OFDM Standard for Wireless LAN and Beyond. *Wireless Personal Communications*, 37(3-4):445–453, 2006.

[59] Dong Ngo. WiGig Alliance to consolidate activities in Wi-Fi Alliance, Jan. 2013. http://www.cnet.com/news/wigig-alliance-to-consolidate-activities-in-wi-fi-alliance/.

[60] Dragos Niculescu and Badri Nath. Ad Hoc Positioning System (APS) Using AoA. In *Proceedings of the IEEE Conference on Computer Communications (Infocom 2003)*, 2003.

[61] Jianxia Ning, Tae-Suk Kim, Srikanth V. Krishnamurthy, and Carlos Cordeiro. Directional Neighbor Discovery in 60 GHz Indoor Wireless Networks. In *Proceedings of the ACM International Conference on Modeling, Analysis and Simulation of Wireless and Mobile Systems (MSWiM 2009)*, 2009.

[62] Thomas Nitsche, Carlos Cordeiro, Adriana B. Flores, Edward W. Knightly, Eldad Perahia, and Joerg Widmer. IEEE 802.11ad: Directional 60 GHz Communication for Multi-Gigabit-per-Second Wi-Fi. *IEEE Communications Magazine*, 52(12):132–141, Dec. 2014.

[63] Thomas Nitsche, Adriana B. Flores, Edward W. Knightly, and Joerg Widmer. Steering with Eyes Closed: mm-Wave Beam Steering without In-Band Measurement. In *Proceedings of the IEEE Conference on Computer Communications (Infocom 15)*, Apr. 2015.

[64] Hyunhee Park, Yongsun Kim, Taewon Song, and Sangheon Pack. Multi-band Directional Neighbor Discovery in Self-Organized mmWave Ad-Hoc Networks. *IEEE Transactions on Vehicular Technology*, 64(99):1143–1155, June 2014.

[65] Minyoung Park. IEEE 802.11ac: Dynamic Bandwidth Channel Access. In *IEEE International Conference on Communications (ICC 2011)*, June 2011.

[66] Minyoung Park, Carlos Cordeiro, Eldad Perahia, and Lily Yang. Millimeter-Wave Multi-Gigabit WLAN: Challenges and Feasibility. In *Proc. IEEE PIMRC*, 2008.

[67] Pasternack and Vubiq. V60WGD03 60 GHz Waveguide Development System. http://www.pasternack.com/60-ghz-development-systems-category.aspx.

[68] Patrick Murphy and Ashutosh Sabharwal and Behnaam Aazhang. Design of WARP: A Flexible Wireless Open-Access Research Platform. In *Proceedings of the European Signal Processing Conference (EUSIPCO 06)*, 2006.

[69] Bob Pearson. Complementary Code Keying Made Simple. *Intersil Application Notes AN9850*, 2000.

[70] Klaus I. Pedersen, Guillaume Monghal, Istvan Z. Kovacs, Troels E. Kolding, Akhilesh Pokhariyal, Frank Frederiksen, and Preben Mogensen. Frequency Domain Scheduling for OFDMA with Limited and Noisy Channel Feedback. In *Proceedings of the IEEE Vehicular Technology Conference (VTC 2007)*, Oct. 2007.

[71] Eldad Perahia and Robert Stacey. *Next Generation Wireless LANs: 802.11n and 802.11ac*. Cambridge University Press, New York, NY, USA, 2nd edition, 2013.

[72] Oscar Punal, Humberto Escudero, and James Gross. Power loading: Candidate for future WLANs? *Proceedings of the IEEE International Symposium on a World of Wireless, Mobile and Multimedia Networks (WoWMoM 12)*, 2012.

[73] Oscar Punal and James Gross. Combined Subcarrier Switch Off and Power Loading for 80 MHz Bandwidth WLANs. In *Proceeding of the 18th IEEE Workshop on Local Metropolitan Area Networks (LANMAN 11)*, Oct. 2011.

[74] Jian Qiao, Lin X. Cai, Xuemin Shen, and Jon W. Mark. Enabling Multi-Hop Concurrent Transmissions in 60 GHz Wireless Personal Area Networks. *IEEE Transactions on Wireless Communications.*, 10(11):3824–3833, Nov. 2011.

[75] Jian Qiao, Xuemin Shen, Jon W. Mark, Zhiguo Shi, and Neda Mohammadizadeh. MAC-layer Integration of Multiple Radio Bands in Indoor Millimeter Wave Networks. In *Proceedings of the IEEE Wireless Communications and Networking Confernce (WCNC 13)*, Apr. 2013.

[76] H. Radi, M. Fiacco, M. A. Parks, and S.R. Saunders. Simultaneous Indoor Propagation Measurements at 17 and 60 GHz for Wireless Local Area Networks. In *Proceedings of the 48th IEEE Vehicular Technology Conference (VTC 98)*, May 1998.

[77] Theodore. S. Rappaport. *Wireless Communications: Principles and Practice*. Prentice Hall PTR, Upper Saddle River, NJ, USA, 2nd edition, 2001.

[78] Theodore S. Rappaport, Robert W. Heath Jr, Robert C. Daniels, and James N. Murdock. *Millimeter Wave Wireless Communications*. Pearson Education, 2014.

[79] Ashutosh Sabharwal, Ahmad Khoshnevis, and Edward W. Knightly. Opportunistic Spectral Usage: Bounds and a Multi-band CSMA/CA Protocol. *IEEE/ACM Transactions on Networking*, 15(3):533–545, June 2007.

[80] Ralph O. Schmidt. Multiple Emitter Location and Signal Parameter Estimation. *IEEE Transactions on Antennas and Propagation*, 1986.

[81] Peter Schmulders. Exploiting the 60 GHz Band for Local Wireless Multimedia Access: Prospects and Future Directions. *IEEE Communications Magazine*, 40(1):140–147, Jan. 2002.

[82] Souvik Sen, Naveen Santhapuri, Romit R. Choudhury, and Srihari Nelakuditi. AccuRate: Constellation based Rate Estimation in Wireless Networks. In *Proceedings of the 7th USENIX Conference on Networked Systems Design and Implementation (NSDI 10)*, Berkeley, CA, USA, 2010. USENIX Association.

[83] Zukang Shen, Jeffrey G. Andrews, and Brian L. Evans. Adaptive Resource Allocation in Multiuser OFDM Systems with Proportional Rate Constraints. *IEEE Transactions on Wireless Communications*, 4(6):2726–2737, Nov. 2005.

[84] Eugene Shih, Paramvir Bahl, and Michael J. Sinclair. Wake on Wireless: An Event Driven Energy Saving Strategy for Battery Operated Devices. In *Proceedings of the ACM Annual International Conference on Mobile Computing and Networks (Mobicom 2002)*, 2002.

[85] Sumit Singh, Raghu Mudumbai, and Upamanyu Madhow. Distributed Coordination with Deaf Neighbors: Efficient Medium Access for 60 GHz Mesh Networks. In *Proceedings of the IEEE Conference on Computer Communications (Infocom 2010)*, Mar. 2010.

[86] Sumit Singh, Raghuraman Mudumbai, and Upamanyu Madhow. Interference Analysis for Highly Directional 60-GHz Mesh Networks: The Case for Rethinking Medium Access Control. *IEEE/ACM Transaction on Networking*, 19(5):1513–1527, Oct. 2011.

[87] Dionysios Skordoulis, Qiang Ni, Hsiao-Hwa Chen, Adrian P. Stephens, Changwen Liu, and Abbas Jamalipour. IEEE 802.11n MAC Frame Aggregation Mechanisms for Next-Generation High-Throughput WLANs. *IEEE Wireless Communications*, 15:40–47, Feb. 2008.

[88] Patrick Svedman, Sarah K. Wilson, Leonard J. Cimini, and Bjoern Ottersten. Opportunistic Beamforming and Scheduling for OFDMA Systems. *IEEE Transactions on Communications*, 55(5):941–952, May 2007.

[89] Mineo Takai, Jay Martin, Rajive Bagrodia, and Aifeng Ren. Directional Virtual Carrier Sensing for Directional Antennas in Mobile Ad Hoc Networks. In *Proceedings of the ACM International Symposium on Mobile Ad Hoc Networking and Computing (MobiHoc 02)*, Lausanne, Switzerland, 2002.

[90] Xiaozheng Tie, Kishore Ramachandran, and Rajesh Mahindra. On 60 GHz Wireless Link Performance in Indoor Environments. In *Passive and Active Measurements (PAM)*, pages 147–157, Berlin, Heidelberg, Mar. 2012. Springer-Verlag.

[91] Fouad A. Tobagi and Leonard Kleinrock. Packet Switching in Radio Channels: Part II–The Hidden Terminal Problem in Carrier Sense Multiple-Access and the Busy-Tone Solution. *IEEE Transactions on Communications*, 23(12):1417–1433, Dec. 1975.

[92] Alberto Valdes-Garcia, Scott Reynolds, Arun Natarajan, Dong Kam, Duixian Liu, Jie-Wei Lai, Yen-Lin Oscar Huang, Ping-Yu Chen, Ming-Da Tsai, Jing-Hong Conan Zhan, Sean Nicolson, and Brian Floyd. Single-Element and Phased-Array Transceiver Chipsets for 60-GHz Gb/s Communications. *IEEE Communications Magazine*, 49(4):120–131, Apr. 2011.

[93] Vincent Vermeer. Wireless LANs; Why IEEE 802.11 DSSS? In *Proceedings of the Wescon Conference (Wescon 97)*, Nov. 1997.

[94] Yu Wang, Hari Krishna Garg, and Mehul Motani. Directional Medium Access Control for Ad Hoc Networks: A Cooperation-Based Approach. In *Proceedings of the IEEE International Conference on Networks (ICON 13)*, Dec. 2013.

[95] Carl Wong, Richard Klukas, and Geoffrey Messier. Using WLAN Infrastructure for Angle-of-Arrival Indoor User Location. In *Proceedings of the IEEE Vehicular Technology Conference (VTC 2008)*, 2008.

[96] Cheong Yui Wong, Roger S. Cheng, Khaled B. Lataief, and Ross D. Murch. Multiuser OFDM with Adaptive Subcarrier, Bit, and Power Allocation. *IEEE Journal on Selected Areas in Communications*, 17(10):1747–1758, Oct. 1999.

[97] Jie Xiong and Kyle Jamieson. Towards Fine-grained Radio-based Indoor Location. In *Proceedings of the ACM International Workshop on Mobile Computing Systems and Applications (HotMobile 2012)*, 2012.

[98] Jie Xiong and Kyle Jamieson. ArrayTrack: A Fine-grained Indoor Location System. In *Proceedings of the USENIX Symposium on Networked Systems Design and Implementation (NSDI 2013)*, 2013.

[99] Li Xiong. A Selective Model to Suppress NLOS Signals in Angle-of-Arrival (AOA) Location Estimation. In *Proceedings of the IEEE Annual International Symposium on Personal, Indoor, and Mobile Radio Communications (PIMRC 1998)*, 1998.

[100] Hao Xu, Vikas Kukshya, and Theodore S. Rappaport. Spatial and Temporal Characteristics of 60-GHz Indoor Channels. *IEEE Journal on Selected Areas in Communications*, 20(3):620–630, 2002.

[101] Hao Xu, Vikas Kukshya, and Theodore S. Rappaport. Spatial and Temporal Characteristics of 60-GHz Indoor Channels. *IEEE Journal on Selected Areas in Communications*, 20(3):620–630, 2002.

[102] Kaixin Xu, Mario Gerla, and Sang Bae. How Effective is the IEEE 802.11 RTS/CTS Handshake in Ad Hoc Networks. In *Proceedings of the IEEE Global Telecommunications Conference (GLOBECOM 02)*, Nov. 2002.

[103] Haibing Yang, Peter Smulders, and Matti H.A.J. Herben. Frequency Selectivity of 60-GHz LOS and NLOS Indoor Radio Channels. In *Proceedings of the IEEE Vehicular Technology Conference (VTC 2006)*, May 2006.

[104] Siew Bee Yeap, Zhi Ning Chen, and Xianming Qing. Gain-Enhanced 60-GHz LTCC Antenna Array With Open Air Cavities. *IEEE Transactions on Antennas and Propagation*, 59(9):3470–3473, Sept. 2011.

[105] Su-Khiong Yong, Pengfei Xia, and Alberto Valdes-Garcia. *60GHz Technology for Gbps WLAN and WPAN: from Theory to Practice*. John Wiley & Sons, 2011.

[106] Takeshi Manabe Yuko, Miura, and Toshio Ihara. Effects of Antenna Directivity and Polarization on Indoor Multipath Propagation Characteristics at 60 GHz. *IEEE Journal on Selected Areas in Communications*, 14(3):441–448, Apr. 1996.

[107] Yibo Zhu, Yengbin Zhang, Yhinus Marzi, Chris Nelson, Upamanyu Madhow, Ben Y. Zhao, and Haitao Zheng. Demystifying 60GHz Outdoor Picocells. In *Proceedings of the ACM Annual International Conference on Mobile Computing and Networks (Mobicom 14)*, 2014.

[108] Thomas Zwick, Troy J. Beukema Nam, and Haewoon. Wideband Channel Sounder with Measurements and Model for the 60 GHz Indoor Radio Channel. *IEEE Transactions on Vehicular Technology*, 54(4):1266–1277, July 2005.

Publications

International Magazine Articles

Authors Thomas Nitsche, Carlos Cordeiro, Adriana B. Flores, Edward W. Knightly, Eldad Perahia, Joerg Widmer

Title IEEE 802.11ad: Directional 60 GHz Communication for Multi-Gigabit-per-Second Wi-Fi

Venue IEEE Communications Magazine, Dezember 2014

Abstract With the ratification of the IEEE 802.11ad amendment to the 802.11 standard in December 2012, a major step has been taken to bring consumer wireless communication to the millimeter wave (mm-Wave) band. However, multi-Gbps throughput and small interference footprint come at the price of adverse signal propagation characteristics and require a fundamental rethinking of Wi-Fi communication principles. This paper describes the design assumptions taken into consideration for the IEEE 802.11ad standard and the novel techniques defined to overcome the challenges of mm-Wave communication. In particular we study the transition from omni-directional to highly directional communication and its impact on the design of IEEE 802.11ad.

International Conference and Workshop Papers

Authors Thomas Nitsche, Adriana B. Flores, Edward W. Knightly, Joerg Widmer

Title Steering with Eyes Closed: mm-Wave Beam Steering without In-Band Measurement

Venue The 34th IEEE International Conference on Computer Communications (IEEE INFOCOM 2015), 26 April - 1 May 2015, Hong Kong, China

Abstract Millimeter-wave communication achieves multi-Gb/sec data rates via highly directional beamforming to overcome pathloss and provide the desired SNR. Unfortunately, establishing communication with sufficiently narrow beamwidth to obtain the necessary link budget is a high overhead procedure in which the search space scales with the product of the sender-receiver beam resolution. In this paper, we design, implement, and experimentally evaluate Blind Beam Steering

(BBS), a novel architecture and algorithm that removes in-band overhead for directional mm-Wave link establishment. Our system architecture couples mm-Wave with legacy 2.4/5 GHz bands in a novel way that exploits the unique propagation properties of each. We utilize omni-directional transmissions at 2.4/5 GHz bands to obtain the line-of-sight path using angle of arrival analysis to then establish (overhead-free) Multi-Gb/sec directional communication in the mm-Wave band. By removing in-band overhead, we leverage mm-Waves very high throughput capabilities, beam-width scalability and provide robustness to mobility. We demonstrate that BBS achieves 97.8% accuracy estimating direction between pairing nodes using at least 5 detection band antennas. Further, BBS successfully detects unobstructed direct path conditions assuring highest mm-Wave throughput with a rate of 96.5% and reduces the IEEE 802.11ad beam forming training overhead by 81%.

Authors Alexander Kuehne, Adrian Loch, Thomas Nitsche, Joerg Widmer, Matthias Hollick, Anja Klein

Title BER Enhancements for Practical Interference Alignment in the Frequency Domain

Venue The 11th International Symposium on Wireless Communication Systems (ISWCS 2014), 26-29 August 2014, Barcelona, Spain

Abstract The K user interference alignment scheme with symbol extensions proposed by Cadambe and Jafar achieves K/2 degree of freedom in theory for high signal-to-noise ratios (SNRs). However, lower SNR ranges appear in many practical scenarios. Thus, further improvements of the Cadambe-Jafar scheme are demanded to enable interference alignment in more realistic settings. In this work, we propose a new precoding vector optimization that improves bit error rates (BER) using zero-forcing at the receivers. Furthermore, we compare and combine our approach with existing performance enhancement techniques for interference alignment such as orthonormalizing the precoding matrices or using lattice decoding instead of zero-forcing at the receiver. Finally, we implement interference alignment with symbol extension in the frequency domain along with the presented BER enhancement techniques on a software defined radio platform to validate our approaches. Both simulation results and testbed measurements show significant BER improvements for different M-QAM schemes compared to the original interference alignment mechanism. Moreover, our precoding optimization scheme based on zero-forcing outperforms lattice decoding in practical systems due to its lower sensitivity to real-world effects.

Authors Adrian Loch, Thomas Nitsche, Alexander Kuehne, Matthias Hollick, Joerg Widmer, Anja Klein

Title Practical Interference Alignment in the Frequency Domain for OFDM-based Wireless Access Networks

Venue The 15th IEEE International Symposium on a World of Wireless, Mobile and Multimedia Networks (IEEE WoWMoM 2014), 16-19 June 2014, Sydney, Australia

Abstract Interference alignment (IA) is often considered in the spatial domain in combination with MIMO systems. In contrast, aligning interference in the frequency domain among multiple subcarriers can also benefit single-antenna OFDM-based access networks. It allows for flexible operation on a per-subcarrier basis. We investigate the gains achievable by frequency IA in practice for a scenario with multiple access points and clients. Previous work is predominantly theoretical and focuses on idealized cases where all nodes have the same average signal-to-noise ratio (SNR). On the contrary, in practical networks, nodes typically have heterogeneous SNRs depending on channel conditions, which might have a significant impact on IA performance. We tackle this problem by designing mechanisms that adaptively choose which nodes shall perform IA on which subcarriers depending on current channel conditions. We implement and validate our approach on software defined radios. To the best of our knowledge, this is the first practical implementation of IA in the frequency domain. Our measurements show that (1) frequency IA is feasible in practice, and (2) choosing appropriate nodes and subcarriers overcomes the main limitations due to heterogeneous SNRs. Our mechanisms enable IA in scenarios where it would be infeasible otherwise, achieving throughput gains close to the 33% theoretical maximum.

Authors Thomas Nitsche, Joerg Widmer

Title Sub-carrier Switch Off in OFDM-Based Wireless Local Area Networks

Venue The 10th IEEE International Conference on Sensing, Communication and Networking (IEEE SECON 2013), 24 - 27 June 2013, New Orleans, USA

Abstract OFDM based wireless communication systems split the available frequency band into so-called sub-carriers, and data is transmitted on each of these sub-carriers in parallel. With frequency selective fading, sub-carriers may experience different channel qualities. Thus, choosing a different modulation and coding scheme (MCS) per sub-carrier improves performance. However, this comes at an increase in transceiver complexity and no current wireless system adapts the MCS at such a fine granularity. Some OFDMA based systems such as LTE allow to adapt the MCS per user, whereas wireless local area networks as specified by IEEE 802.11 use the same MCS on every sub-carrier. The performance of such wireless systems that use a single MCS in a frequency selective fading channel can be significantly improved through Sub-Carrier Switch

Off (SSO), a simple but powerful alternative to adaptive MCS. SSO deactivates weak sub-carriers that excessively raise the error probability to improve the overall throughput. In this paper, we implement and test SSO in a software-defined radio testbed based on the Wireless Open Access Research Platform (WARP). We present a novel light-weight method for selecting the sub-carriers to be switched off based on the per-sub-carrier channel quality. The results we obtain from our measurements indicate that throughput increases of up to 250% are possible and thus SSO is a highly promising and very low complexity mechanism for future wireless local area networks.

Authors Thomas Nitsche, Joerg Widmer, Adrian Loch, Matthias Hollick

Title EVM and RSSI Link Quality Measurements in Frequency Selective Fading Channels

Venue The 14th IEEE International Workshop on Signal Processing Advances for Wireless Communications (IEEE SPAWC 2013), 16 - 19 June 2013, Darmstadt, Germany

Abstract In this paper, we discuss the suitability of error vector magnitude (EVM) and received signal strength indicator (RSSI) as wireless quality metrics. We evaluate these metrics in a software defined radio testbed and provide detailed measurement results for frequency selective fading channels. We show that EVM is well suited as a packet loss estimator and discuss a case where receiver implementation inefficiencies show up in the EVM.

Authors Adrian Loch, Matthias Hollick, Thomas Nitsche, Joerg Widmer, Alexander Kuehne, Klein Anja

Title CSI Feedback in OFDMA Wireless Networks with Multiple Sender-Receiver Pairs

Venue The 14th IEEE International Workshop on Signal Processing Advances for Wireless Communications (IEEE SPAWC 2013), 16 - 19 June 2013, Darmstadt, Germany

Abstract In wired or wireless distribution systems, as well as wireless mesh networks, multiple senders often need to deliver data to multiple receivers in the same interference domain. OFDMA enables interference avoidance by assigning disjoint sets of subcarriers to each sender. However, optimal subcarrier allocation requires CSI feedback to the transmitters, thus incurring overhead. We evaluate an allocation mechanism inspired in subcarrier switching techniques, which allows nodes to locally decide which subcarriers they prefer. Hence, feedback is minimal, as only preference values need to be shared. We implement this approach on software defined radios and compare it to standard CSI feedback mechanisms. Despite our approach only requires local information, the results show that it performs close to an ideal solution based on full CSI knowledge.

Authors Thomas Nitsche and Thomas Fuhrmann

Title A Tool for Raytracing Based Radio Channel Simulation

Venue Proceedings of the 4th International ICST Conference on Simulation Tools and Techniques,Barcelona, Spain, 21-25 March 2011

Abstract In this paper, we briefly report on our ongoing work to extend the GNU Radio software suite with a ray tracing based radio channel simulator. Radio channel simulation is an important aspect in the design and evaluation of wireless protocols because noise and interference can have a crucial impact on the performance of a protocol. However, the calculation of radio wave propagation is computationally demanding. Thus, most network simulation frameworks rely on simple statistical radio channel models that do not account for site-specific propagation characteristics. So, these simulators miss important details that might impact a protocol significantly in specific propagation environment. Our radio channel simulator uses ray tracing techniques to overcome this limitation. It precomputes the channel characteristics of a given scene so that it can then efficiently simulate the corresponding links. Our implementation seamlessly interfaces with the GNU Radio software defined radio (SDR) framework, replacing its statistical channel simulation component. Furthermore, using GNU Radios various modulation components, our simulator can provide a complete PHY layer simulation interface for other simulators such as ns-3 or OMNeT++. All in all, our simulator enables SDR developers and wireless protocol engineers to quickly assess their design in more realistic simulated environments.

Technical Reports

Authors Adrian Loch, Thomas Nitsche, Alexander Kuehne, Matthias Hollick, Joerg Widmer, Anja Klein

Title Practical Challenges of IA in Frequency (Technical Report TR-SEEMOO-2013-01)

Abstract Interference Alignment (IA) is a promising technique at the physical layer which allows to increase the Degree-of-Freedom (DOF) of a communication by aligning all interfering signals into the same dimension, while the desired signal lies unaffected in an orthogonal dimension. IA has been widely studied in theory, but only limited practical work exists, since it poses significant challenges for real-world deployments. In this report, we study issues which are key to enable IA in practice.
